

Study on the Dynamic Response of Container Stacks Using Non-Linear Finite Element Analysis



THE UNIVERSITY OF TOKYO

Vinícius Aguiar de Souza
Graduate School of Frontier Sciences
Adviser: Professor Katsuyuki Suzuki

A thesis submitted for the degree of

Doctor of Philosophy

2010

I would like to dedicate this thesis to my Grandparents: Norma Aguiar, Jose Felicio Aguiar, Nery Engracia de Souza, and Pedro Reis de Souza, and my son: Pedro Moraes Aguiar. I firmly believe that much can be said of a character of a men just by analyzing his ancestors. I hope I can provide to my son an example (*vita non est vivere sed valere vita est*) at least close to those superb that thou taught me. I love and miss thou beyond thou can imagine. *In Memoriam*

Acknowledgements

I would like to thank from the bottom of my heart the Japanese Ministry of Education and Science for supporting this kind of program, aimed to foreigners, which make possible this challenge of studying in Japan. This experience changed my life in a way that I find difficult to describe in words. Following that I own my advisor professor Katsuyuki Suzuki more than just gratitude. In the distant year of 2005 I was in the brink of leaving Japan. Without his incentive and support I would never be able to became a doctor. More than just giving me academic advice he presented me with a limitless source of inspiration and example. Additionally, this work would not be possible without your kind help. Thank you so much for being a marvelous advisor. A long time has passed since I started this journey.

To all Graduate School of Frontier Sciences employees. They were always supportive, helpful, and most important of all: kind. Thank you so much. To my colleagues in professor Suzuki laboratory. Thanks for the Japanese lessons and help. To Ana Paula Bortoleto, Kelly Midori Vargas, Rafael Takai, Marcos Fukase Maeda, Lirian Mina Nozawa, Marcia Sayuri Kondo and Pedro Ivo Lages de Macedo who were close friends sharing my agony during my worst period in Japan. Without your assistance I would have abandoned my dream in March of 2005. Muchas gracias hermanos!!!!!!Special thanks to Pedro Ivo for all Winning Eleven hours. They made many bad moments just disappear (Thanks to KONAMI for making such wonderful game. Love you guys).

Special thanks to doctor Levent Kirkayak who was always there for me. Without him, I would not complete this task. He helped me in every aspect of my life in Japan, not only technical aspects but personal as well. I will never forget his first day in the laboratory when after a short introduction he turn around and said: " no need to say who is the Brazilian guy". Among many qualities, he is a master in breaking the ice. I am really glad that I can call him my brother. To doctor Huseyin Tekin Darama for his help regarding seismic isolation devices. He was really supportive contributing greatly for the

implementation and improvement of this work. For both of you I will use a old Latin saying: *Amici probantur rebus adversis*.

To all technical members of the Monohakobi Technology Institute (MTI-NYK) in Yokohama. Without their technical support and know-how this work would loss in quality.

To the members of my doctor's committee: professors Hidetoshi Sueoka, Yutaka Toi, Hosaka Hiroshi and Watanabe Hiroshi for their valuable advice and pertinent questions that helped to increase the quality of this manuscript. To the L^AT_EX: community for proving a reliable platform to write a decent dissertation. Special thanks to professor Donald Knuth who was the creator of such great computer typesetting system. To Sport Club Internacional for showing some great soccer and becoming South American Champions once again. To doctor Sergio Jun Ono Fonseca for recommending me to this laboratory. To the Japan Karate Association for helping me to release my stress. Honor mention to master Mitsuo Inoue who recommended me to one of the most famous Karate clubs in Japan: Komazawa university Karate club. To master Takeshi Oishi and Shinzo Izumiya who received me with open arms. To my master and idol master Seiji Osaka for all valuable lessons not only as a true Karate master but as a marvelous human being as well.

To professor Milton Antonio Zaro for the help with the data filtering. To René Marcelino A Britta Teixeira for his help with the layout in Latex environment.

To professors Koichi Hattori and Beate Heissig and friends from the Institute of Medical Sciences (Stem cells research laboratory) for the nice three years I spend working with them. To Petrônio Nagahara Ribeiro, Caroline Grahl Fabiano Alves, Daniela Santos Machado and Cristiane Moraes da Silva for babysitting my son while I was writing this dissertation. Special mention to Petrônio Nagahara Ribeiro who was my close friend and ally during the most turbulent period: two weeks before the final defense, when he left his family and job just to look after my son. Words are not enough to thank your help. For you my brother I paraphrase the same saying I wrote before: *Amici probantur rebus adversis*.

To my wife Cristina Moraes de Souza who that despite all adversity was there for me. To my parents and relatives who always believe that I could come to Japan and make my dreams come true. I will always remember your lessons: *Perfer et obdura; dolor hic tibi proderit olim*.

To my friends and brothers Sebastiao Bernard Fontenele, Marlo Lustosa da Silveira, Leonardo Castilhos Silveira, Cristian Job Salaini, Deivis Cristovao Lima Chagas, Adriano Lauck, Elton Alexandre Schuck, Renato Passos Moreira, Paulo Ricardo Geyer da Costa and Hervandil Morosini Sant'Anna. My life in Japan was not perfect because they were not around. . To my friends in the volleyball team that helped me relief the stress associate with the PhD course: Fabio Terabe, Fernando Nogueira, Haeng-ja Chung, Misa Tsutsui, Paulo Vinícius Queiróz de Souza, Tatiana Victorovna Martsinkevich and many others.

To Jorge Cham for his hilarious PhD Comics that reflect in a humorous way what graduate students face. To Playstation for proving some funny moments to relax through some memorable games. Finally, to Minwoo Park, Benjamin Rossman, Moses Mwalye and Dan Cook who kindly helped me with the English grammar revision.

Abstract

During the centuries that followed the Age of Discovery, when Europeans, notably Portugal and Spain, started to cruise the Seven Seas, the first navigators faced a dilemma that threatened their well being and the success of their enterprise: how to transport goods safely and efficiently across the oceans? Moreover, how to do it avoiding deterioration and consequent losses? The final answer for these questions was the creation of containers: a geometrically simple structure that facilitated maritime transportation. Nowadays, sea surface transportation accounts for 99% of all international transportation. Of this amount, the biggest part of the fleet corresponds to container ships. The use of containers to transport numerous manufactured goods is relatively new. Since this piece of equipment was invented in 1937 by Malcolm MacLean, a revolution was seen in maritime transportation, with consequent improvements in efficacy and reliability.

Despite its young age, containers became broadly popular and their use quickly spread around the globe. Nowadays, about 90 % of all non-bulk cargo maritime transportation worldwide is performed employing containers stacked in container ships. However, such popularization brought some concerns: tight schedules allied a recent increase in the height of stacks carried on deck and the growing size of container, coinciding with a substantial increase in the number of containers lost at sea. This number is estimated to be around ten thousand each year, and although the total number involved is a matter of controversy among experts, this still represents a significant economical loss to the liner industry. Often, extreme sea conditions that eventually induce parametric rolling in the vessel are considered the most probable culprit behind those losses. However, present regulation and norms for securing equipment are calculated based on static loads, an unrealistic approach considering the dynamic nature of the conditions faced by containers during maritime transportation. Thus, questions have been raised about the safety of prolonged use of these standards, which might underestimate real values of forces acting on container stacks and their securing elements.

In this panorama, the problem of container stack dynamics must be addressed properly to understand the mechanisms behind container losses, in an effort to set new standards and promoting valuable advice to the liner industry. To achieve this goal, the authors propose the study of the container loss problem in the light of science using a strong methodology. The study was divided in four main stages: scaling of a 20 ft ISO freight container, pilot study using scaled model in a two-tiers single stack arrangement (2x1), container stack dynamics study using scaled model in a seven-tiers single stack arrangement (7x1) and the same study of a seven-tiers three stack arrangement (7x3). These stages were segregated in two sub-stages: experimentation using shaking table testing, and numerical simulation employing finite element method. For both sub-stages a set of control variables were idealized: amplitude and frequency of the driving excitation, payload added to the scaled models, horizontal rotation of the stack base, and twist lock's gap size. Additionally, 2x1, 7x1, and 7x3 systems' linking connectors, denominated twist locks were modeled for both cases (experimental and numerical).

The first part of the research presents a method to scale down 20 ft containers using dimensional analysis, similarity theory and finite element analysis. The scaling study was separated into four sub-stages: determination of similitude parameters using Froude scaling laws, design testing (Finite Element Method - F.E.M.), scaled model manufacture and experimental validation (static and dynamical). The physical (dimensions, mass, and moments of inertia) and structural (longitudinal, transversal and torsional stiffness) characteristics of the scaled models were decided based on two dimensionless numbers: ratios between gravity force and inertia force, and elastic force divided by inertia force, through experimental and numerical analysis. Furthermore, the choice of each similitude parameter and its determination using dimensional analysis are presented in detail. Additionally, model geometrical design based on finite element analysis, posterior static and dynamic validation are explained thoroughly. In conclusion, study qualifications and limitations are logically presented with further prospect.

The second part of the research presents a pilot study used to identify some important points before the last two stages of the study. Among these points the following issues are emphasized: adequacy of the instruments and their operations, checking the design of the research protocol, assessing whether the research protocol is realistic and workable, establishing whether the sampling frame and technique are effective, identifying logistical problems which

might occur using proposed methods, estimating variability in outcomes to help determining sample size, collecting preliminary data, assessing the proposed data analysis techniques to uncover potential problems, and the assess the adequacy of the control variables.

The third part of the research describes an approach to simulate the 7x1 system, subjected to dynamical load induced by its base. Series of experiments with controlled parameters (amplitude and frequency of driving excitation, payload, shaking table base rotation and gap size) were performed using a shaking table test to understand the effects of each variable in the container stack dynamics and present enough data to validate the numerical model. Finally, the last stage describes an approach to simulate the 7x3 system using shaking table test in three cases only. The main goal of this stage is to identify and quantify the contact among stacks in order to calibrate the numerical model.

The study helped to elucidate some points regarding the system's fundamental mechanical behavior, where correlation of dynamic properties depending on amplitude and frequency of the input vibration, base rotation, container load and twist lock gap size, were obtained and used to calibrate and validate a numerical model. After this strenuous validation, the scaled numerical model was used as a valid tool to simulate the behavior of multi-stack configuration in some simple situations faced by containers during maritime transportation. Among these situations some common ship's motion were studied in detail: heaving, pitching and rolling, employing cases reported in the literature. Additionally, the problem of how simple changes in basic variables affect force in the bottom twist lock was addressed, the result of which provides useful advice for the industry, for maintaining the problem complexity to a minimum. Undoubtedly, this is one of the most significant findings to emerge from this study. In this panorama, it may contribute significantly to the understanding of container stack dynamics, an area where intuition and old standards are still preferred over more solid scientific principles.

Contents

1	Introduction	1
1.1	Background and Historical Highlights	1
1.2	Objects of Study	6
1.2.1	Container	6
1.2.2	Twist lock	6
1.3	Posing the Problem: Container Loss	12
1.4	Relevance: Economical Importance of Container ships	17
1.5	Container Lashing Components	20
1.6	Defining Goals	24
1.7	Literature Review	25
1.8	Outline of Structure	27
2	Methodology	28
2.1	Research Design Overview	28
2.2	Experimental Facility and Apparatus	31
2.2.1	Shaking Table Testing	31
2.2.2	Transducers	31
2.3	Physical Parameters Modeled	36
2.4	Defining Input and Output Variables	37
2.5	Data Analysis	39
2.6	Experimental Data Filtering	42
2.7	Terminology	45
3	Scaled Model	49
3.1	Brief Overview	49
3.2	Similarity Theory	50
3.2.1	Geometric Similarity	51
3.2.2	Kinematic Similarity	53
3.2.3	Dynamic Similarity	53

3.3	Buckingham π 's Numbers Used for Scaling	54
3.4	Design and Testing Parameters	54
3.5	Similitude Parameters Used for Model Construction	56
3.6	Design Evaluation Using Finite Element Analysis	56
3.6.1	Static Analysis	58
3.6.2	Frequency Extraction	58
3.7	Experiments for Design Evaluation	60
3.7.1	Static Validation	60
3.7.2	Dynamic Validation	61
3.8	Considerations about the Scaled Model	62
4	Experimental Investigation for the 7x1 and 7x3 Cases	69
4.1	Seven-tiers Single Stack (7x1)	69
4.2	Seven-tiers Three Stacks (7x3)	71
5	Numerical Model	73
5.1	Container Model Structure	73
5.2	Twist Lock Non-Linear Behavior	73
5.2.1	Experimental Investigation	76
5.2.1.1	Slamming Test	76
5.2.1.2	Tensile Test	77
5.2.2	Numerical Analysis	77
5.2.3	Data Analysis	79
5.3	Damping	83
5.3.1	Rayleigh Damping	84
5.4	Contact	92
5.5	Failure	94
5.6	Euler Buckling	94
5.7	Time Increment	94
6	Pilot Study	97
6.1	Objectives and Significance	97
6.2	Research Design (2x1)	98
6.2.1	Objects of Study (2x1)	98
6.2.2	Driving Excitation and Physical Parameters (2x1)	98
6.2.3	Experimental Investigation and Apparatus (2x1)	99
6.2.4	Numerical Investigation: Finite Element Analysis (2x1)	101
6.3	Results and Discussion (2x1)	102

6.3.1	Amplitude (2x1)	102
6.3.2	Frequency (2x1)	104
6.3.3	Payload (2x1)	104
6.3.4	Gap size (2x1)	104
6.4	Final Considerations about the Pilot Study	109
7	Calibration of Numerical Model	114
7.1	Seven-tiers Single Stack (7x1)	114
7.1.1	Numerical Investigation: Finite Element Analysis (7x1)	114
7.1.2	Numerical Model Validation (7x1)	115
7.1.2.1	Amplitude (7x1)	115
7.1.2.2	Frequency (7x1)	116
7.1.2.3	Payload (7x1)	117
7.1.2.4	Base rotation (7x1)	117
7.1.2.5	Gap size (7x1)	120
7.1.3	Discrepancies (7x1)	120
7.2	Seven-tiers Three Stacks (7x3)	128
7.2.1	Numerical Investigation: Finite Element Analysis (7x3)	128
7.2.2	Numerical Model Validation (7x3)	128
7.2.3	Discrepancies (7x3)	129
8	Simulation Results and Discussion	137
8.1	Predictions and Advice (7x1)	137
8.1.1	Gap Effect on Heaving	138
8.1.2	Damper Effect on Heaving	138
8.1.3	Payload Effect on Heaving	142
8.1.4	Stiffness Effect on Heaving	142
8.2	Predictions and Advice (7x3)	148
8.2.1	Pitching	148
8.2.1.1	Pitching Frequency	148
8.2.1.2	Gap Effect on Pitching	148
8.2.1.3	Damper Effect on Pitching	149
8.2.2	Rolling	149
8.2.2.1	Rolling Amplitude	151
8.2.2.2	Rolling Frequency	151
8.2.2.3	Gap Effect on Rolling	155
8.2.2.4	Damper Effect on Rolling	155
8.2.2.5	Joining Adjacent Corner Castings Effect on Rolling	155

8.3	Limitations of the Study	159
9	Conclusions	161
9.1	Summary of Findings	161
9.2	Answer to the Central Question of this Dissertation	162
9.3	Future Work	163
A	Full scale model	165
	References	177

List of Figures

1.1	Example of old break bulk method.	3
1.2	Malcom MacLean: consider “father” of container.	3
1.3	A picture taken from the deckhouse in the stern direction.	5
1.4	Picture of 20 and 40 foot containers.	7
1.5	General information about container construction.	7
1.6	Container nomenclature for the back and side portions.	8
1.7	Container nomenclature for the bottom portion.	8
1.8	Two important components of the securing system.	10
1.9	Example of semi-automatic twist lock.	11
1.10	Total collapse of containers stacks with subsequent loss of top tiers.	14
1.11	Another example of container stack collapse.	15
1.12	An example of adverse sea conditions. Picture of MSC Napoli.	15
1.13	Example of container loss.	16
1.14	Percentage of total fleet.	18
1.15	Global Containerized Trade, 2001 to 2011.	18
1.16	Annual growth of the total capacity of container ships.	19
1.17	Fixed fittings attached to the ship.	20
1.18	Loose fittings in common use.	21
1.19	Loose fittings in less common use.	22
1.20	Lashing components being placed on a container ship.	23
2.1	Schematic representation of the approach used for this study.	29
2.2	Schematic representation of the divisions of the experimental stage.	30
2.3	Schematic representation of the experimental facility.	32
2.4	Technical specifications for the shaking table.	34
2.5	Transducers used for the experiments.	35
2.6	Dimensions of the accelerometer.	35
2.7	Summary of physical phenomena modeled.	37
2.8	Fourier expansion.	42

2.9	Effect of filtering for horizontal and vertical directions.	44
2.10	Harmonic content of the horizontal and vertical displacements.	47
2.11	Residual analysis to decide the value of the cut-off frequency.	48
2.12	Graphic representation of terminology regarding ship motion.	48
3.1	Terminology for container testing (ISO).	56
3.2	Scaled model design for a 20 ft container.	57
3.3	Boundary conditions.	59
3.4	Finite element results.	60
3.5	Constructed scaled model.	60
3.6	Schematic representation of static experiments.	61
3.7	Static experiment results.	61
3.8	Placement of the accelerometers on the scaled model.	63
3.9	Characteristic signal obtained in the impact hammer test.	64
3.10	Eigenfrequencies obtained from the impact hammer test.	65
3.11	Summary of results for static cases studied.	67
3.12	Frequency comparison between experiment and numerical analysis.	68
4.1	Physical parameters and labeling.	70
4.2	Physical parameters, labelling and details of the linking components.	72
5.1	Profile of the beams used for the numerical model.	75
5.2	Details of the numerical model.	75
5.3	Twist lock experiments.	76
5.4	Step function used as driving excitation (vertical direction).	77
5.5	Tensile test results.	78
5.6	Cut view of corner casting-twist lock system.	78
5.7	Twist lock non-linear relation.	79
5.8	Twist lock numerical model.	79
5.9	Discrepancies observed for experimental data.	80
5.10	Comparison between experimental and numerical data.	82
5.11	Comparison between dashpot and Rayleigh coefficients approach.	85
5.12	Relation of damping ratio (ζ_i) and natural frequency ($\alpha = \beta = 1$).	86
5.13	Rayleigh damping calculation algorithm.	89
5.14	Plot of the four approximations.	90
5.15	Details of the contact element used for the numerical simulation.	95
5.16	Failure modeling.	96
6.1	The two setups used for experimentation (2x1).	98

6.2	Scaled twist lock.	98
6.3	Schematic representation of the gap used as a variable.	99
6.4	Details of the linking components and labeling (2x1).	100
6.5	Finite element model of the two-tier single stack case (2x1).	101
6.6	Amplitude of response for point 1 (2x1–5Hz–non loaded).	105
6.7	Amplitude of response for point 1 (2x1–10Hz–non loaded).	106
6.8	Response comparison of RMS value for point 1 (2x1–5 Hz).	107
6.9	Response comparison of RMS value for point 1 (2x1–10 Hz).	108
6.10	Frequency-response function for the experimental data (2x1).	109
6.11	Effect of inclusion of payload (2x1).	110
6.12	Fourier analysis of 15 Hz–loaded case (2x1).	111
6.13	Load effect on response (2x1).	112
6.14	Some other effects on response (2x1).	113
7.1	Finite element model of the seven-tier single stack case (7x1).	115
7.2	Amplitude comparison (relative motion–7x1).	116
7.3	Frequency comparison (relative motion–7x1).	118
7.4	Payload comparison (relative motion–7x1).	119
7.5	Rotation comparison (relative motion–7x1).	121
7.6	Gap size comparison (relative motion–7x1–2 Hz).	122
7.7	Gap size comparison (relative motion–7x1–5 Hz)	123
7.8	Local motion of point 1 in the lateral direction (7x1).	125
7.9	Discrepancies for the response observed in point 1 (7x1).	126
7.10	Discrepancies for the driving excitation (7x1).	127
7.11	Finite element model of the seven-tier three stacks case (7x3).	129
7.12	Rotation effect using RMS value comparison (relative motion–7x3).	130
7.13	Comparison of relative motion for case: 7x3–0 degree.	131
7.14	Comparison of relative motion for case: 7x3–2 degrees.	132
7.15	Comparison of relative motion for case: 7x3–10 degrees	133
7.16	Driving excitation discrepancy (7x3).	135
7.17	Lateral displacement discrepancy (7x3).	136
8.1	Effect of decreasing the gap size (heaving)	139
8.2	Effectiveness of dampers (heaving).	140
8.3	Damper inclusion and gap decrease effect (heaving).	141
8.4	Payload effect (heaving).	143
8.5	Stiffness change effect (heaving–time history).	145
8.6	Stiffness change effect (heaving–RMS).	146

8.7	Effect of changes in racking stiffness on twist lock's force.	147
8.8	Effect of changes in pitching period on twist lock's force (RMS value). . . .	149
8.9	Effect of gap size and damper inclusion (pitching).	150
8.10	Rolling amplitude effect on twist lock's force (Time history comparison). . .	152
8.11	Rolling amplitude effect on twist lock's force (Peak value comparison). . .	153
8.12	Effect of changes in rolling period on twist lock's force (RMS value).	154
8.13	Effect of changes in gap size (rolling).	156
8.14	Effectiveness of dampers (rolling).	157
8.15	Effectiveness of joining adjacent stacks (rolling).	158
9.1	Quantification and identification of the sources of the system non-linearities.	164
A.1	Comparison of full and scaled model results (linear case).	166
A.2	Comparison of full and scaled model results (nonlinear case).	167

List of Tables

1.1	General properties of 20 foot and 40 foot containers.	9
1.2	Global fleet information.	17
2.1	Technical specification of shaking table	32
2.2	Technical specification of the accelerometers	33
2.3	Technical specification of laser distance meters	33
2.4	Technical specification of high-speed cameras	33
2.5	Terminology used to refer to the displacement-time response data	42
2.6	Terminology of the ship motions	45
2.7	Terminology used to refer to study cases regarding the structure	46
3.1	Summary of similarity studies	52
3.2	Dimensionless numbers used for scaling the model	54
3.3	Scaling laws for the model (Froude scaling)	55
3.4	Geometric scaling of the models	57
3.5	Stiffness scaling	57
3.6	Numerical values obtained from finite element analysis	58
3.7	Eigenfrequencies obtained from finite element analysis	58
3.8	Comparison of the geometric similitude parameters	63
3.9	Comparison of the scaled model data	66
3.10	Eigenfrequencies of the scaled model	66
4.1	Experimental parameters (7x1)	70
4.2	Terminology of the displacement-time response data (7x1)	71
4.3	Experimental parameters (7x3)	72
4.4	Terminology of the displacement-time response data (7x3)	72
5.1	General information about the frame section	74
5.2	Eigenvalue analysis results	88
5.3	Values for the Linear damping ratio	90

5.4	Values for the full, half range and average approximations	91
5.5	A summary of contact algorithms [97]	93
6.1	Pilot study experimental conditions (2x1)	101
6.2	Experimental and numerical results for the cases studied (2x1)	103
8.1	Driving excitation conditions for the pitching cases	148
8.2	Driving excitation conditions for the rolling cases	151
8.3	Values of force obtained from rolling simulation	151
A.1	Geometric scaling of the full scale model	168

Chapter 1

Introduction

1.1 Background and Historical Highlights

Nowadays, the most significant part of goods transportation around the globe is done through maritime routes, elevating maritime industry to a prominent role in the world economy. Its efficiency is crucial to keep the flow of, not only, manufactured goods but raw materials necessary to perform such manufacturing. Consequently, transportation of such items in an appropriate way is essential, in a first moment, to keep the production flow bursting world economy.

In addition to that, it is important to mention that improving the means of storage and transportation increases ship and crew safety, decreases losses and increases industry reliability. However, the merchant marine industry waited too many years before finding an initial answer to the simple question: how to transport a wide range of products and materials in an efficient way across sea, avoiding deterioration and losses? Such a question permeated the mind of Naval Engineers for centuries, and although much effort was made toward a solution, little progress was observed.

Since the first explorers, notably Portugal and Spain, started the Age of Discovery, they faced this significant problem that could put in check the very success of their enterprise. At that time, inappropriate storage of goods and raw materials had in most cases deadly consequences, causing ships to sink or subjecting the crew to starvation and consequent death. Sailing the Seven Seas was not an easy task and even though, in the mainstream of this problem, early naval engineers and related researchers tried to find a solution for it, not until the 20th century was a proper and original idea introduced to address the problem.

The 20th century was spectacular for the development of the merchant marine: steel hull, internal combustion engines and propellers catapulted the industry to a superior level. The total amount of goods that could be transported increased drastically, whilst

1.1 Background and Historical Highlights

time required moving it across sea decreased wondrously. However it was not these inventions that solved the problem regarding the transportation, storage and preservation of goods and raw materials. The problem persisted.

Until half of the 20th century, break bulk was the most common method to transfer cargo from, or to, the ship and to other means of transportation, e.g., trucks or trains. This process was slow, because the cargo was loaded or unloaded individually, usually using barrels, boxes, crates, drums and bags, mainly by humans sometimes using very rudimentary tools (Figure 1.1). The personnel contingent, known as stevedores or dockers, involved in such activity was enormous and time consuming, sometimes as much time as it did sailing. Not to mention theft and cargo damage. A certain progress was made by the introduction of pallets and skids but, again, the problem persisted.

Thus, we cannot stop asking ourselves: what was the original idea that revolutionized the industry? Well, let's look at an overview the history about it. Everything started in 1937 in the United States when a young man named Malcolm MacLean, (Figure 1.2) a truck company owner, had an idea to make more agile and efficient the slow process of stowing cotton bundles in New York port: store it beforehand in big metal boxes, the early containers, and then stowed them in the ship. In his own words: "There has to be a better way than loading cargo aboard ship piece by piece. Why couldn't an entire truck be hoisted aboard ship, for instance, and then used for delivery purposes at the other end of the line?" The man was a visionary, foreseeing something that was to come: intermodalism. As mention by Cudahy [25], in 1937 the word itself has not even been created. Nowadays, intermodalism refers to the efficient interlinked system of ships, trucks and trains that transport containers around the globe. No further words are necessary about MacLean's idea.



Figure 1.1: Example of old break bulk method: stevedores on a New York dock loading barrels of corn syrup onto a barge on the Hudson River. Photograph by Lewis Hine, 1912.



Figure 1.2: Malcom MacLean: consider “father” of container. Photo: Maersk Line, Ltd.

1.1 Background and Historical Highlights

The idea that started being shaped in 1937 finally received some body in April of 1956. The idea was delayed for that long because of the Second World War and some experimentation. However, without further ado, MacLean created the first containership to sail: *Ideal X*. Originally this vessel was a common T-2 tanker that was adapted to receive the bodies of 58 trailer trucks, detached from their running gear, becoming containers. The ship cast off from Port Newark, New Jersey, and six days later docked in Houston, Texas. When the 58 trailers were hoisted off *Ideal X*, no stevedores were employed in the process: they were directly attached to running gear and headed to their destination. The local impact was tremendous. However, something even bigger was to come: MacLean's company sent a ship with containers to Europe.

The year was 1966, and the ship was called *SS Fairland*. The industry would never be the same. The impact of such an invention could be observed soon after. As mentioned before, until that time the number of stevedores necessary to move the cargo on and off ship was tremendous. The *SS Fairland* docked in Amsterdam, the biggest port on the planet, in the same year carrying fifty containers. At that time, Amsterdam port had twenty five companies using nine thousand employees. One year later, MacLean's invention reduced that number to five companies with an astoundingly small number of 208 employees managing the new system.

In a really short period of time the impact of the container use for marine transportation could be seen: improvement in port handling, lowering costs, decreasing losses and increasing profits. The advantages of MacLean's idea made containers popular and they quickly spread around the planet. Overseas trade was never the same, assuming extraordinary proportions. Nowadays, this process of changing from the old break bulk method to MacLean's invention was baptized *Containerization*. Hitherto, with exception of some goods that are transported by specialized ships like petroleum products, cement, chemicals, coal, dry edibles, grain, minerals – these categories being denominated bulk cargo – cars, and some high valued commodities, just about everything else is transported by the so called container ships. According to specialists, like Levinson [47], approximately 90% of non-bulk cargo worldwide moves by containers stacked on transport ships. That is an impressive number.

In the main stream of this process, containerization changed logistics modus operandi worldwide, increasing efficiency and companies profits. To have an idea about the size of the business, the Marine Conservation Society estimated that more than 100 million containers are transported worldwide in a year. It is not an exaggeration to claim that containerization has played a crucial role in the trade globalization. Economical impact of containerization will be debated in section 1.3. For those who still are unbelievers, they cannot deny this process as one of the most flourishing developments in the freight



Figure 1.3: A picture taken from the deckhouse in the stern direction (NYK, THEMIS) during container loading procedure in Tokyo, Japan. The hatch and lashing bars can be clearly seen in the spots where additional containers still can be placed.

transport sector ever. According to Levinson [47] all these factors summed, are enough to catapult the containerization to one of the most important innovations of 20th century logistics. To finish this section, let's summarize the benefits of the containerization:

- Facilitates transportation of goods in lots which are too small for traditional bulk transport,
- At the same time, it avoids poor handling that results from bulk transport system,
- As consequence of the previous two advantages, container transportation is the best option for high-value and delicate commodities,
- Almost abolish human and natural factors, e.g., theft and deterioration, increasing safety and reliability,
- Substantial amount of time, including waiting and transit time, and labor cost is saved during the load and unload process, increasing companies profits,
- Perishable goods have a proper mode of storage and can be transported everywhere not depending on the transport route,

- Reduced inventory costs benefiting companies.

1.2 Objects of Study

1.2.1 Container

Container geometric features are quite simple. However in its simplicity lies its robustness. If one has to explain it to a infant a very simple and elegant way would be: just a big metal box with a side door. The Merriam-Webster dictionary defines as follows:

” A portable compartment in which freight is placed (as on a train or ship) for convenience of movement.”

Obviously, containers have to pass through a standardization process like almost everything in modern industry, obeying guidelines from International Standards and Organization (ISO). Kirkayak (2009) [44] provides the information that among all types of containers, the highest incidence of use lies on 20 and 40 foot length ones. Resuming from the previous information, containers must satisfy some basic specifications, e.g., structural stiffness. More details about container stiffness will be presented in the next section of this work.

However is interesting to present some basic information about the most common containers, 20 and 40 foot (these categories of containers can be seen in the Figure 1.4) as mentioned before, to increase the understanding about one of the links in our study. The following table 1.1 shows the weights and dimensions of these two types of containers. Extra information about container construction is depicted in Figure 1.5. Moreover is important to present the nomenclature related to containers. This terminology is depicted in Figures 1.6 and 1.7.

1.2.2 Twist lock

Twist locks are mechanical devices designed to connect container to ship’s deck and successive containers stacked on it, becoming a primordial component in the marine cargo transportation securing system. Moreover, this component is widely employed to fix containers during terrestrial transportation, e.g., semi-trailer truck and railway container trains, as well as for lifting using gantry cranes. It is connected to a container through a particular element in its structure, named corner casting, which contrarily to the twist locks have no moving parts. The linking process is quite simple and similar to the mechanism behind a Kensington lock: twist lock is inserted through a hole in the base of the corner casting, and then its top portion is rotated 90° , which it will avoid removal. Nowadays, both parts follow guidelines provided by the International Organization for



Figure 1.4: Picture of 20 and 40 foot containers.

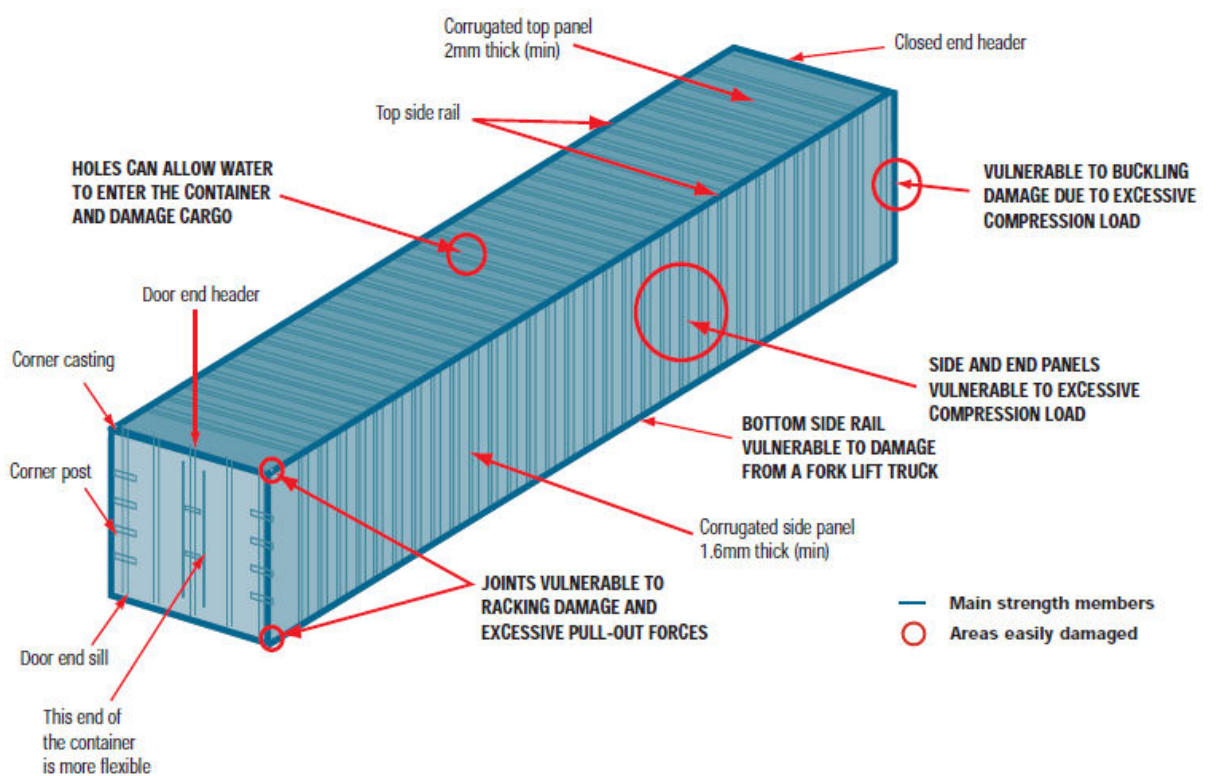


Figure 1.5: General information about container construction [53].

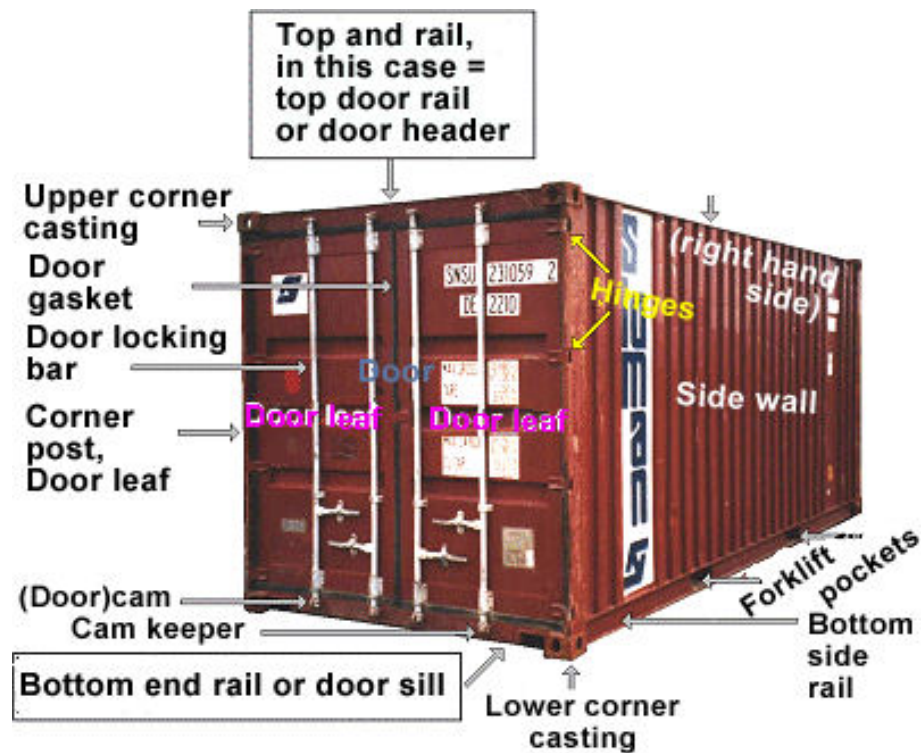


Figure 1.6: Container nomenclature for the back and side portions (Source: Container Handbook, GDV).

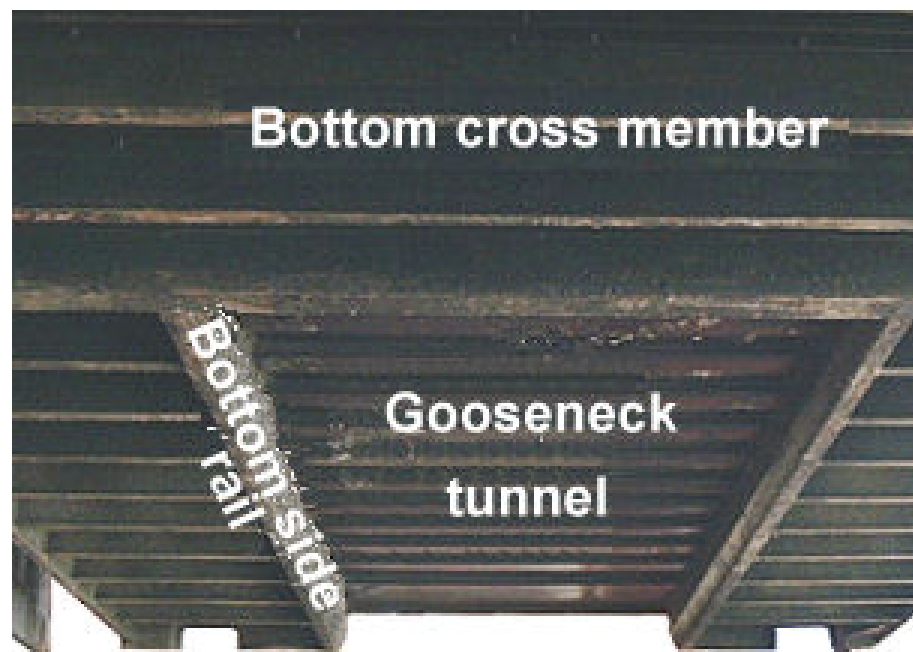
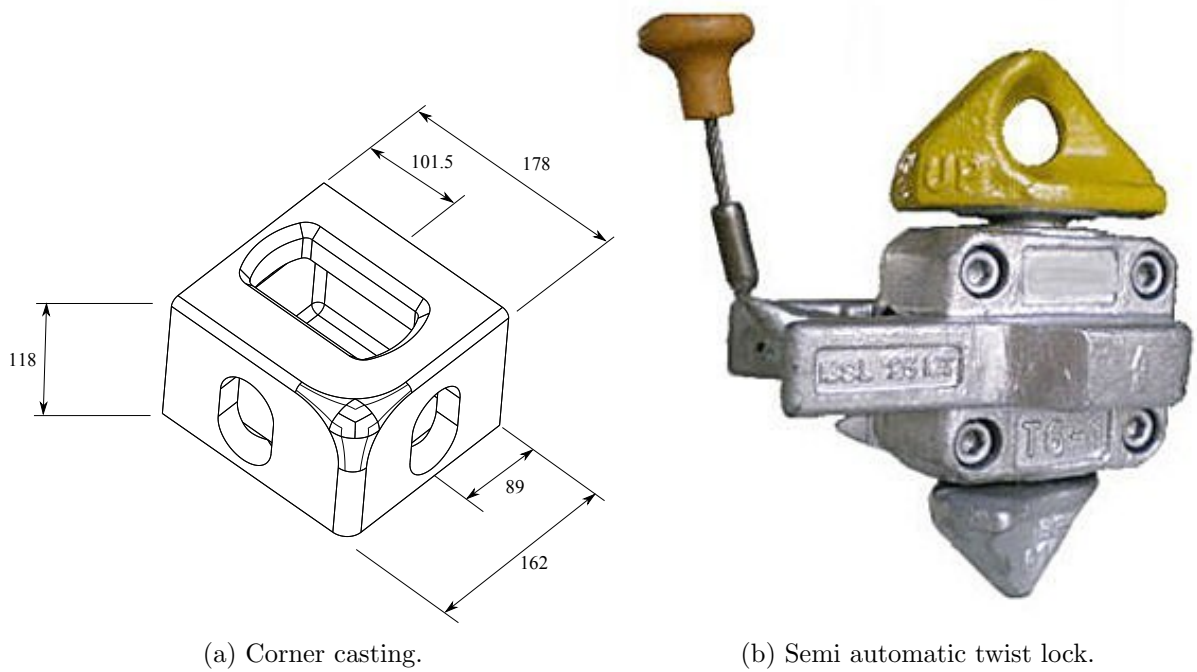


Figure 1.7: Container nomenclature for the bottom portion (Source: Container Handbook, GDV).

Table 1.1: General properties of 20 foot and 40 foot containers based on information by [36]. Weights and dimensions quoted below are averages. It may slightly vary in actual size and weight according to the manufacturer of container [44].

		Container Size	
		20 foot	40 foot
External dimensions	length[m]	6.198	12.192
	width[m]	2.438	2.438
	height[m]	2.591	2.591
Internal dimensions	length[m]	5.898	12.032
	width[m]	2.352	2.352
	height[m]	2.385	2.385
Door aperture	width[m]	2.343	2.343
	height[m]	2.28	2.28
Volume[m ³]		33.1	67.5
Maximum gross mass[kg]		24000	30480
Empty weight[kg]		2330	4000
Net load[kg]		21770	26480

Standardization: ISO 1161 (1984) and ISO 3874 (1997), for corner castings and twist locks, respectively. Female and male components of container securing system analyzed in this study are depicted in Figures 1.8a and 1.8b. Moreover, relevant technical information about twistlock is presented in Figure 1.9.



(a) Corner casting.

(b) Semi automatic twist lock.

Figure 1.8: Two important components of the securing system.

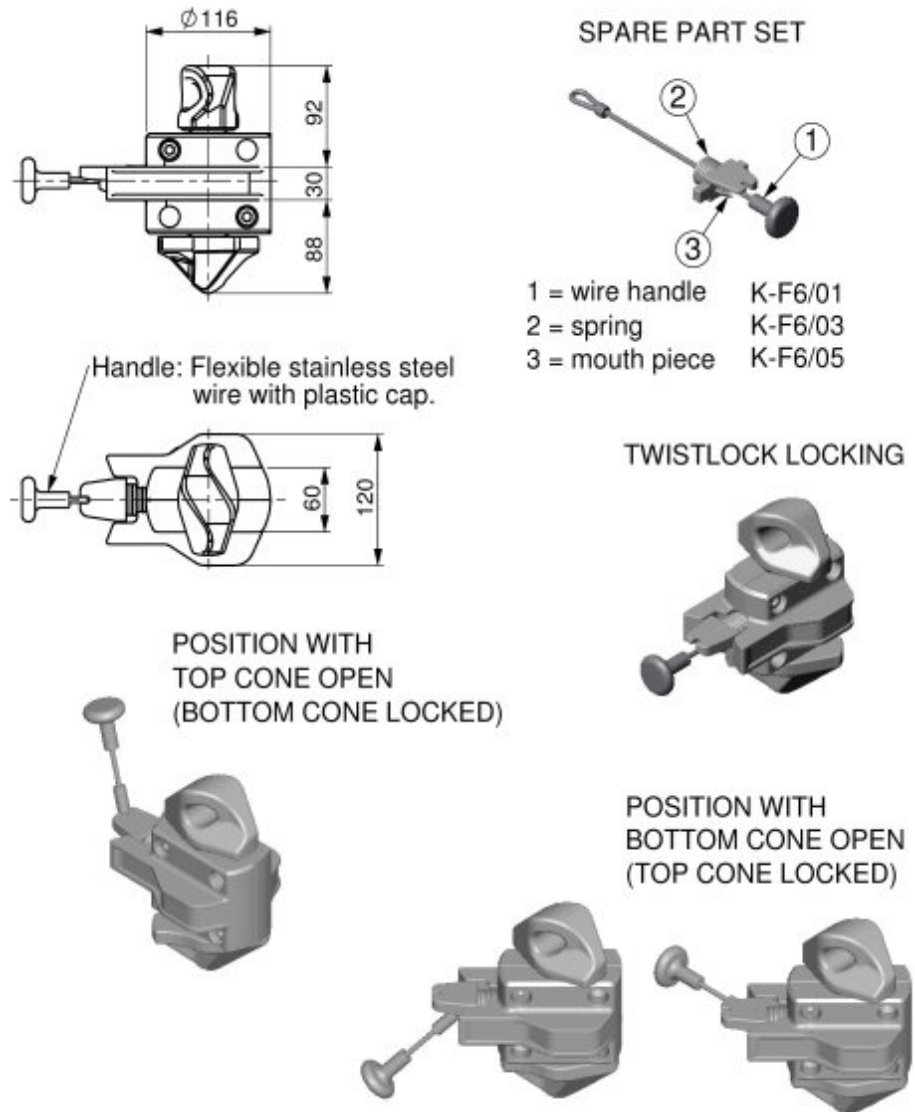


Figure 1.9: Example of semi-automatic twist lock (Source: Container Technics N.V.).

1.3 Posing the Problem: Container Loss

According to various sources, e.g., Marin Conservation Society report, a number between two thousand five hundred and ten thousand containers are lost at sea each year (Figure 1.10 and Figure 1.11)[58]. France [27] reported the loss of about four hundred containers aboard of MV¹ APL China in 1998, which is credited as the biggest cargo loss since the dawn of containerization. More recently, container ships: MV OOCL America (2000), MV Sea-Land Hawaii (2000), MV Sea-Land Pacific(2000), MV Xin Qing Dao (2004), MV Saga Spray (2006) MV Jeppesen Maersk (2006), MV Ital Florida (2007), and MV CMA CGM Dahlia (2008) just to mention a few, also lost containers at sea. Considering that those containers may carry goods as such as electronic equipment, the total loss of a single container can easily reach an amount around a million dollars. This amount can increase significantly if the cargo is a customized good or precision equipment. Multiply this value to the number of losses in a year and one can have an idea about the size of this problem. Another point to be added is that the container ship sector is growing steadily each year, which increases the possibility of material and economical losses. See section 1.4, Figures 1.16 for more details. In an obvious manner, this problem did not pass unnoticed to the competent authorities that started to research the factors behind it.

The first container ships were designed with their deck-house at the forward end of the ship, where stacks two or three high were stored. This design concept had the main goals of protecting the containers from boarding seas and to assist navigational control. Engineers responsible for designing modern container ships kept the same goals from an early age, however some factors out of the design table started to impact Naval engineering: increase in competition, ship's cost, size and velocity. With increase in the container ships size elastic behavior of the hull started to become significant for the cargo stowed on the deck-house, but surprisingly this behavior is not taken into account when calculating lashing systems. And still, when containers are lost aboard, it is believed that critical sea conditions, like abnormal swell, typhoons and storms, are the main factors inducing container losses during transportation (Figure 1.12).

Furthermore, some extra factors may play a significant role in these losses. The first one is the constant increase of containers stacked on the deck in recent years. At the beginning of container transportation era, most of the containers were stowed below deck, and the containers above it were rarely stacked over four tiers. Nowadays, an inversion occurred: up to 60% of the containers are transported on deck, and it is not uncommon observing stacks up to ten tiers. Albeit, they are considerably lighter than the ones stowed below deck, the total number of containers exposed to the intemperate weather without

¹MV or M/V is a common nomenclature meaning merchant vessel or motor vessel

additional protection is alarming. Furthermore, bridge visibility is lessened, increasing the likelihood of collisions.

Additionally, high deck loadings may have other serious consequences: compromising of ship's stability, caused by the excessive number of containers stowed, plus the uncertainty regarding their real weight. Add to the equation that such big number of containers create a massive wall comprising a vast surface that is exposed to wind, so here we identify the second factor. The third factor comes indirectly from the sea state: ship motion, e.g. parametric rolling, whipping, pitching, etc. Such motions are culprits in the events that lead to damage and container losses, being pointed out as the main factors causing elevated values of radial force in the containers in the upper tiers on deck. The last factor in our equation is the sea water that sometimes collides against the ship and its cargo exerting non negligible loads on it.

The last point to be analyzed is the securing system of the containers: lashings equipment, and twist locks. These equipments will be presented in details in the next section. Although container structure and geometry is basically the same since its creation in the middle of the 20th century, there still a lot room for some improvements in the securing systems that fix container stacks to deck. In fact such equipment is out of date, i.e., their design is unchanged for the last 35 years, and despite the efforts of competent authorities, new international standards will have to wait few years until its implementation. To complicate the situation even more, there is a handful of research regarding container dynamics and lashing equipment. Actually, most of the studies and standards used by the industry correspond to static situation, which is distant from the real situation, as can be seen in the previous paragraphs.

In this panorama, a more realistic approach should be addressed, accounting for dynamical effects. Such approach is a bold step towards a more rational method to deal with such problem, and is one of the goals in this study. Our purposes will be presented in a logical way in the next section. Before that, it is interesting to present some of the consequences of containers losses at sea.

Although economical losses are the immediate consequences of such accidents, there is another vicissitude involved: containers lost at sea may not sink, becoming a hazard for navigation, especially small boats. This can be clearly seen in the Figure 1.13. Moreover, locating and rescuing such containers is not an option because of the elevate costs involved in such operation. Add the fact that containers are lifted by specially designed gantry cranes located at ports. For example, it cost several hundred thousand euros, to perform such rescue operation in three containers containing drums of wood preservative that fell overboard off the Dutch coast in December 2003.

1.3 Posing the Problem: Container Loss

What brings another aspect of container losses: environmental impact. This problem cannot be neglect because often containers are loaded with chemicals and hazardous materials. As we can infer from the information provided, preventing container losses is a monumental task that will bring benefits not only to Maritime industry but just everyone else.



Figure 1.10: Total collapse of containers stacks with subsequent loss of top tiers.



Figure 1.11: Another example of container stack collapse.



Figure 1.12: An example of adverse sea conditions. Picture of MSC Napoli.



Figure 1.13: Example of containers that were lost due to extreme sea conditions but were drifted ashore.

1.4 Relevance: Economical Importance of Container ships

According to a report entitled "Valuation of the Liner Shipping Industry: Economic Contribution and Liner Industry Operations" publish by the Global Insight, Inc. in December of 2009, until July of 2009, the global fleet showed the following distribution:

Table 1.2: Global fleet information (Source: Lloyd's Register – Fairplay Research)

Vessel Type	Number of Vessels	Dead-Weight Tons
Container	4684	165774103
Vehicle	443	11375691
Ro-Ro	1753	7423240
Total	7210	184573034

Analyzing this data one can infer that container ships represent the biggest slice in the liner industry with about 65% of the world fleet. Hitherto, container ships represent highest growth rate in the maritime industry (See Figure 1.14 for reference). Just to have an idea about the size of the business, the liner industry transported about 60% of the total value of global seaborne trade of US\$7.7 trillion in 2007. Considering that 65% of this industry consists of container ships is easy to recognize containers economical importance: the total number is around US\$4.3 trillion, placing container ships as the largest sector of Maritime industry when measuring the value of world trade transported. Apart from that, liner industry global operations and ship building in 2007 is estimated to be 436.3 billion, and generated 13.5 million direct and related jobs.

And the business is still growing: global containerized trade has grown at an annual rate of 12 percent from 2001 to 2005. The predictions for the period 2005 to 2011 still positive: 6.5 growth rate per year. According to their data, in 2011, global containerized trade is expected to reach 134 million TEU ², 2.3 times bigger than the one recorded in 2001. See Figure 1.15 for more details. According to specialist this is just the beginning: new standards and ships will place the industry at a level never thought before (Figure 1.16). The measure in this Figure is DWT³ in thousands.

²Is an inexact unit of cargo capacity often used to describe the capacity of container ships and container terminals. This unit is based on the volume of a 20-foot-long (6.1 m) intermodal container [65].

³Dead weight ton (DWT) is a measure of how much weight a ship is carrying or can safely carry including cargo, fuel and stores [80]

1.4 Relevance: Economical Importance of Container ships

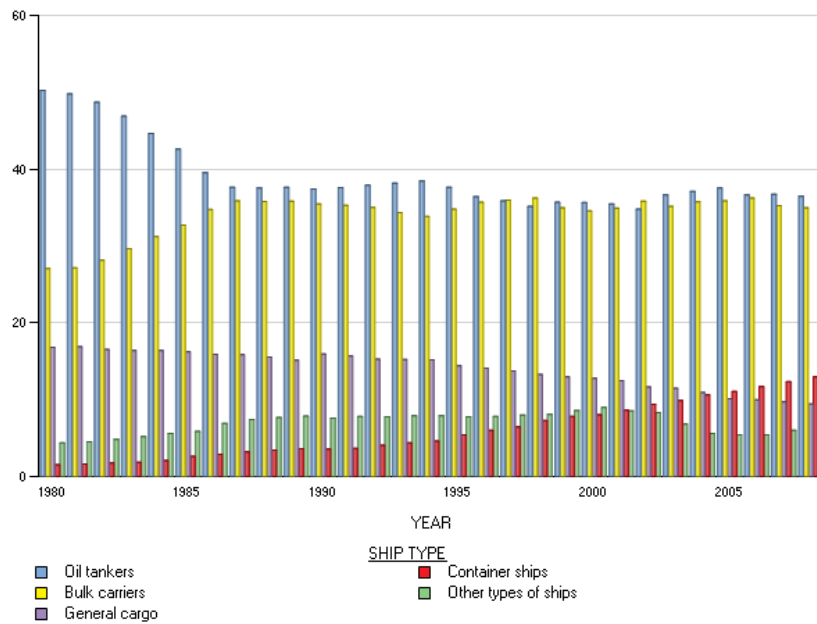


Figure 1.14: Percentage of total fleet. Containerships is the only sector of the maritime transportation industry that presents a significant annual growth. Source: United Nations Conference on Trade and Development–UNCTAD–Handbook of Statistics 2009.

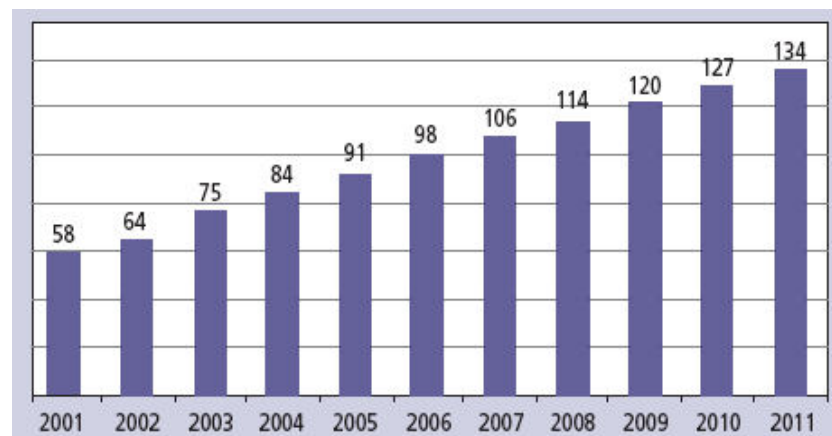


Figure 1.15: Global Containerized Trade, 2001 to 2011 (Forecast), in Million TEU (Source: Global Insight, Inc. World Trade Service). Data representing maritime trade in fully loaded containers.

1.4 Relevance: Economical Importance of Container ships

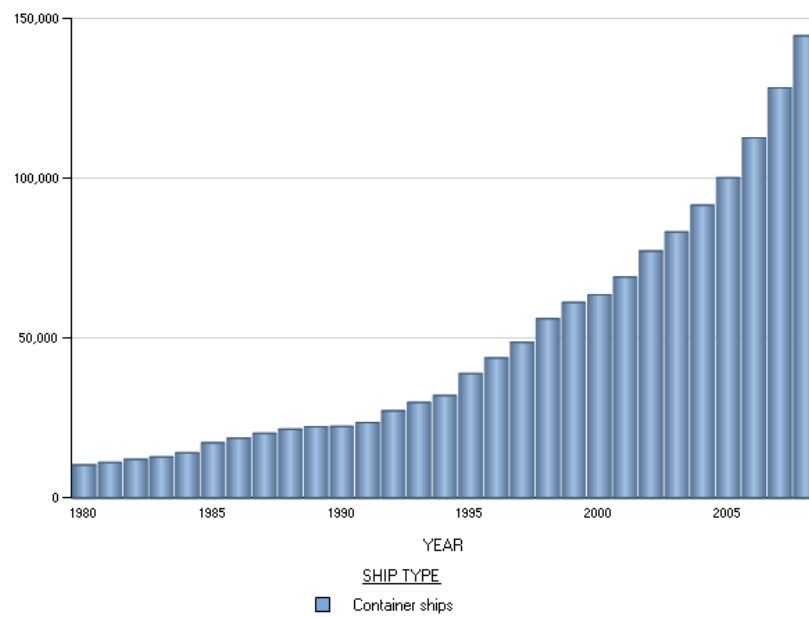


Figure 1.16: Annual growth of the total capacity of container ships. Source: United Nations Conference on Trade and Development–UNCTAD–Handbook of Statistics 2009. UNITS:DWT.

1.5 Container Lashing Components

We do not want to discuss the merits and demerits of the lashing components that have been used for the past years. The goal of this section is just to describe and present them without any assertion, i.e., this section is strictly descriptive. Obviously, there are an enormous variety of components in the market, however the figures below represent the majority of them [53].

DESCRIPTION	PURPOSE	IMAGE	NOTES
Flush Socket	Locating of base twistlocks or stacking cones in the cargo hold.		Normally fitted over a small recess to ensure watertightness. Clean and remove debris before use.
Raised Socket	Locating of base twistlocks or stacking cones on deck.		Clean and remove debris before use.
Lashing Plate or 'Pad-eye'	Tie down point for turnbuckle on deck or hatchcover.		Designed only for in-plane loading. An out-of-plane load could bend the plate and may crack the connecting weld.
D Ring	Alternative tie down point for a turnbuckle.		Corrosion of the pin ends can weaken a D Ring. Suitable for in-plane and out-of-plane loading.
Dovetail Foundation	Base for sliding twistlock.		Clean before use. Check for damage or wear.
Fixed Stacking Cone	To prevent horizontal movement of 20-foot containers in 40-foot cell guides.		Often found at the base of a cell guide.
Mid-bay Guide	To prevent transverse movement of 20-foot containers in 40-foot guides. Fitted at tank top level.		Does not interfere with general stowage of 40-foot containers

Figure 1.17: Fixed fittings (components of the lashing system that are attached to ship- [53]).

1.5 Container Lashing Components

DESCRIPTION	PURPOSE	IMAGE	NOTES
Lashing Rod	To provide support for container stacks on deck. Used in conjunction with a turnbuckle.		Resists tensile loads. Very long lashing bars can be difficult to handle and difficult to locate in a container corner casting. They can have eyes at each end.
Extension Piece	To extend a lashing rod when securing 'high cube' containers.		Fit at the base of a lashing rod and connect to the turnbuckle.
Turnbuckle (Bottle screw)	To connect a lashing rod to a lashing plate or D ring. Tightening puts tension into a lashing rod.		Resists tensile loads and is used to keep the lashing tight. Regularly grease its threads. Ensure the locking nut or tab is locked.
Penguin Hook	Used as a supporting device in conjunction with a special lashing rod with an eye-end.		Likely to be put in place when container on shore because of difficulty in fitting when on board. Risk of injury if it falls out when container is lifted onboard.
Stacking Cone	Placed between containers in a stack and slots into corner castings.		Resists horizontal forces. Many types exist. May be locked into bottom corner castings prior to lifting a container on board.
Twistlock	Placed between containers in a stack and slots into corner castings.		As above but also resists separation forces. Each fitting requires locking after fitting. Left and right-hand types exist, causing uncertainty whether a fitting is locked or open.
Semi-automatic Twistlock	Placed between containers in a stack and slots into corner castings.		As above. Can be fitted on shore and automatically locks into the lower container when placed on top. It is easier to determine whether it is locked or not when compared to manual twistlocks. Unlocked manually.
Fully automatic Twistlock	Placed between containers in a stack and slots into corner castings.		A new and innovative design. Automatic unlocking during lifting. Usually opened by a vertical lift, with a twist/tilt.
Sliding Twistlock	To connect bottom containers to the ship.		Fits into a dovetail foundation. Used on hatch covers and in holds when a raised socket can cause an obstruction.

Figure 1.18: Loose fittings in common use [53].

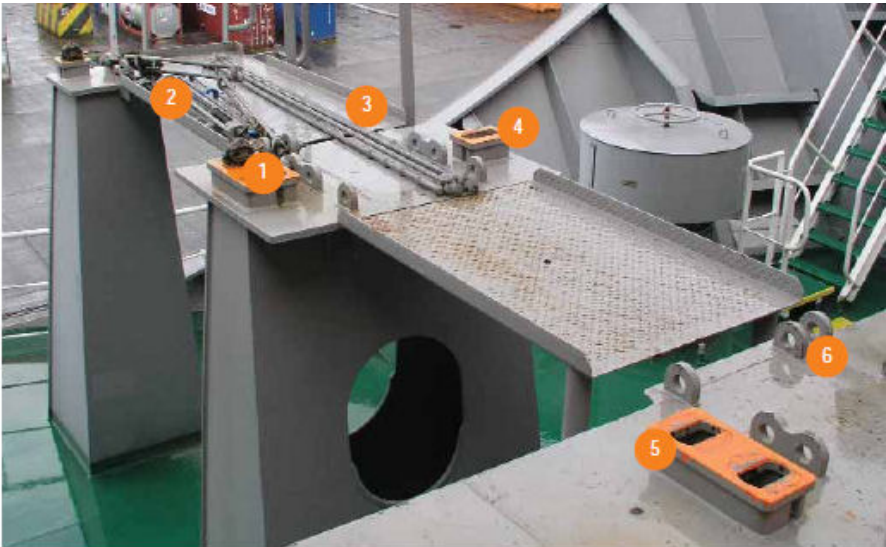
1.5 Container Lashing Components

DESCRIPTION	PURPOSE	IMAGE	NOTES
Bridge Fitting	To link top containers of two adjacent stacks together. Can be used on deck or in a hold.		Resists tensile and compressive forces. Potential fall hazard for stevedores during placement.
Mid-Lock	Placed between containers in a stack, and slots into corner castings. Used on deck between 20-foot containers in 40-foot bays at mid-bay position.		Resists lateral and separation forces. Fitted to underside of container on shore and automatically locks into lower container when placed on board.
Buttress	External support for container stacks in a hold.		Can resist compressive and tensile forces. Must be used in conjunction with higher strength double stacking cones or link plates and aligned with side support structure.
Double Stacking Cone	To link adjacent stacks, particularly those in line with buttresses.		Resists horizontal forces. More commonly used on con-bulkers below deck.
Load Equalising Device	To balance the load between two paired lashings.		Enables two connections to two containers with both lashing rods being fully effective. Can only be used with designated lashing rods.

Figure 1.19: Loose fittings in less common use [53].

1.5 Container Lashing Components

- 1 Twistlock
- 2 Turnbuckle
- 3 Lashing Rod
- 4 Single Raised Socket
- 5 Double Raised Socket
- 6 Lashing Plate



- 1 D Rings
- 2 Dovetail Foundation
- 3 Turnbuckle



Figure 1.20: Lashing components being placed on a container ship [53].

1.6 Defining Goals

There are many unanswered but fundamental questions regarding the mechanical behavior of container stacks. Answering all of them, or finding an alternative approach to such problems would involve a colossal work that would require a great deal of logistics, human effort, time, and consequently money. This work has the ambition of helping answering a more modest set of questions regarding this dynamical event, contributing positively to existing regulations. Our research questions can be formulated as follows:

1. Is dynamic effect an important phenomena in container stack dynamics, or it is negligible?
2. Does impact between adjacent stacks have importance in container stack dynamics, or it is negligible?

These goals were formulated based on reports of specialists like Murdoch (2006) [53] who highlights the fact that neither the dynamic response of the separate tower stacks nor the effects of the interaction between adjacent stacks is well considered in the design of the cargo securing system, and as mentioned before, most standards used by the maritime transportation industry correspond to static conditions. In order to find meaningful insight into these questions we proposed a systematic study of the effect of some parameters involved in container stack dynamics, in a variety of situations, initial and boundary conditions, that emulate as realistically as possible those encountered by containers in maritime transportation. Our questions will be answered through a numerical model that was validated by a series of experiments that will be explained in the next sections.

1.7 Literature Review

To the extent of our knowledge, scientific studies regarding containers as structures are quite rare. Most of the works published, like [78], [87], and [54] are decision-making rules to optimize container terminal operations, e.g., space, transfer and stowage. Additionally, an overview of the literature regarding these kind of operations was published by Stahlbock [75] in 2008. So far as the literature review goes, the first study about container stack dynamics, considering container elastic deformation, was published in 2009 by Suzuki and colleagues [77]. In his work a complete description of an one-fourth scaled model construction and validation is thoroughly presented. Moreover, the model constructed was used to determine experimentally the mechanical behavior of a two tiers stack, through a shaking table test. The next study, published by Kirkayak [45] in the same year, is a natural continuation of the work performed by Suzuki and colleagues. This study consists of the construction of a valid numerical model validated against the acquired experimental data. This paper provides in-depth numerical analysis of the problem presenting some predictions and advice.

In the same year, Kirkayak [44] wrote the most complete synthesis to date of fundamental behavior of container stack dynamics. In this work, which includes experimental and numerical analysis based on a scaled model, effects of vibrational and physical variables on a single stack are completely understood for a high stack of seven containers. However, the main weakness of the study is the failure to address how friction and contact affect structural response. Moreover, regarding the numerical model, damping was included in the system as discrete elements, i.e., dashpots connecting corner castings. This discrete approach induced beating phenomenon in some of the numerical cases and is strongly dependent on frequency. Additionally, in the numerical model the four nodes corresponding to the bottom-corner castings are kinematically coupled to a node in the geometrical center. This node has the function of matching the mass and moments of inertia of the real model, through simple addition. However, although it is not the study case, this rigid body modeling would underestimate elastic deformation leading to wrong predictions in buckling analysis.

The works of Aguiar *et al.* [3, 4], are the first to approach the problems faced by Kirkayak and colleagues, expanding their work to a more complex model. Based on experimental data, a numerical model of a seven-tier scaled container was built and validated. The study presented some new approaches: the use of Rayleigh damping and the removal of the over-constraints. The Rayleigh damping approach avoided the beating problem faced by Kirkayak and colleagues. On the other hand, the removal of the bottom-corner casting coupling constraints allowed each individual container to deform more naturally.

However, the model excluded friction and contact, two physical phenomena of crucial importance when the container stack is inclined.

The next work published by Aguiar [5] presented an extension of the previous study: a numerical model of three stacks of seven tiers calibrated against experimental data. In this work one important physical phenomenon was included in the numerical model: contact between adjacent containers. However, as in previous works of the authors, the model failed to include contact and friction among corner castings of the same stack. Despite these limitations, the model presented a high level of agreement with numerical data, which allowed some numerical predictions in situations faced in maritime transportation, e.g., rolling.

1.8 Outline of Structure

To close the introduction we would like to present a summary about our study aiming simplicity and clearness.

Chapter 1: Defines the main question of the study with its goals, significance and review of previous studies.

Chapter 2: Describes research methodology, i.e., a research design, synthesis, characterization and evaluation of the problem in order to answer the main question and its nuances. Presents our approach divided in its main stages: experimental and numerical for full containers and scale model. Additionally, present information about the experimental variables, apparatus, data filtering and data analysis.

Chapter 3: Begins by laying out the theoretical dimensions of the scale model used for experiments, after a short overview and literature review about scaling. Additionally presents details about the scaled model design, construction and validation.

Chapter 4: Describes the main experiments (7x1 and 7x3) with details of the experimental facility, apparatus and experimental conditions for each trial. Furthermore depicts labeling of areas of interest and positioning of the sensors.

Chapter 5: Presents an extended overview about the numerical model used for simulation and how each relevant parameter was modeled. Among these parameters one can find structural stiffness, twist lock's stiffness and damping.

Chapter 6: Presents a pilot study involving a two-tier single stack of container models. The study itself was performed to assess the adequacy of the research design employed in the 7x1 and 7x3 cases. Additionally, presents some interesting trends and limitations that were used to identify potential problem for the main experimental stage (7x1 and 7x3).

Chapter 7: Debates about results and its interpretation for the 7x1 and 7x3 cases and consequent validation of the numerical model. Additionally, present a rationale about discrepancies observed in the experiments, helping to qualify the numerical model.

Chapter 8: This section presents only numerical simulation that was employed to identify important points in the container stack dynamics. Here, force on the bottom twist locks (nonlinear springs) was used to provide a means of comparison. Furthermore, this section presents some advice for the maritime industry based on the numerical predictions.

Chapter 9: Presents a summary of the findings, suggestions and limitations of the study with further prospect for a future studies.

Chapter 2

Methodology

2.1 Research Design Overview

Our specific plan for studying the research problem, providing the glue that holds the major parts of the research project together was divided roughly in many stages that included: container scaling, data acquisition for full scale and scaled container, and numerical simulation constructed and validated based on the experimental data. Our strategy of attack on the central research problem is facilitated by this division, that is a common *modus operandi* in many fields. All stages were divided into sub-stages that will be explained thoroughly in the next chapters. The objects of this study are a 20 foot dry freight container and twist locks, both in full and small scale in a variety of dispositions: single, two, and seven tiers (one and three stacks). Moreover, container size was chosen based on its incidence in the industry as explained in section 1.2.1. Twist lock size is invariant regarding container size, however the mechanism has two versions: semi and full automatic. The study focused in semi-automatic version of this mechanism. Please refer to Figure 2.2 for understanding how the experiments, and posterior numerical simulation, were conducted and segregated.

Regarding the numerical analysis, it is necessary to emphasize that the model built had two ways to be validated: conceptual and result validation. Conceptual validation was performed through intense theoretical discussion about the various methods used to model the physical phenomena included in our model. Thus, as will be seen in the results section of this work, the phenomenon modeled were sufficient to emulate container stack dynamics within a reasonable margin of error. On the other hand, data acquired during experiments are the reference used to calibrate the numerical model, and consequent numerical model validation. The overall approach can be seen in Figure 2.1.

The research itself, with rare exceptions, was focused in the study of a scaled model based on a 20 ft dry freight container. The reasons behind this choice were presented

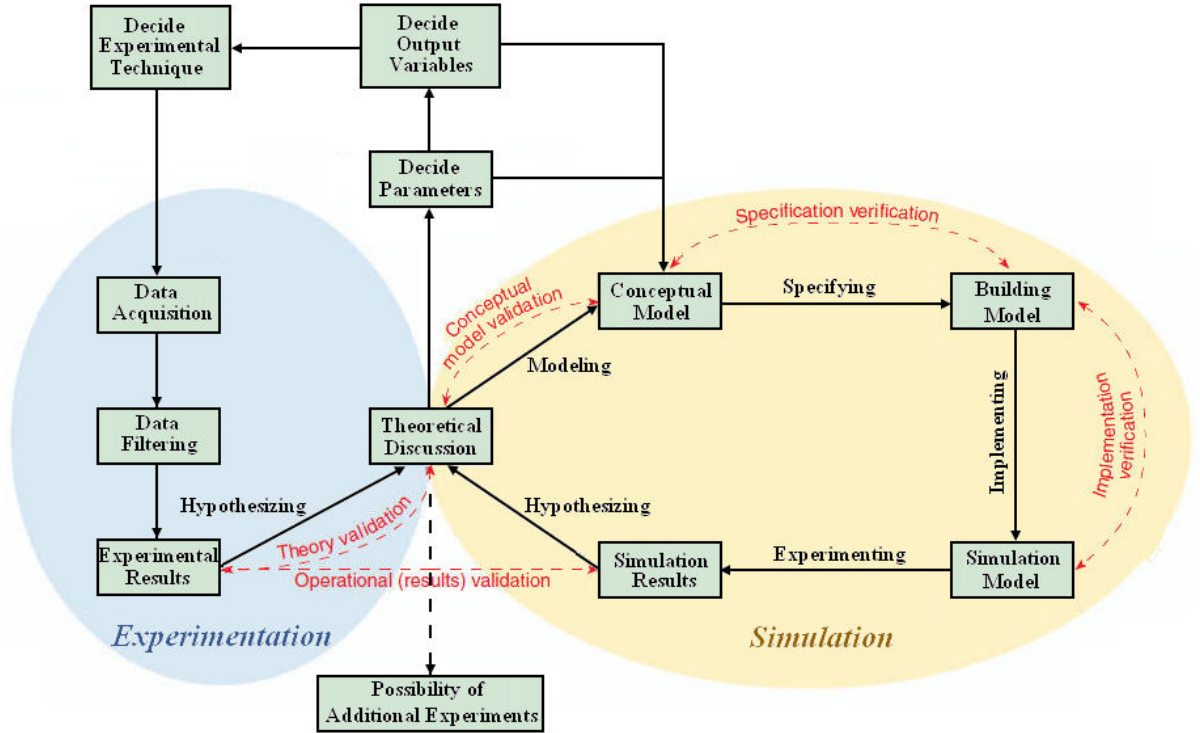


Figure 2.1: Schematic representation of the approach used for this study. The conceptual diagram was based on a diagram created by Dr. R. G. Sargent *apud* [57].

and discussed in section 1.4. In the exception cases are included two studies: slamming of a single container, and random noise of a two tiers stack. Regarding the study for a scaled model, some constraints influenced the choice of this approach. Firstly, the non-existence of any experimental facility able to perform experiments in dispositions of two tiers for full scale containers, which would defeat the final goal of studying high stacks. Secondly, testing scaled models is significantly cheaper than testing real containers, which requires specialized transportation and lifting. In 1999, Vassalos estimated the total cost of a testing model as a small fraction (around 1%) of the overall capital involved in full scale testing. Thirdly, the process of testing such a big and heavy structure in various driving excitations can be risky and accident-prone, which could pose an unnecessary risk to researchers involved. Moreover, in extreme cases, e.g., fall or structural damage, small scale models can be easily replaced and repositioned. Fourthly, scaled models are prominent tools to calibrate numerical models, offering a better option to control study variables, and the possibility of isolating the ones of particular interest. And last, but not least, the development of a valid scaled model opens the possibility of simulating container stacks in a wide variety of situations faced during maritime transportation, which can provide a realistic approach for the problem of container loss.

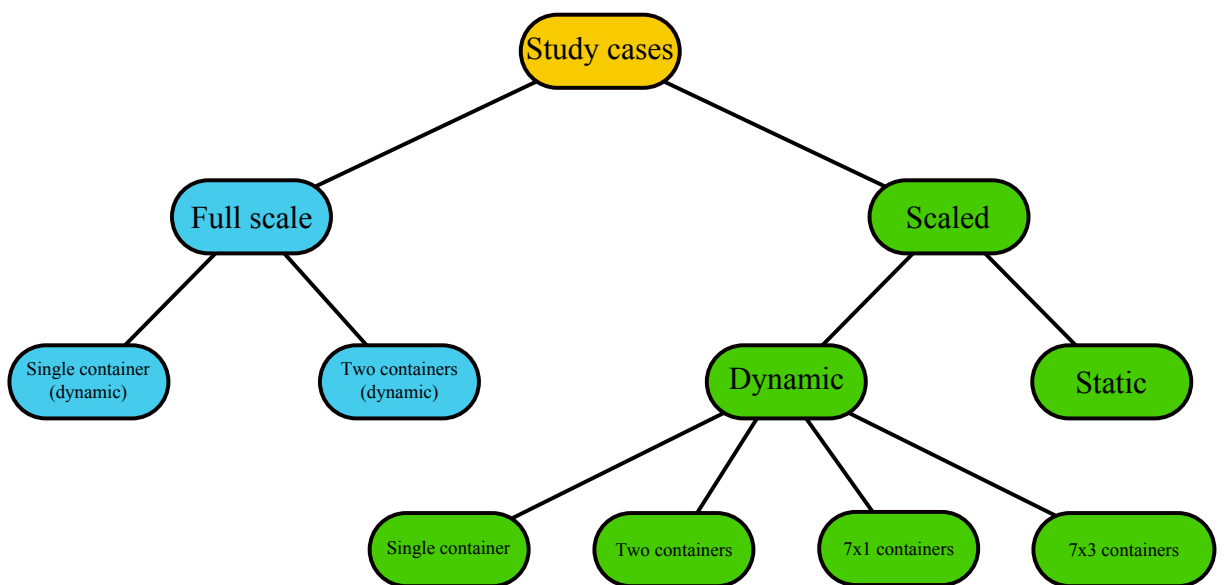


Figure 2.2: Schematic representation of the divisions of the experimental stage of this study, and posterior numerical simulation.

2.2 Experimental Facility and Apparatus

2.2.1 Shaking Table Testing

All vibrational experiments performed during this study, with the exception of hammering test, employed a shaking table. The use of a shaking table to study the dynamic response of structures to given driving excitation is not new: the technique has been employed successfully since the 80's [96], becoming one of the most respectable procedures to study structures subject to vibration. Although most studies using this technique are oriented to civil engineering applications [34] with emphasis in seismology [17, 20, 28, 46, 48, 50, 51, 55, 67, 76, 86, 95], our choice is based on its advantage of allowing a great deal of control over vibrational variables like amplitude and frequency, as well possibility of vibration input following special functions, e.g., transient, non-transient, random, recorded, etc. Furthermore, shaking tables allow driving excitation in six degrees of freedom (multi-axis), and easier experimental measurements [59].

All vibrational tests mentioned in this dissertation were performed using a shaking table located in the experimental facility of Monohakobi Technology Institute (MTI) in Yokohama, Japan. The main dimensions of the shaking table are 2.6 x 6.2 m, with a maximum loading weight of 20 tons and maximum rotation angle of ± 20 degrees. The device can vibrate with maximum acceleration of 2 and 3 g in the horizontal and vertical directions, respectively. Additionally, it presents a maximum velocity of 0.6 meter per second for both directions and a maximum displacement of 0.2 and ± 0.25 m for horizontal and vertical directions, respectively. The frequency of the input waveform can range from 0.1 to 80 Hz. This shaking table is denominated multi cargo simulator (MCS). A graphic representation of the experimental facility is shown in Figure 2.3. A summary of the technical specifications for the shaking table are described in table 2.1.

2.2.2 Transducers

This section will describe the technical information about the instrumentation used for the experiments. Their disposition and placement during data acquisition for the different stages of this study will be presented in each pertinent section. Three types of transducers were employed for the experiments: uni-axial accelerometers, laser distance meter and high-speed cameras. Laser distance meters were employed in only one of the experiments involving full scale container (see section 5.2). Whereas accelerometers were used in all experiments, high-speed camera were the main transducers used to acquire the dynamical response of the structure. Accelerometers were used to double check the dynamical response obtained from image analysis and the results will be presented when

2.2 Experimental Facility and Apparatus

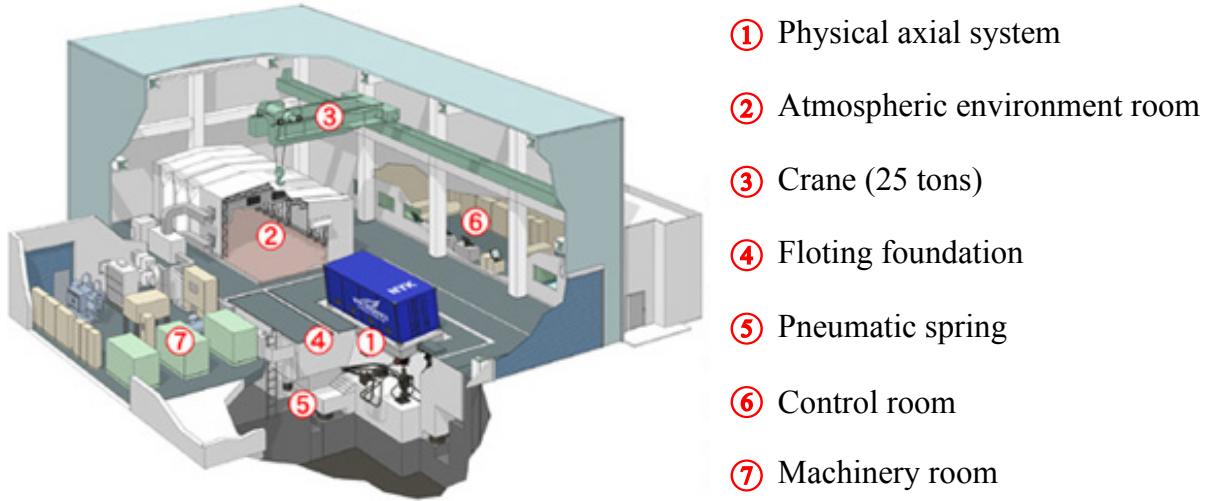


Figure 2.3: Schematic representation of the experimental facility (NYK-MTI, Yokohama, Japan).

Table 2.1: Technical specification of shaking table

Specification	6 DOF
Dimensions [m]	2.6 x 6.2
Maximum loading weight [ton]	20
Maximum rotation angle [degrees]	± 20
Frequency range [Hz]	80
Maximum acceleration [g]	horizontal: 2 vertical: 3
Maximum velocity [m/s]	horizontal: 0.6 vertical: 0.6
Maximum displacement [m]	horizontal: ± 0.2 vertical: ± 0.25

relevant. The choice of one sensor over the other as the major transducer was based on two reasons. Firstly, despite their popularity, the accelerometer signal may be prone to present high levels of noise, mostly caused by collisions between the two scaled models and non-linearity induced by the twist locks gaps. Moreover, such technique would require a careful and lengthy analysis of frequency domain to identify the relevant part of the spectrum. Secondly, accelerometer data needs to be integrated twice to be converted to displacement which can introduce round-off errors in the estimate. Relevant technical specifications for the accelerometers, laser distance meters and high-speed cameras are

2.2 Experimental Facility and Apparatus

presented in tables 2.2, 2.3 and 2.4 respectively.

Table 2.2: Technical specification of the accelerometers (model ARF-200A, Tokyo Sokki Kenkyujo Co. Ltd.)

Mass [kg]	0.013
Capacity [m/s^2]	200
Amplitude limit [g]	20.40
Frequency response [Hz]	310
Natural frequency [Hz]	520
Non-linearity [%]	1

Table 2.3: Technical specification of laser distance meters (model LK-500, Keyence Corporation)

Pulse duration [μs]	3 to 994
Reference distance [mm]	350
Measuring distance [mm]	± 100
Minimum spot diameter [mm]	0.7
Linearity [%]	± 0.1
Sampling frequency [μs]	1024

Table 2.4: Technical specification of the high-speed cameras (model NVC-SL, PHOTRON, USA, Inc.) .)

Sensor [pixels]	512x512
Shutter [s]	16.7 ms to 3.7 μs
Shock [g]	100 any axis
Dimensions [mm]	109.2(H), 90(W), 235(D)
Mass [kg]	1.76

2.2 Experimental Facility and Apparatus

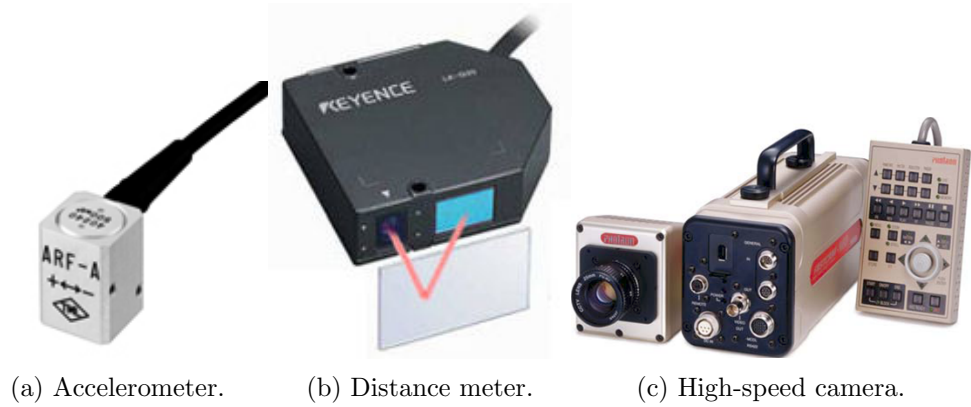


Figure 2.5: Transducers used for the experiments.

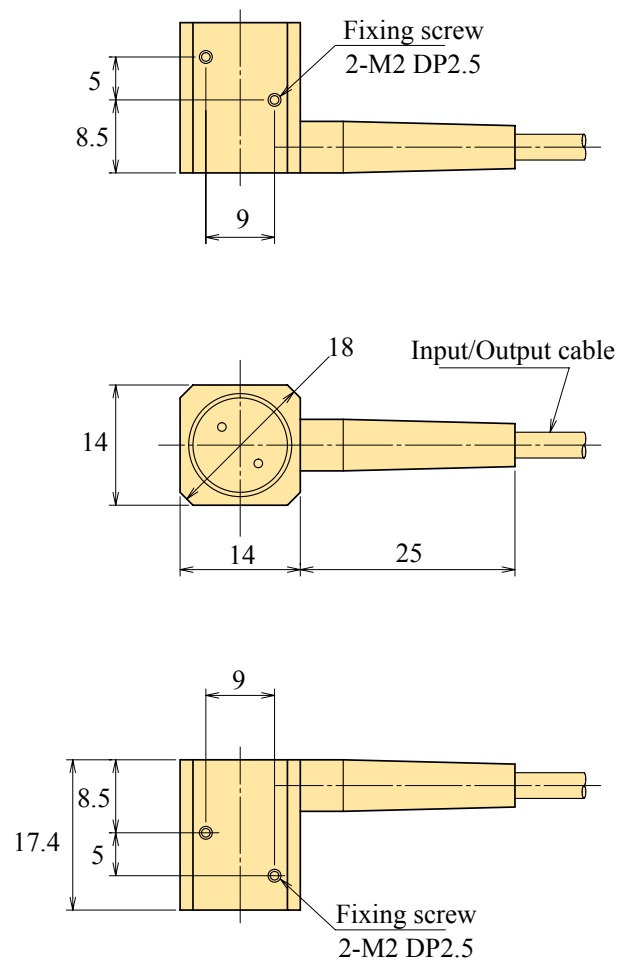


Figure 2.6: Dimensions of the accelerometer.

2.3 Physical Parameters Modeled

To model and understand all the variables involved in container stack dynamics is a herculean task require such a considerable amount of time, that it may be outside the scope of a Ph.D. dissertation. Therefore it is important to selectively identify the main physical phenomena that are responsible for dictating structural behavior. In this study, these crucial phenomena are:

- Driving excitation

Obviously, the first parameter in question here is the cause of container dynamical behavior. Thus, a complete study of how ship's motion like whipping, rolling and pitching affect it is a key point in this study.

- Elastic deformation of containers

Rigid body models are easy to implement, and its computational cost is low. However, in such big structure, keeping in mind that a container stack height can reach up to 20 meters, elastic deformation is an important physical phenomena and must be accounted for. Moreover, non-linearities that have origins in large displacement must be included in the study.

- Container weight

Although, container load is a simple variable its effects are not fully understood. Moreover, it is a common belief in the industry that this parameter is crucial during securing of containers.

- Twist lock non-linear behavior

In our understanding, twist lock behavior is one of the main sources of non-linearity observed in a container stack. Thus an appropriate treatment and modeling of its mechanical properties is essential to accurately emulate this system. During the course of this dissertation this phenomena will be also referred to as backlash or gap effect.

- Collision between stacks

The other clear source of non-linearity in our study is contact between adjacent stacks. Like twist lock behavior, a careful approach for such physical phenomena must be addressed.

- Buckling

This non-linear phenomenon is important to understand the collapse of the stack under extreme conditions.

- Twist lock failure

To completely model the collapse of the container stack, twist lock failure must be taken into account.

To visualize the physical phenomena modeled in this study a schematic representation of the most complex case in our study is depicted in Figure 2.7.

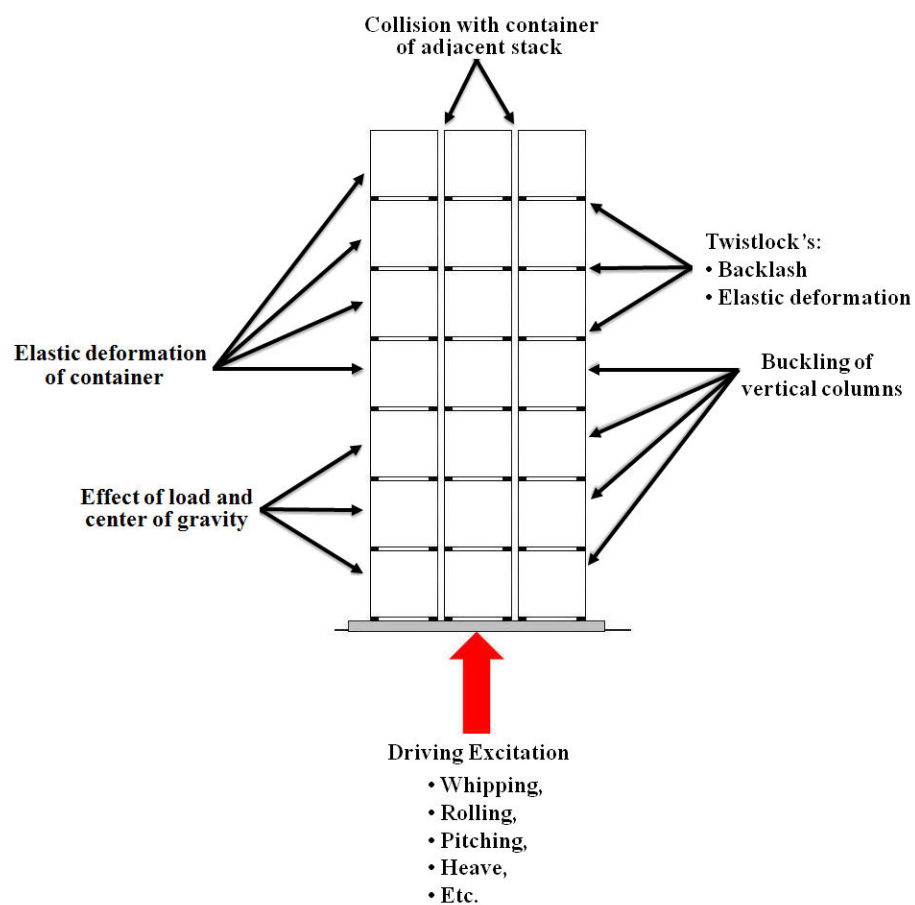


Figure 2.7: Summary of physical phenomena that are included in the numerical model.

2.4 Defining Input and Output Variables

For all dynamical cases, with exception to hammering test, the input variable was displacement, through a sinusoidal driving excitation applied to the system by the shaking

2.4 Defining Input and Output Variables

table. For all cases a series of physical variables were idealized to serve as parameters to understand their effects on container stack dynamics. Two of them belong to the driving excitation and three others have physical characteristics. Namely:

- Amplitude of driving excitation,
- Frequency of driving excitation,
- Additional payload added to some tiers in multi-tier arrangement,
- Rotation of the shaking table in the horizontal plane,
- Increase in the gap size existing between corner casting and twist locks.

Following the example of the input variable, displacement was elected as an output variable. The study limited the analysis of displacement of the top corner of each individual container using high-speed camera technique. Moreover, in multi-stack disposition, the highest container was used for evaluation purposes. The points in question will be presented with details and illustrations in the pertinent section of this dissertation. It is important to emphasize that displacement will be analyzed in time, i.e., displacement-time response.

2.5 Data Analysis

The data will be analyzed using two techniques: time history and coefficients of Fourier expansion comparison, and when convenient, RMS⁴ value comparison. For time history comparison a simple comparison between signals of interest is enough to ascertain the effect of the input variables on the displacement-time response. RMS value for a discrete distribution was calculated based on the expression [88]

$$RMS(x) = \sqrt{\frac{\sum_{i=1}^N x_i^2}{n}} \quad (2.1)$$

On the other hand, the maximum value of Fourier expansion coefficients and RMS value comparison are quite useful to identify how the structure responds to changes in the control parameters. A brief theoretical approach for Fourier expansion is presented below. Fourier Analysis assumes that any stationary sample record $f(t)$ with a period of T_p , and consequently, fundamental frequency $f_1 = \frac{1}{T_p}$, can be expanded using Fourier series as follows

$$f(t) = \frac{a_0}{2} + \sum_{q=1}^{\infty} a_q \cos q\pi f_1 t + b_q \sin q\pi f_1 t \quad (2.2)$$

Where the angular frequency is given by

$$\omega_p = 2\pi f_1 = \frac{2\pi}{T_p} \quad (2.3)$$

Remembering that $f(t)$ must satisfy Dirichlet conditions, named after Johann Peter Gustav Lejeune Dirichlet (1805-1859):

- $f(t)$ it must have a finite number of extrema in any given interval,
- $f(t)$ it must have a finite number of finite discontinuities in any given interval,
- $f(t)$ it must be absolutely integrable over a period, and
- $f(t)$ it must be bounded.

It persists the need of calculating the coefficients a_q and b_q in the expansion. They can be calculated using the orthogonality of the trigonometric basis. Analytically, orthogonality for a given set $\{\phi_i, i = 1, 2, \dots, \infty\}$ over the interval $[a, b]$, with weight $\rho(t)$ is given by the condition $\int_a^b \phi_i(t) \phi_j(t) \rho(t) dt = 0$ for $i \neq j$. Considering that the basis for Fourier

⁴The root-mean-square of a variate X, sometimes called the quadratic mean, is the square root of the mean squared value of x [88]

series expansion is trigonometric functions, sine and cosine, it is important to emphasize their orthogonal relations

$$\begin{aligned} \int_a^b \cos(\omega_i t) \cos(\omega_j t) dt &= \frac{T}{2} \delta_{ij} \\ \int_a^b \sin(\omega_i t) \sin(\omega_j t) dt &= \frac{T}{2} \delta_{ij} \\ \int_a^b \sin(\omega_i t) \cos(\omega_j t) dt &= 0 \end{aligned} \tag{2.4}$$

Where δ_{ij} is the *Kronecker* delta. Thus, multiplying the equation 2.2 for the trigonometric basis yields both coefficients

$$\begin{aligned} a_q &= \frac{2}{T} \int_0^T f(t) \cos(2\pi q f_1 t), \quad q = 0, 1, 2, \dots \\ b_q &= \frac{2}{T} \int_0^T f(t) \sin(2\pi q f_1 t), \quad q = 0, 1, 2, \dots \end{aligned} \tag{2.5}$$

As can be seen, equations 2.2 and 2.5 above consider a continuous interval. Moreover the function $f(t)$ is assumed to be periodic in an infinite range. However, during an experiment a discrete number of samples is acquired, so the previous equations are not directly suitable for the Fourier expansion. A good formal approach about the Fourier series procedure for discrete data was done by Bendat [10]. The procedure consists of three assumptions that enable the use of previous theory for discrete data.

Firstly, one must assume that a sample record $f(t)$ is of finite length $T_r = T_p$, the fundamental period of the data. Secondly, one must assume that the record is sampled at an even number of N equally spaced points a distance h apart. This assumption is redundant because sampling rate during our experiment was fixed for every case. The important point in the second assumption that must be addressed carefully is the choice of h . This value must be selected to produce a sufficiently high cutoff frequency defined analytically by $f_c = \frac{1}{2h}$. In our case $h=0.02$ and 0.04 s, corresponding to cutoff frequencies of 250 and 125 Hz, respectively. Remembering that the analysis is restricted to a finite time interval $[0, T]$, which leads to a Fourier series with discrete frequencies and a periodic function of time. Therein lies the importance of an appropriate choice of h . The last assumption considers the initial point of the record to be zero and denotes the transformed data values, as before, by

$$x_n = (nh) \tag{2.6}$$

In possession of the three assumptions one must proceed now to calculate the finite version of a Fourier series which will pass through these N data values. Based on the equation 2.2, for any point t in the interval $(0, T_p)$, the result is

$$f(t) = A_0 + \sum_{q=1}^{\frac{N}{2}} \cos\left(\frac{2\pi qt}{T_p}\right) + \sum_{q=1}^{\frac{N}{2}-1} \sin\left(\frac{2\pi qt}{T_p}\right) \quad (2.7)$$

At the particular points $t = nh$, $n = 1, 2, \dots, N$, where $T_p = Nh$,

$$f(t) = A_0 + \sum_{q=1}^{\frac{N}{2}} \cos\left(\frac{2\pi qn}{N}\right) + \sum_{q=1}^{\frac{N}{2}-1} \sin\left(\frac{2\pi qn}{N}\right) \quad (2.8)$$

Thus using orthogonality of the basis the coefficients A_q and B_q s are given by

$$\begin{aligned} A_0 &= \frac{1}{N} \sum_{n=1}^N f_n = \bar{f} = 0 \\ A_q &= \frac{2}{N} \sum_{n=1}^N f_n \cos\left(\frac{2\pi qn}{N}\right), \quad q = 0, 1, 2, \dots, \frac{N}{2} - 1 \\ A_{\frac{N}{2}} &= \frac{1}{N} \sum_{n=1}^N f_n \cos q\pi \\ B_0 &= 0 \\ B_q &= \frac{2}{N} \sum_{n=1}^N f_n \sin\left(\frac{2\pi qn}{N}\right), \quad q = 0, 1, 2, \dots, \frac{N}{2} - 1 \\ B_{\frac{N}{2}} &= 0 \end{aligned} \quad (2.9)$$

Often the coefficients B_0 and $B_{\frac{N}{2}}$ are included for symmetry. Note that the corresponding sine function factors evaluate to zero, leaving these two coefficients arbitrary. Thus, aiming at simplicity one can assume them to be zero. A simple routine in MATLAB was written to calculate the coefficients. Fourier expansion presents itself as good approximation in our case, because the driving displacement imposed on the system is a sinusoidal function with a fixed angular frequency for each case. The effect of this method can be seen in the Figure 2.8.

Another technique used during this study is the subtraction of the displacement-time response and driving excitation. In this dissertation the result of this operation is denominated *relative motion* and will be employed in most cases. Additionally, the nomenclature *local motion* is employed denoting displacement-time history without any algebraic operation. This information is summarized in table 2.5.

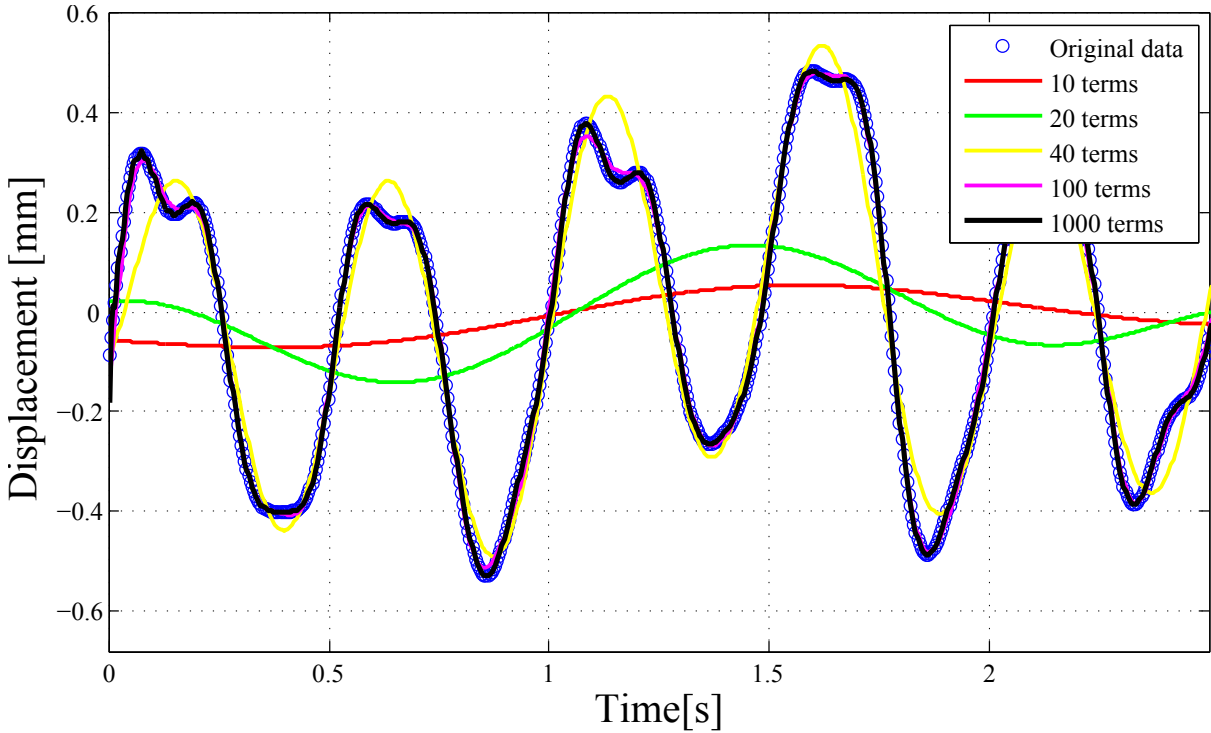


Figure 2.8: Fourier expansion.

Table 2.5: Terminology used to refer to the displacement-time response data

Description	Nomenclature
Displacement with relation to a fixed reference (ground)	<i>Local motion</i>
Subtraction of displacement-time driving excitation and displacement-time response	<i>Relative motion</i>

2.6 Experimental Data Filtering

Digital signal processing, attended by the acronym DSP, is an important step towards understanding and interpreting information contained in a digital signal through various mathematical techniques. A well known method to perform such an action is called, by its short name, filtering, or more commonly digital signal filtering. Digital signal filtering is useful for denoising, i.e., removing noise from data preserving only the pertinent part of the spectrum. In other words one is interested in removing noise as much as possible without distorting the original data.

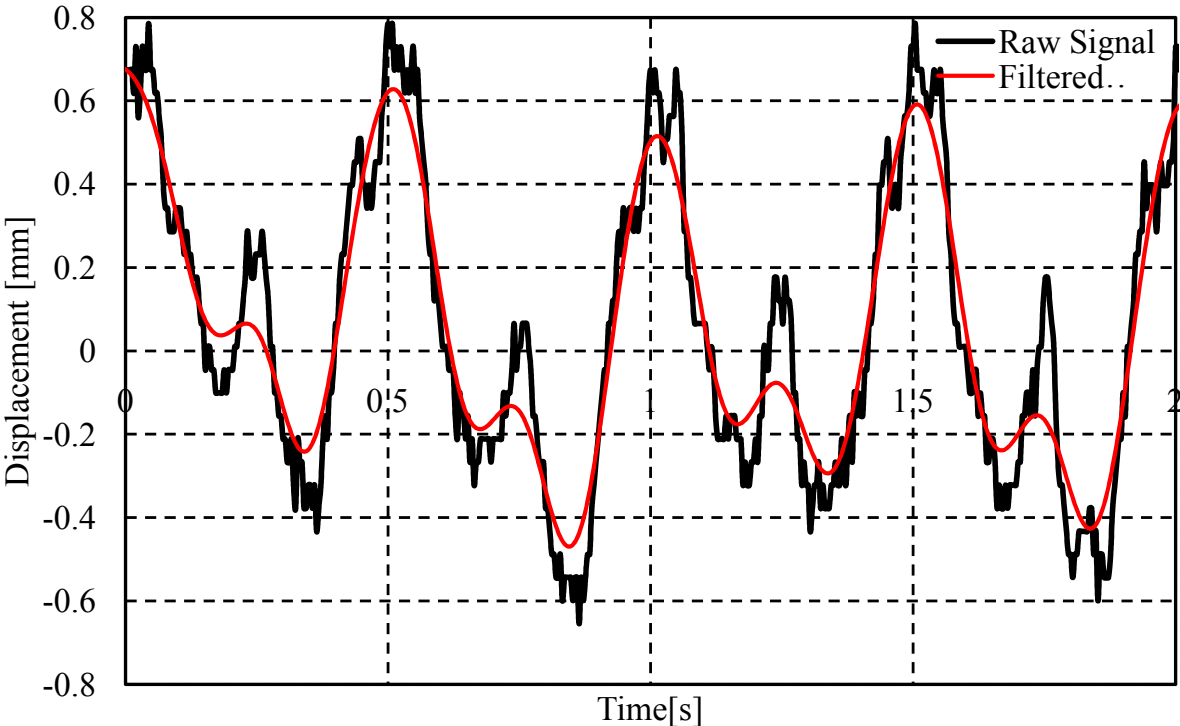
There are many techniques in filtering, each one with its own peculiarities, e.g. noise-spike, high-pass, low-pass, and band-pass to mention but a few. Roughly, filters can be classified in three categories: time domain, used for smoothing and DC removing;

frequency domain, applicable for separating frequencies, and custom, used for deconvolution. The appropriate choice depends strongly on a previous understanding of the physical phenomenon recorded. In our case, a driving frequency set in advance facilitates this process. During the experiment the whole system was excited with a defined and constant frequency. Thus filtering in frequency domain is perfectly suitable in this case, e.g., band-pass, band-reject, high-pass and low-pass. As mentioned previously, excitation frequency for the experiment was constant for every trial, thus low-pass filter is the best option to denoise the signals. Moreover, Hamming window was employed as a base line for the low-pass filter. However, after deciding the method it is necessary to go a step further and calculate the cut-off frequency to be used for filtering. There are specific methods to calculate an appropriate cut-off frequency. The next paragraphs will discuss this choice on a mathematical basis.

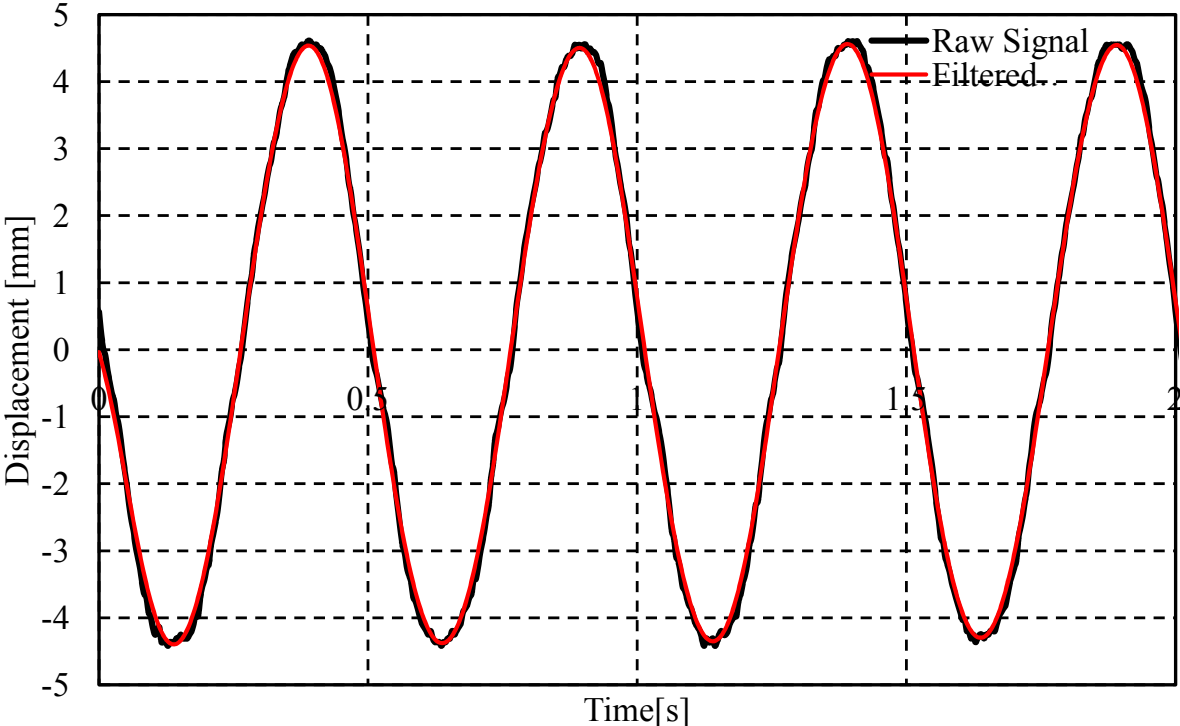
For this study two methods were employed: harmonic analysis and residual analysis. The reasons behind the choice of these methods will be explained in the next paragraphs. Physically the noise observed during experiment was expected to have equal levels in both directions: horizontal and vertical, both originated from camera sensibility. However in the vertical direction signal is clearly smoother than it is in the horizontal direction. The probable reason behind this observation is the shaking table excitation, strictly vertical following a well behaved sinusoidal function. Moreover, amplitude in vertical direction is considerably higher than horizontal direction, helping to identify what is noise and what it is not. This can be easily observed in Figure 2.9a and Figure 2.9b. Vertical direction motion is clearly governed by a sinusoidal function with frequency of 2 Hz, making it easy to identify the noise component.

For the vertical direction raw data, harmonic analysis was chosen because of its simplicity and quickness. As mentioned above data in this direction is smoother and as consequence a simple inspection of harmonics is enough to decide the cut-off frequency. Thus, just by analyzing the power in each component, it is easy to decide based on simple inspection, how much power to accept and how much to reject [89]. The drawback in such an approximation is the assumption that the filter is ideal and has an infinitely sharp cut-off. In our case harmonic analysis is depicted in Figure 2.10. Based on the harmonic analysis, vertical direction motion data cut-off frequency was chosen in 5.5 Hz.

For the horizontal motion data residual analysis presents itself as a better method to decide the cut-off frequency. Residual analysis consists of a difference between filtered and unfiltered signals over a wide range of cut-off frequencies and can be calculated using



(a) Horizontal direction.



(b) Vertical direction.

Figure 2.9: Effect of filtering for horizontal and vertical directions.

the expression presented by Winter

$$R(f_c) = \sqrt{\frac{1}{N} \sum_{i=1}^N (X_i - \hat{X}_i)^2} \quad (2.10)$$

Where

X_i : is the raw data i th sample

\hat{X}_i : is the filtered data at the i th sample

The important point in this method regards where the cut-off frequency (f_c), should be chosen. Winter concludes: "To preserve the meaningful information contained in the original signal one must find a balance between the amount of signal distortion versus the amount of noise allowed through". A best option might be equal weights for both, then a simply projection of a vertical line from the intersection of the horizontal line created from the linear coefficient obtained from the best fit linear regression of the residual curve. An example of residual analysis for one study case (7x3-0 degree-2 Hz-6 mm) is illustrated in Figure 2.11.

2.7 Terminology

There are some specific terms that must be explained for better understanding during the reading of this dissertation. The first part regards the jargon of ship motion. Like any other object in space, ship movement is divided into translational and rotational motion, defining the six degrees of freedom that it can experience. The main difference in Naval engineering is the existence of a special terminology to denominate each motion, depending on the type of movement (translation and rotation) and the ship's main axis (longitudinal, transverse and vertical). Table 2.6 presents a summary of the ship's motion. Furthermore Figure 2.12 represents this terminology graphically.

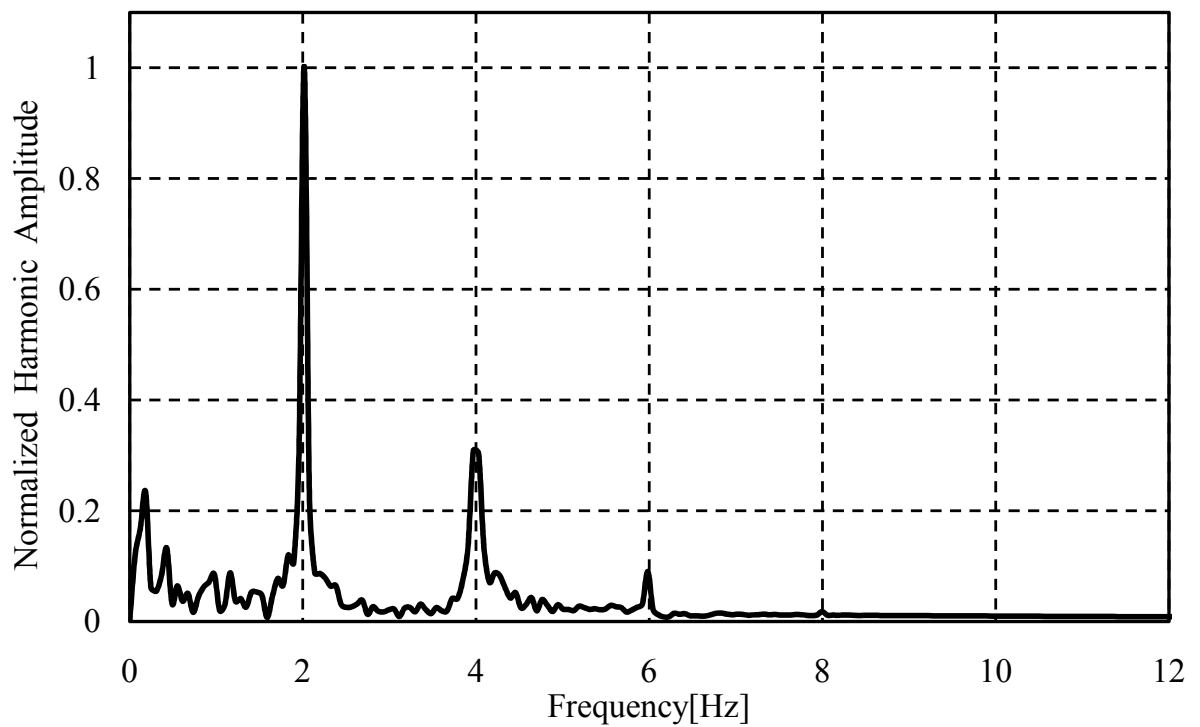
Table 2.6: Terminology of the ship motions

Axis	Translational (linear)	Rotational (rotation)
Longitudinal	Surge	Roll
Transverse or Lateral	Sway	Pitch
Vertical	Heave	Yaw

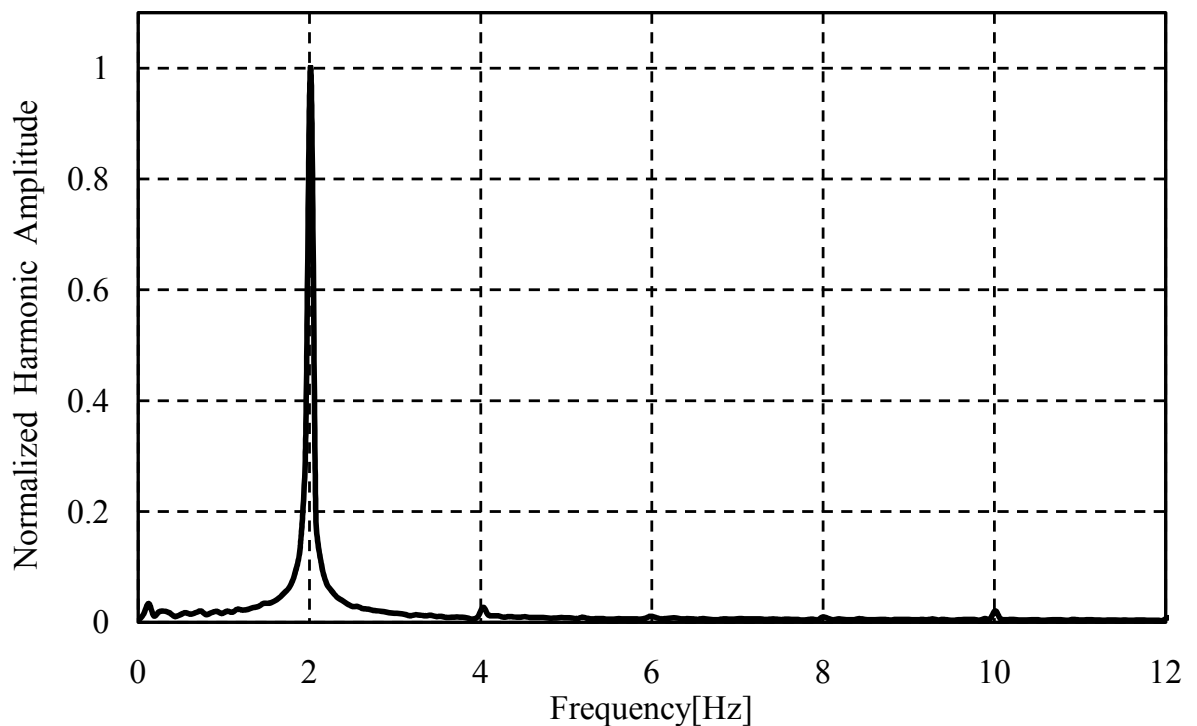
Moreover, some terms will be used in this dissertation that may not be familiar. To facilitate understanding, the terms regarding the disposition of the structure are summarized in table 2.7.

Table 2.7: Terminology used to refer to study cases regarding the structure

Study case description	Acronym
Two tiers	2x1
Seven tiers, one stack	7x1
Seven tiers, three stacks	7x3



(a) Horizontal direction.



(b) Vertical direction.

Figure 2.10: Harmonic content of the horizontal and vertical displacements of point 1 in a 7x3 experimental configuration. The first harmonic (driving frequency of 2 Hz) is normalized at 1.00. For the vertical direction over 99 % of power is contained below the 2th harmonic.

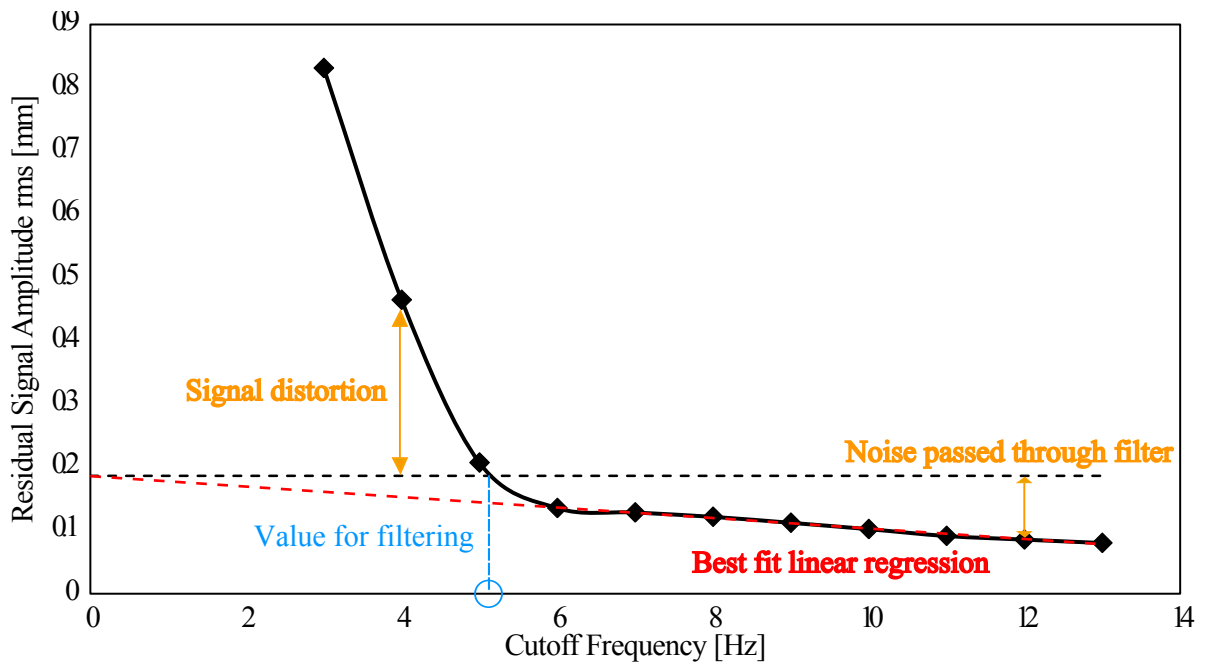


Figure 2.11: Residual analysis to decide the value of the cut-off frequency.

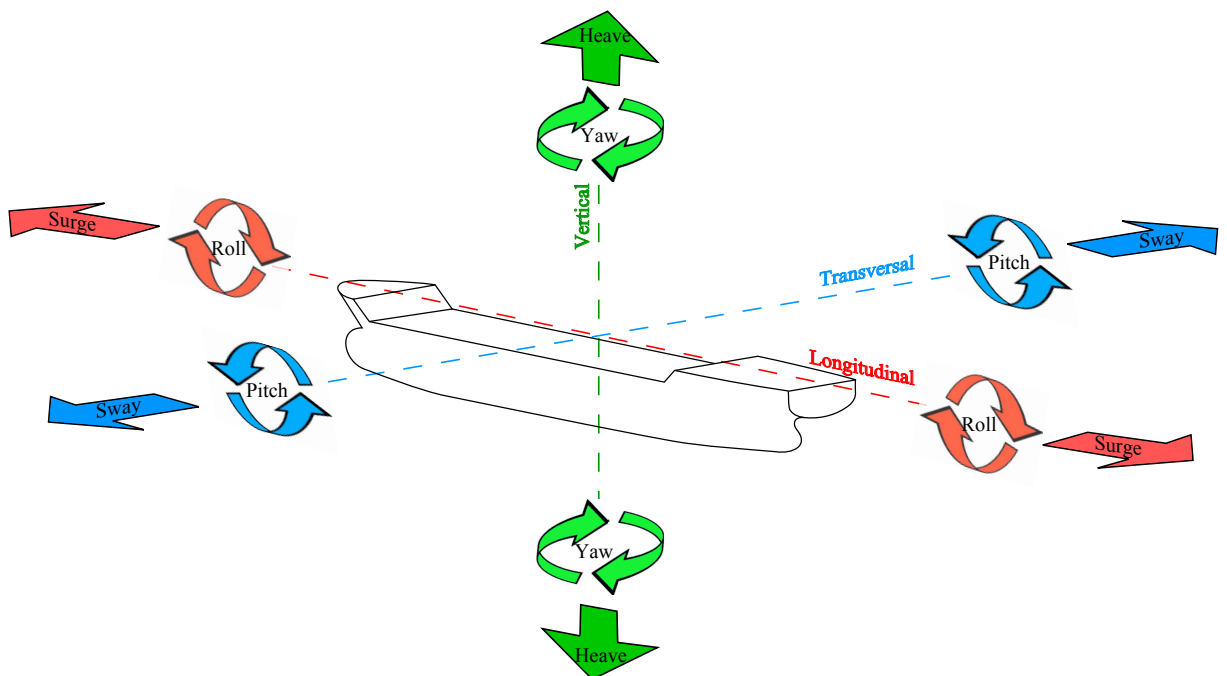


Figure 2.12: Graphic representation of terminology regarding ship motion.

Chapter 3

Scaled Model

3.1 Brief Overview

The use of scaled models by scientists as a tool to experiment, evaluate and analyze complex physical behavior was firstly recorded in human history by Leonardo da Vinci (1425-1519)[85]. However, despite his fertile and genial intellect, most of Leonardo's models were impractical, and were never built in full-scale. The next researcher related to scaling was Galileo Galilei (1564-1642) who is often credited, amidst many more in various fields, as the first scientist to successfully apply scaling for practical situations. Amidst that period, most model building have only geometric resemblance to the real world structures they were mimicking. It is what we refer nowadays as geometric scaling, an approach where proportions (lengths) between prototypes and models are kept constant.

Although geometric scaling provided a reasonable insight in some situations, there was a need for a wider theory. Around that time Euclidean theory of similar figures and solids contained in Book VI of the Elements was the pillar of geometrical scaling. However, Euclidean geometry was insufficient when it came to reliably scaling artifacts because neglects the forces acting on these objects. To illustrate the limitation of geometrical scaling it is enough to say that if a boat is scaled up ten times in the three Euclidean dimensions, then the resulting artifact will be much too weak for practical purposes [30]. Even though Galileo had developed a theory about scaling forces, not until the 19th century this lacuna was filled, and not until then such approach received the approval from the scientific community, and then became accepted as a justifiable methodology. This happened because of the efforts of a Victorian civil engineer called William Froude (1810-1879) who, in 1871, successfully used an accurate scaled model of the vessel *HMS Greyhound* for experimentation in a tank. Officially this was the world's first scaled model experiment, inaugurating a new era in Naval Engineering. Concretely, he introduced a non-dimensional parameter that served as the criterion for dynamic similarity when comparing boats of different hull

lengths [29], which is nowadays referred as Froude number. Scaled model analysis would get another significant contribution soon after: Edgar Buckingham (1867-1940) developed the mathematical background necessary to give a theoretical basis to scaling. His papers, dating to 1914 and 1915, opened a new gamma of applications, catapulting the field to an unprecedented level.

A new field with countless applications was born: Dimensional Analysis, also known as Buckingham's π theory. The main application of the new theory was promptly discovered: to establish the conditions necessary and sufficient to guarantee that prototypes and models, used for experimentation, are physically similar, including not only geometric similarity, i.e., a formal method to obtain the relevant parameters necessary to guarantee physical similarity. These parameters are denominated *similitude* or *similarity parameters*. Such parameters have an unique characteristic: are **equal** for the model and the prototype (real world).

They realized that if the ratios between physical parameters that govern a system are assumed to be constant, i.e., the ratios do not vary, like in the geometric similarity, there is a unique set of numbers that independently satisfy that criterion and are valid for both systems. By construction, they are dimensionless, which can prove a valuable feature because its independence on the sizes of the fundamental units [12]. A formal mathematical treatment of this theory is lengthy and outside the scope of this dissertation, which used it as a tool to obtain the similitude parameters necessary for scaling coherently the model. If the reader has interest in knowing it thoroughly please refer to the papers entitled *On Physically Similar Systems; Illustrations of the use of Dimensional Analysis* [12] and *Model experiments and the forms of empirical equations* [13]. Additionally, to understand how dimensional analysis is applied in a variety of fields, e.g., structural dynamics, naval engineering, biology, fluid dynamics, etc., refer to the pioneer book *Dimensional analysis* by Bridgman [11] with first edition in 1922.

In this dissertation we will just present and explain choice and meaning of the dimensionless numbers (π) used for model construction, what is described in section 3.3, without over-stressing the mathematical basis behind dimensional analysis theory. Please refer to Table 3.1 for an extended list of works involving similarity theory allied with dimensional analysis in a variety of applications.

3.2 Similarity Theory

The use of similarity theory and dimensional analysis theory to find solution for structural problems is relatively seldom documented in the literature. Although an enormous quantity of books about dimensional analysis and similarity, including applications, have being

published since 1922, a very limited number of scholastic papers were published reporting study cases using this technique. Moreover, technical reports about use of models and scaling in simulation are extremely restrict, mostly because many applications regarding it have strategic importance for the industry. However, some researchers present valuable studies about the theme. During the course of this brief literature review, the literature review will focus solely in studies that employed similar research design. Moreover, we will avoid, as much as possible, to refer to studies that are not fully available, e.g., technical reports from famous agencies, proceedings papers, etc. The most prolific researcher regarding the use of these theories in structural dynamics is Wu. He has publish precious papers about a variety of scaled models with no economy in details.

3.2.1 Geometric Similarity

Geometric similarity or similarity of shape is used to refer to systems that the specified physical quantities relating them are lengths, i.e., the ratio of any length of one system to the correspondent length in the other system is a constant [85]. This concept can be extended as a corollary to area, volume, mass, moment of inertia, and stiffness. During this dissertation, the constant, habitually denominated *scale factor*, used to represent the geometric similarity ratio will be denoted as the Greek letter lambda(λ).

The basic geometric features of our model: length, width and height follow a strict numerical relation with a full scale 20 ft container, i.e., its shape is a scaled version of it. Moreover, area, volume, mass, moment of inertia and stiffness also preserve a similar relationship as mentioned before during our inference about geometric similarity. As a matter of convenience, we will denote all physical variables regarding full-scale container with a subscript f . On the other hand, all variables regarding the model will be identified by a subscript m , as used previously by Vassalos [85]. Analytically,

$$\lambda = \frac{L_f}{L_m} \tag{3.1}$$

$$Area_f = \lambda^2 Area_m \tag{3.2}$$

$$Volume_f = \lambda^3 Volume_m \tag{3.3}$$

$$Mass_f = \lambda^3 Mass_m \tag{3.4}$$

$$I_f(mk)^2 = \lambda^5 I_m \tag{3.5}$$

Table 3.1: Summary of studies involving similarity theory and dimensional analysis theory

Author	Year	Problem approached
Soedel	1971	Vibration in thin shells
Qian <i>et al.</i>	1990	Impact damage in fiber composites
Simitses & Rezaeepazhand	1993	Structural similitude for laminated structures
Rezaeepazhand <i>et al.</i>	1995	Laminated cylindrical shells subjected to axial compression
Rezaeepazhand <i>et al.</i>	1996	Vibration response in laminated shells
Vassalos	1999	Similitude for marine structures
Wu <i>et al.</i>	2002	Vibration in a crane structure
Ungbhakorn & Singhatanadgid	2003	Buckling loads of laminated plates subjected to biaxial loads
Ungbhakorn & Singhatanadgid	2003	Buckling and free vibration in symmetric cross-ply laminated circular cylindrical shells
Wu	2003	Vibration characteristics of elastically restrained flat plates subjected to dynamic loads
Wu	2005	Dynamic analysis of rectangular plates under a moving load line
Wu	2006	results comparison of full-size and scaled model of flat plates subject to vibration
Wu	2007	Vibration characteristics of a rotor bearing system
Oshiro & Alves	2007	Cylindrical shells under axial impact
Singhatanadgid & Songkhla	2008	Vibration response of rectangular thin plates
Torkamani <i>et al.</i>	2009	Free vibrations of orthogonally stiffened cylindrical shells

Important to mention that equations 3.3 and 3.4 have this form because of the assumption that both systems have equal values of densities (analytically $\rho_f = \rho_m$). In addition to what has been said, we have to emphasize that geometric similarity itself is not sufficient

to guarantee that the two systems: full-scale and scaled, will present similar behavior. For complete similitude some other requirement are necessary. Such requirements will be presented in sections 3.2.2 and 3.2.3.

3.2.2 Kinematic Similarity

Besides geometric similarity, another feature that similar system must possess is called kinematic similarity. The etymology of the word kinematic is derived from the Greek word *kinema* that means to move. Thus this kind of similarity regards the motion of the two objects of interest: full-scale and model container. Kinematic similarity guarantees that, besides geometry similarity, the two systems have similarity of time, i.e., corresponding time intervals present a fixed ratio. Consequently similarity of velocity and acceleration will be achieved. This kind of similarity will be achieved if geometric and dynamic similarity are present, and normally, there are no separate requirements marking the occurrence of this similarity. Thus, kinematic similarity is achieved in our study as a consequence of Froude scaling (please refer to table 3.3 and section 3.2.3).

3.2.3 Dynamic Similarity

Other than geometric and kinematic similarity, both systems can possess a third one: dynamic similarity. Such similarity is presented when the ratio between forces acting on the system is a fixed ratio. Some of those ratios are notorious dimensionless numbers named after famous scientists that discovered them, e.g., Froude number, Reynolds number, etc. In our case some forces are considered to play a fundamental role in container stack dynamics. Videlicet:

- Inertia Force

$$F_i = \frac{mL}{t^2} \tag{3.6}$$

- Gravity Force

$$F_g = mg \tag{3.7}$$

- Elasticity Force

$$F_{elastic} = E\epsilon L^2 \tag{3.8}$$

Where L is length, m is mass, t is time, g is gravity acceleration, E is Young's modulus, and ϵ is strain.

Table 3.2: Dimensionless numbers used for scaling the model

Delineation	Analytical expression	Nomenclature
$\frac{\text{Inertiaforce}}{\text{Gravityforce}}$	$\frac{L}{gt^2}$	Froude
$\frac{\text{Gravityforce}}{\text{Twistlockelasticityforce}}$	$\frac{mg}{E\epsilon l^2}$	nameless
$\frac{\text{Containerelasticityforce}}{\text{Twistlockelasticityforce}}$	$\frac{E'}{E}$	nameless

3.3 Buckingham π 's Numbers Used for Scaling

In this section, the dimensionless number, most commonly called Buckingham's π numbers, used for scaling will be presented. Such numbers, expressions and nomenclature, when existing, are delineated in table 3.2 below. The expressions for these numbers were found manipulating equations 3.6, 3.7, and 3.8 according to the ratios stipulated in table 3.2.

To close this section we will present a table summarizing our scaling laws for the model. Refer to table 3.3 for details. We would like to emphasize that this set of scaling laws is commonly referred as Froude scaling [15, 85].

Using the expressions in the right column in the table 3.3 and geometric information contained in table 1.1, one can easily calculate the physical parameters necessary to construct the model.

3.4 Design and Testing Parameters

Is practically impossible to match all similitude parameters, characterizing complete similitude, during the construction of a real model. The relaxation of one or more similitude parameters, also known as partial similarity, may induce error between both systems: full-scale and scaled model [64]. The magnitude of this error is strongly dependent on the influence that each similitude parameter has on the overall system behavior. Thus, neglecting parameters representing minor phenomena would not have a major impact in the way the scaled model behaves. Our choice of parameters were based on dominant effects for container stacks, i.e., parameters that would have great influence in the structural dynamics of containers. It is important to mention that these parameters will be used to validate the designed scaled model experimentally and numerically. Namely:

- Mass
- Moments of inertia

Table 3.3: Scaling laws for the model (Froude scaling)

Physical parameter	Full scale	Scaled model
Mass [kg]	m_f	$\frac{m_f}{\lambda^3}$
Length [m]	L_f	$\frac{L_f}{\lambda}$
Time [s]	t_f	$\frac{t_f}{\sqrt{\lambda}}$
Frequency [Hz]	f_f	$\sqrt{\lambda} f_f$
Velocity [m/s]	v_f	$\frac{v_f}{\sqrt{\lambda}}$
Acceleration [m/s ²]	a_f	a_f
Angle [rad]	θ_f	θ_f
Angular Velocity [rad/s]	$\dot{\theta}_f$	$\sqrt{\lambda} \dot{\theta}_f$
Angular Acceleration [rad/s ²]	$\ddot{\theta}_f$	$\lambda \ddot{\theta}_f$
Pressure/Stress [Pa]	P_f	$\frac{P_f}{\lambda}$
Force [N]	F_f	$\frac{F_f}{\lambda^3}$
Moment [N m]	M_f	$\frac{M_f}{\lambda^4}$
Moment of Inertia [kg m ²]	I_f	$\frac{I_f}{\lambda^5}$
Translational Stiffness [N/m]	k_f	$\frac{k_f}{\lambda^2}$
Rotational Stiffness [Nm/rad]	k_f	$\frac{k_f}{\lambda^4}$

- Transversal racking stiffness of front (open) end frames
- Transversal racking stiffness of rear (closed) end frames
- Longitudinal racking stiffness
- Torsional stiffness

Based on these physical parameters, design of scaled models and constructed models were tested according to testing standards approved by ISO [35]. For better understanding of the terminology adopted for testing freight containers, refer to Figure 3.1. Additionally, these standards are depicted in section 3.7.

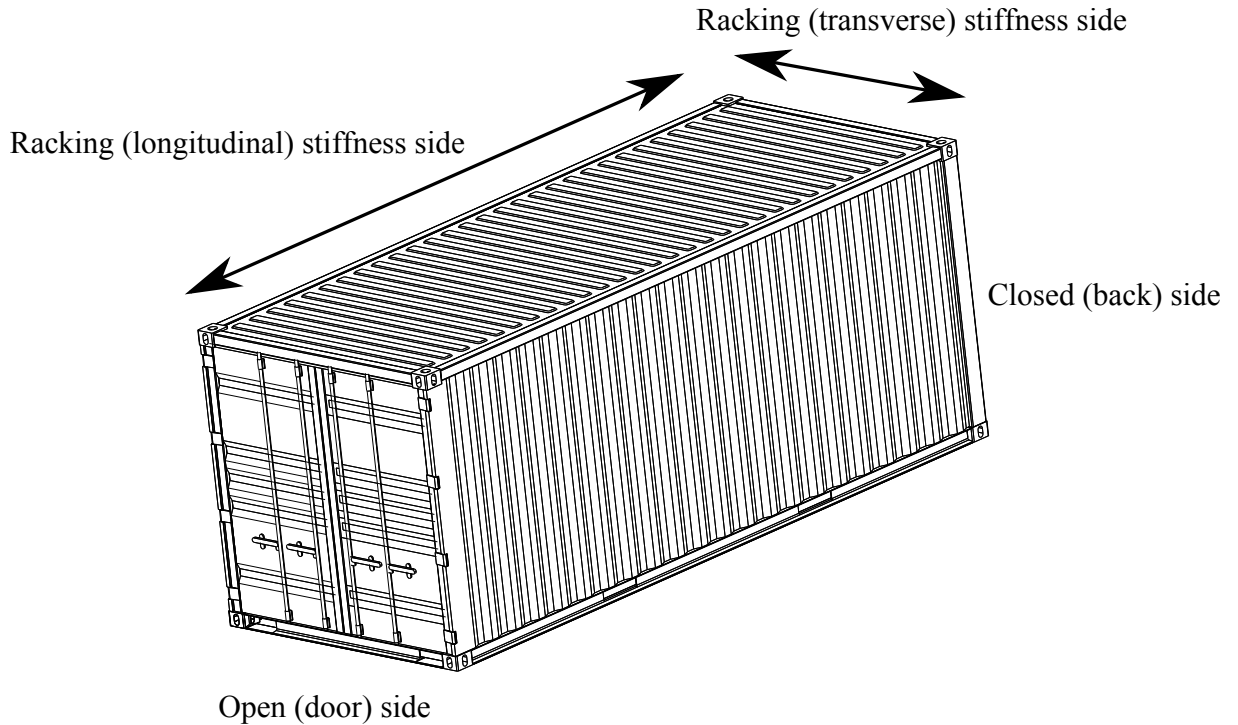


Figure 3.1: Terminology for container testing (ISO).

3.5 Similitude Parameters Used for Model Construction

Values regarding geometry and structural stiffness are presented in table 3.4 and 3.5. Both tables are obtained from scaling laws presented in table 3.3. Using the information provided in the tables 3.4 and 3.5, a scaled model was designed. The proposed model design is depicted in Figure 3.2. To verify the model's design compliance to the ISO standards, the proposed design was tested using finite element analysis.

3.6 Design Evaluation Using Finite Element Analysis

Before the construction of the scaled model, some physical parameters of the proposed design (Figure 3.2) were evaluated through finite element analysis. The proposed geometry was drawn using a CAD capability of a preprocessing commercial program (Hypermesh 8.0, Altair Engineering Inc., 1995-2006). The same software was used to mesh the geometry, and check mesh quality. Scaled model material was assumed to be structural steel (isotropic, linear elastic material: Young's modulus $E=210$ GPa and Poisson ratio $\nu=0.3$). Two types of analysis were performed: static and frequency extraction, accounting for ge-

3.6 Design Evaluation Using Finite Element Analysis

Table 3.4: Geometric scaling of the similitude parameters for the models considering a 20 ft container based on ISO [36]

		Full-scale(20 ft)	Scaled model
External dimensions	length[m]	6.058	1.5140
	width[m]	2.438	0.6095
	height[m]	2.591	0.6478
Mass [kg]		2330	36.41
Moment of Inertia	I_{xx} [kg/m ²]	3765	3.68
	I_{yy} [kg/m ²]	11830	11.55
	I_{zz} [kg/m ²]	11486	11.22

Table 3.5: Stiffness scaling calculated using relation supplied in table 3.3

Structure Stiffness	Stiffness value		
	Full-scale (20 ft)	Scaled model	
Racking [MN/m]	closed	58	3.61
	open	3.41	0.21
Longitudinal [MN/m]	58	3.61	
Torsional [kNm/rad]	3200	12.5	

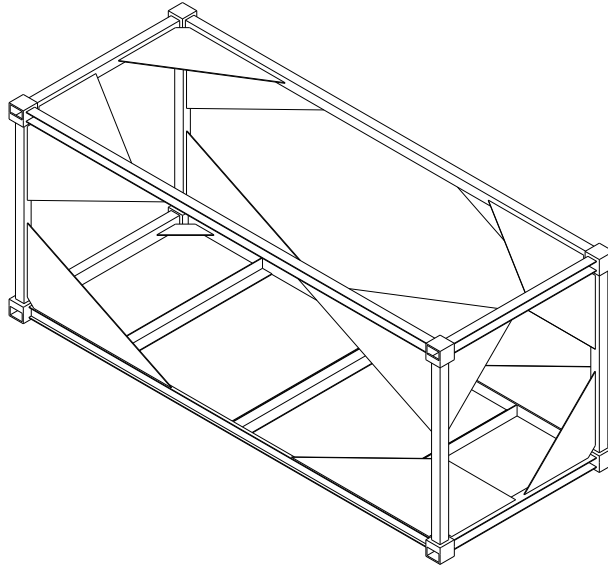


Figure 3.2: Scaled model design for a 20 ft container.

ometric non-linearity. Both analysis were implemented numerically in a commercial finite

element analysis package (ABAQUS, Simulia, version 6.7). Details about constraints and boundary condition for each case is presented in each pertinent section: 3.6.1 and 3.6.2, respectively.

3.6.1 Static Analysis

The first numerical evaluation of the proposed model was performed through a finite element static analysis. Boundary conditions emulate the same ISO specifications described in section 3.4, with constraints specified in Figure 3.3. Convergence analysis was based on mesh density with target results (refer to table 3.5 for details) as parameter. However, due to its simple geometric features, meshing was not overstressed, i.e., the model was meshed using a relatively coarse mesh. Result differences between target and numerical value corroborate with our idea that the meshing process was appropriate for this case (refer to table 3.6). Figure 3.4 shows results for the four cases simulated.

Table 3.6: Numerical values obtained from finite element analysis

Stiffness	Side	Displacement[mm]	Force[kN]	Stiffness
Racking [MN/m]	closed	0.63	2.34	3.72
	open	11.72	2.34	0.20
Longitudinal [MN/m]		0.325	1.17	3.84
Torsional [kNm/rad]				15.8

The design proposed shows good level of agreement (see table 3.9) with the target values stipulated from Froude scaling, leading to a construction of the scaled model depicted in Figure 3.5.

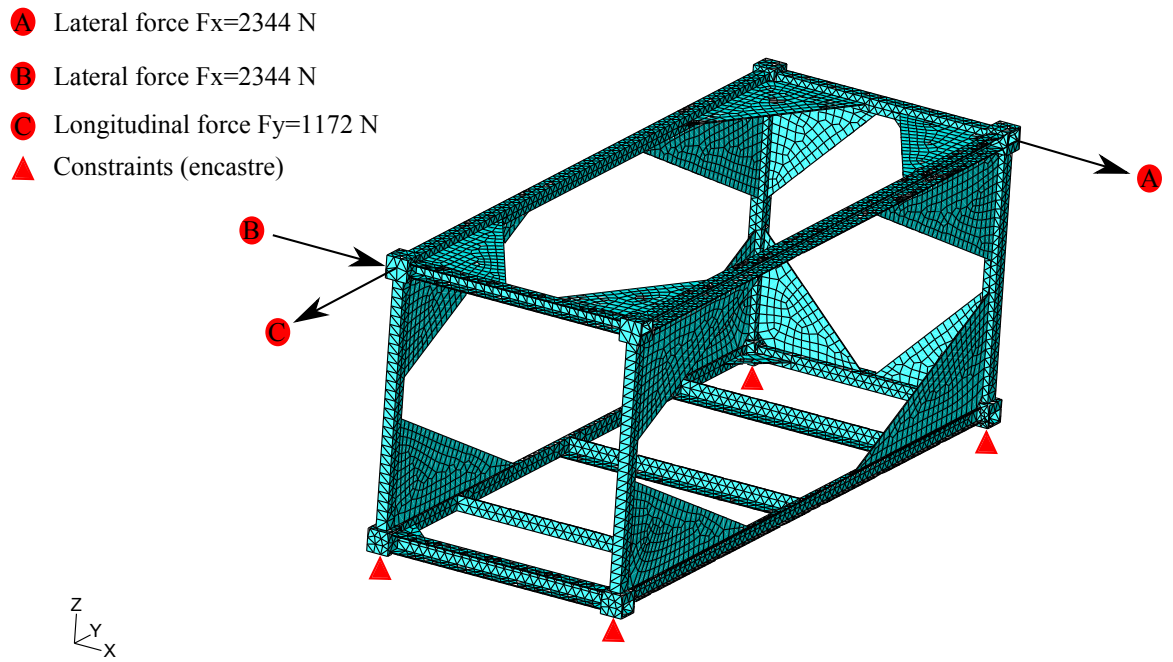
3.6.2 Frequency Extraction

To find another mean to validate the proposed design, frequency extraction by an eigenvalue problem of numerical model was performed. Frequency results for the first five modes are presented in table 3.7.

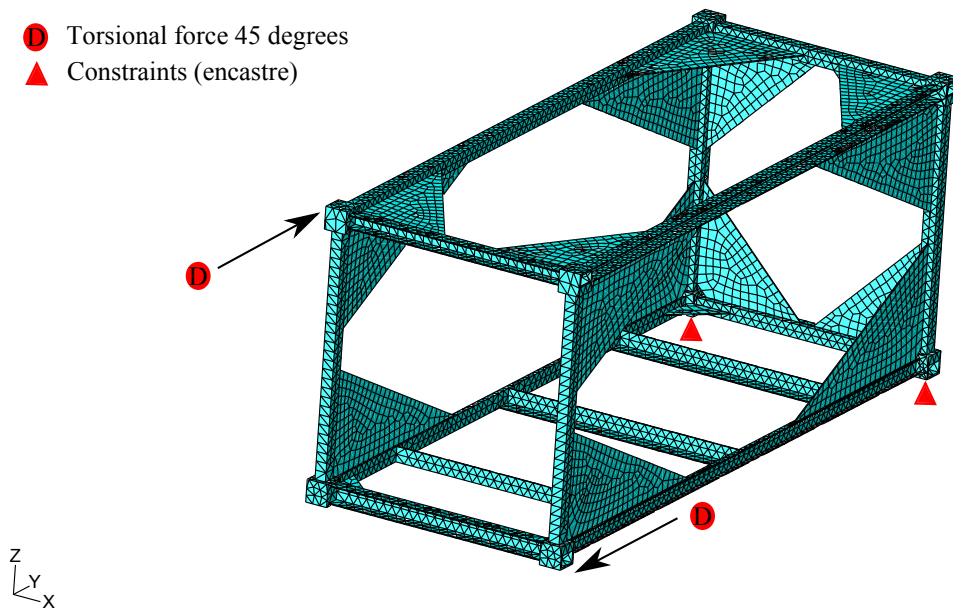
Table 3.7: Eigenfrequencies obtained from finite element analysis

Mode	1	2	3	4	5
Frequency [Hz]-Numerical	39.24	66.37	72.54	74.17	82.76

3.6 Design Evaluation Using Finite Element Analysis



(a) Boundary conditions for the translatory cases.



(b) and for the rotational cases.

Figure 3.3: Boundary conditions.

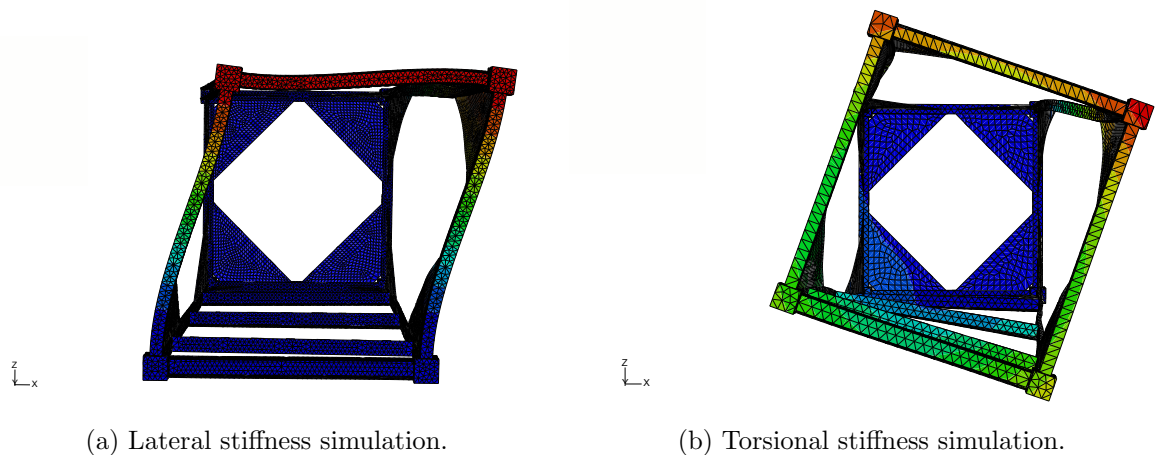


Figure 3.4: Finite element results.



Figure 3.5: Constructed scaled model of a 20 ft container based on Froude scaling.

3.7 Experiments for Design Evaluation

After the construction of the scaled model (Figure 3.5) a succession of experiments were performed to inspect its conformity to the target stiffness presented in table 3.5. Two types of tests were performed: static and dynamic. Static tests were implemented in the scaled model following the same ISO specifications described in section 3.4, and simulated through finite element analysis delineated in section 3.6. Static validation is explained thoroughly in section 3.7.1. On the other hand dynamic test was implemented through a standard measuring technique denominated impact hammer test. Details of this technique are presented in section 3.7.2.

3.7.1 Static Validation

The scaled container was fixated at the bottom cross members to a rigid wall, while a corner casting on the top was gradually loaded up to forty (40) kilograms and then unloaded, with increments of ten (10) kilograms. Please refer to Figure 3.2 for a nomenclature of

scaled model components. Displacement of two corners in the same line of the applied load were recorded using a displacement sensor (micrometer). Load was applied in one end (closed side) and then another (open side). Experiments concentrated in racking because it is a dominant effect during container transportation. For a better understanding about static experiments a schematic representation of each test is depicted in Figure 3.6. Results, and consequent curve fitting, for the two cases performed are presented in Figures 3.7a and 3.7b. The stiffness values for each case were obtained from simple inspection of the angular coefficient of the linear fitting presented in each graphic.

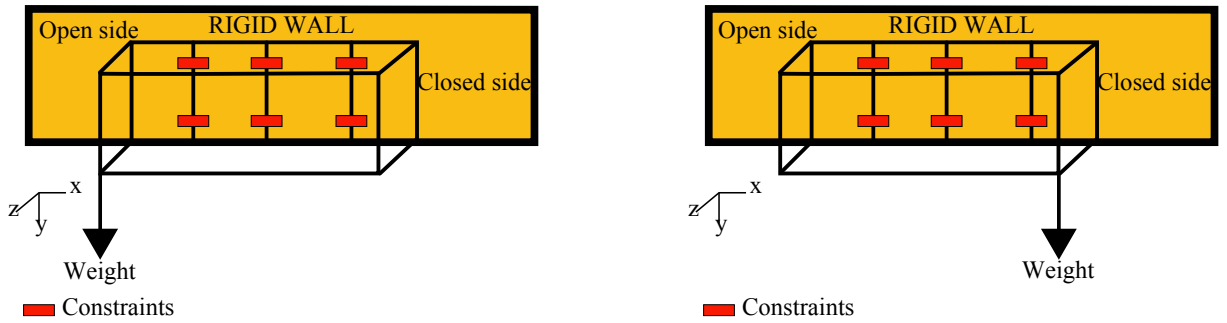
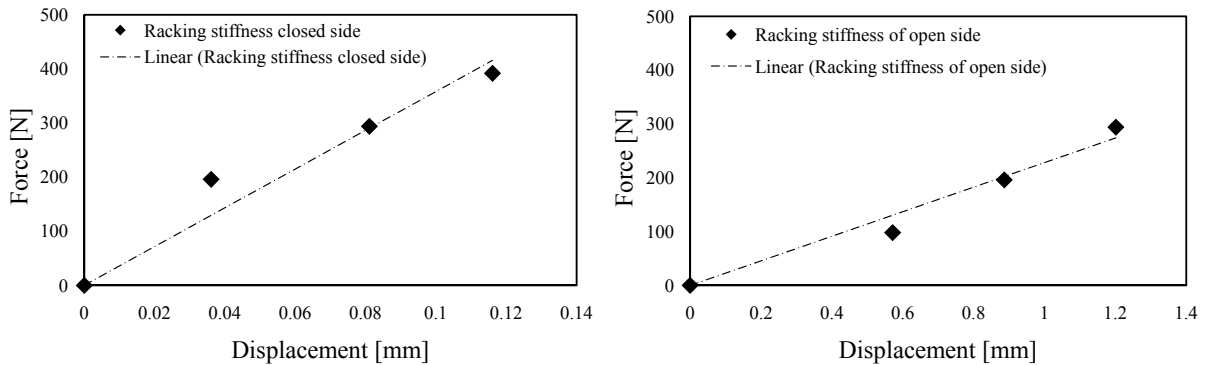


Figure 3.6: Schematic representation of static experiments: racking open side (left) and racking closed side (right).

3.7.2 Dynamic Validation

A pseudo-impulsive force, nomenclature used by *Ege et al.*, was applied on the scaled model with an impact hammer in two distinct points of it (points A and B—please refer to Figure 3.8 for details) to estimate the system vibrations. The system structural response



(a) Results and best fit: $y = 0.23x$, $R^2 = 0.97$.

(b) Results and best fit: $y = 3.58x$, $R^2 = 0.94$.

Figure 3.7: Static experiment results.

was acquired using ten (10) uni-axial accelerometers (see table 2.2 and Figure 2.6 for technical information and dimensions, respectively), with sampling rate of 1000 Hz, placed on the corner fittings of the scaled model (as depicted in Figure 2.5a). The pseudo-impulsive force was applied in direction x and y, alternately. An impact hammer test characteristic signal is depicted in Figure 3.9. Figure 3.9a is a graphic representation of the experiment time domain, where the transient nature of the signal is evident. Moreover, the magnified version of the same signal (Figure 3.9b) presents a clear inference about the system damping. The frequency components of the acceleration signal was analysed through power spectrum function. Results of power spectrum analysis of accelerometers in x and y direction, are depicted in Figures 3.10a and 3.10b, respectively. Results are summarized in table 3.10. Before continuing to the next section, we would like to clarify another point. Because the most important phenomenon regarding container is racking, acceleration for z direction, recorded with four (4) accelerometers, is omitted (another important point about vertical direction is presented in section 3.8).

3.8 Considerations about the Scaled Model

It is interesting to note that in all eight cases of this study the differences, when existing, were within the range expected considering limitations imposed by the study itself. However, is important to properly address every case separately. Following our expectations, this study did not find a significant difference between target and numerical values for length, width and height parameters. These are, without any doubt, the easiest parameters to match. Consequently, discussion about dimensions will not be considered during this section. Following, the next geometric similitude parameter used: mass, the observed difference in between target and numerical model mass was not significant either: about 1.1%. But again, following the example of the first parameter, adjusting it is relatively simple task. The next geometric parameter used for comparison was moment of inertia with respect of the three main axis of the scaled model. Differences regarding moment of inertia about container's longitudinal, transverse and vertical axis are 3.35%, 9.93% and 11.44%, respectively. For an overview about the values refer to table 3.8.

For the remainder parameters tested, Figures 3.11 and 3.12 display the data obtained for the scaled model, in two situations: experimental and numerical. The objective of these figures is to graphically represent a comparison between the target values and the values obtained from simulation (F.E.A.) and experimentation (please refer to tables 3.8, 3.9, 3.10 for an overview of values). As a general trend, there was close data agreement in all procedures, for the range of cases performed during our study. Such agreement, present in all parameters up to now, evidences a consistency in our research design. Important

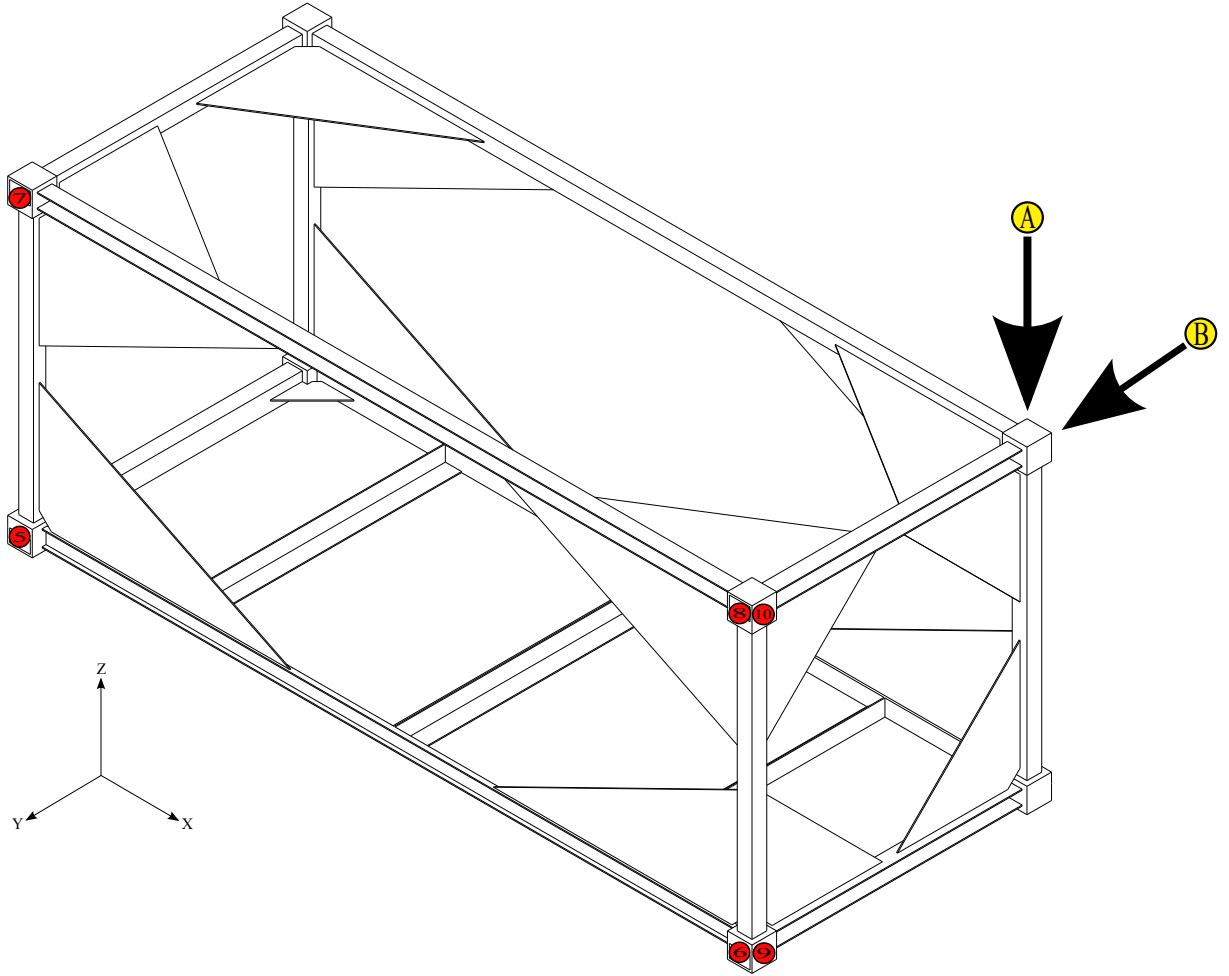
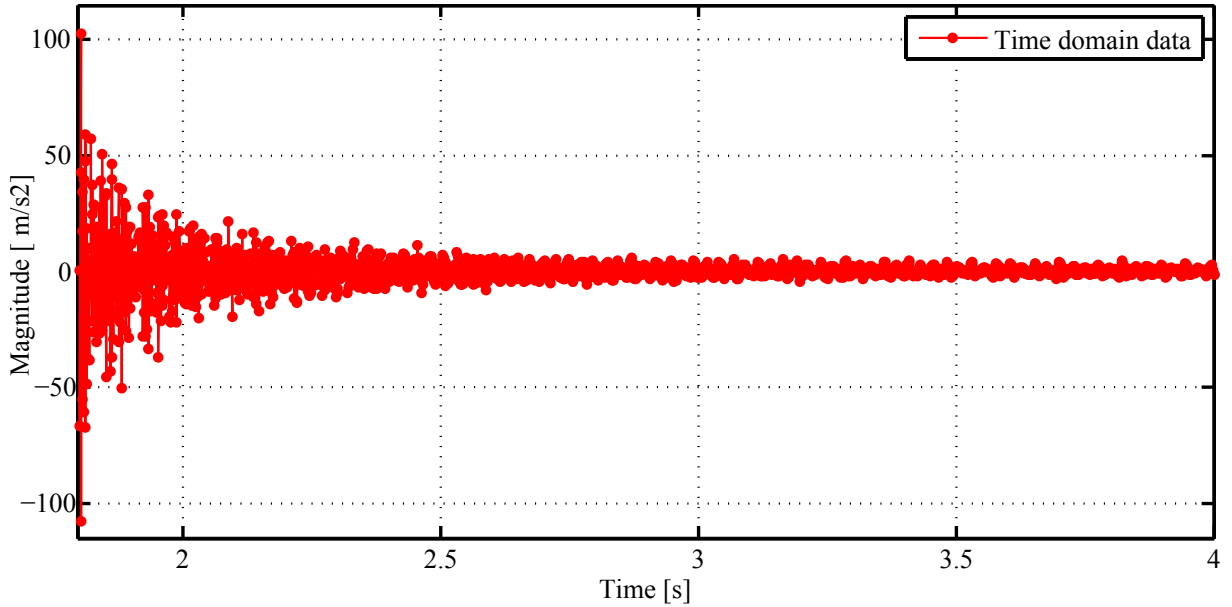


Figure 3.8: Placement of the accelerometers on the scaled model.

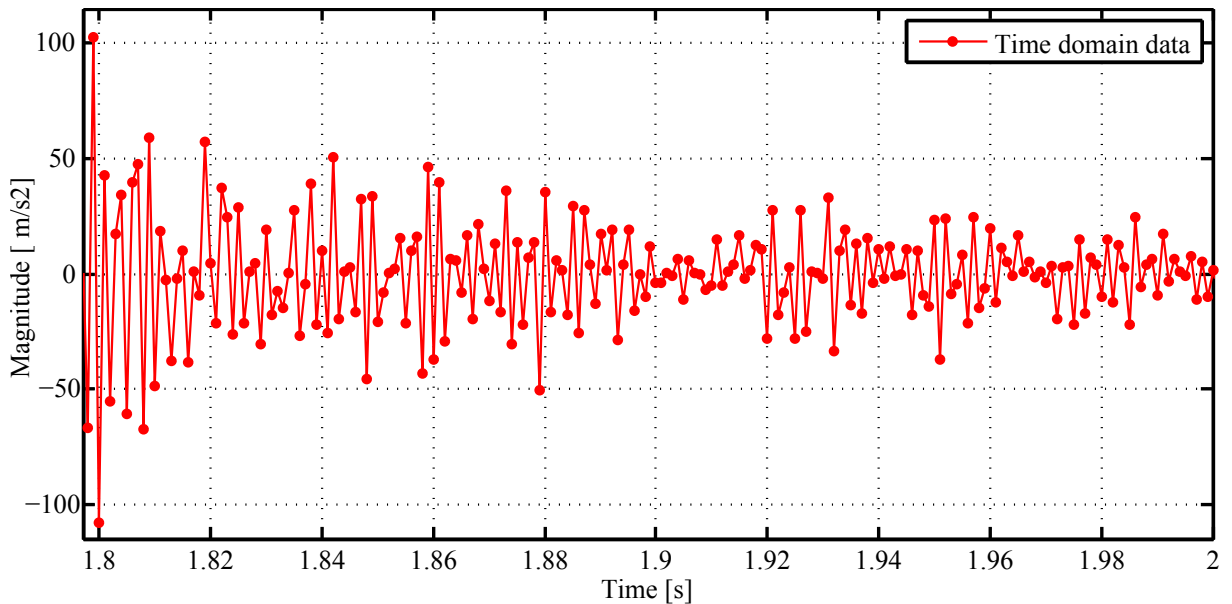
Table 3.8: Comparison of the geometric similitude parameters

	Target values	Numerical model
Mass [kg]	36.41	36.82
Moment of Inertia	I_{xx} [kg/m ²]	3.68
	I_{yy} [kg/m ²]	11.55
	I_{zz} [kg/m ²]	11.22

to emphasize that the parameters chosen for the range of this study, represent what, we believe, are the dominant physical effects regarding a container structure. Although we are completely aware of the fact that real containers during marine transportation are under the influences of many other physical parameters, their selective choice can be excessively lengthy and overwhelming, involving a lot of theoretical and conceptual discussion. Thus, dominant effects were prioritized.



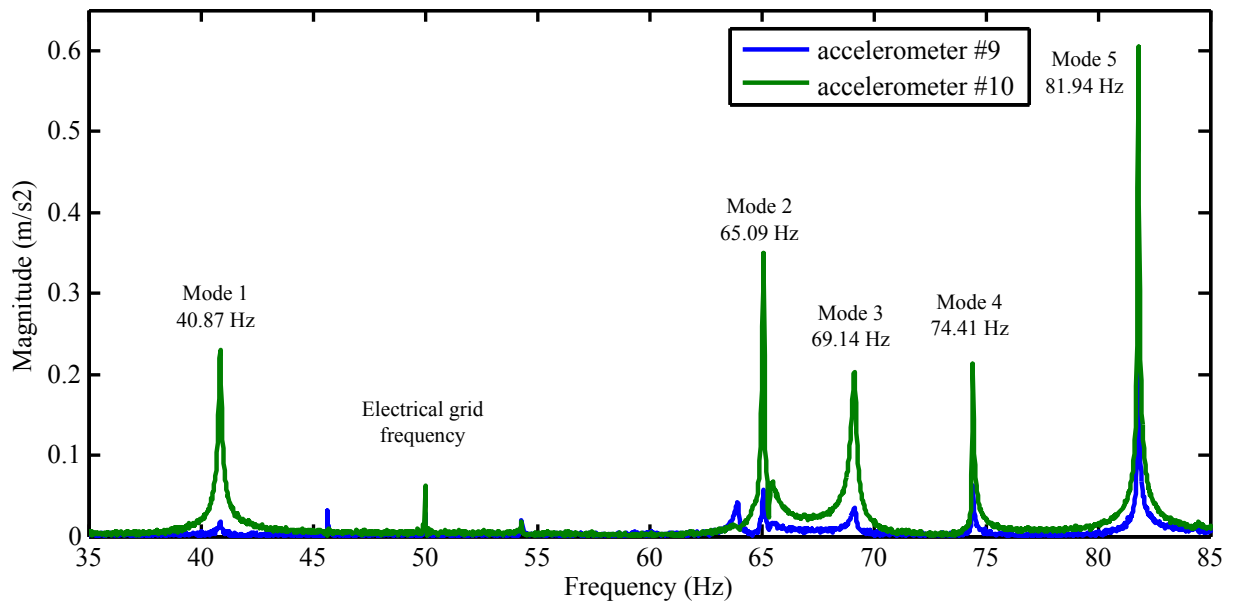
(a) Time domain.



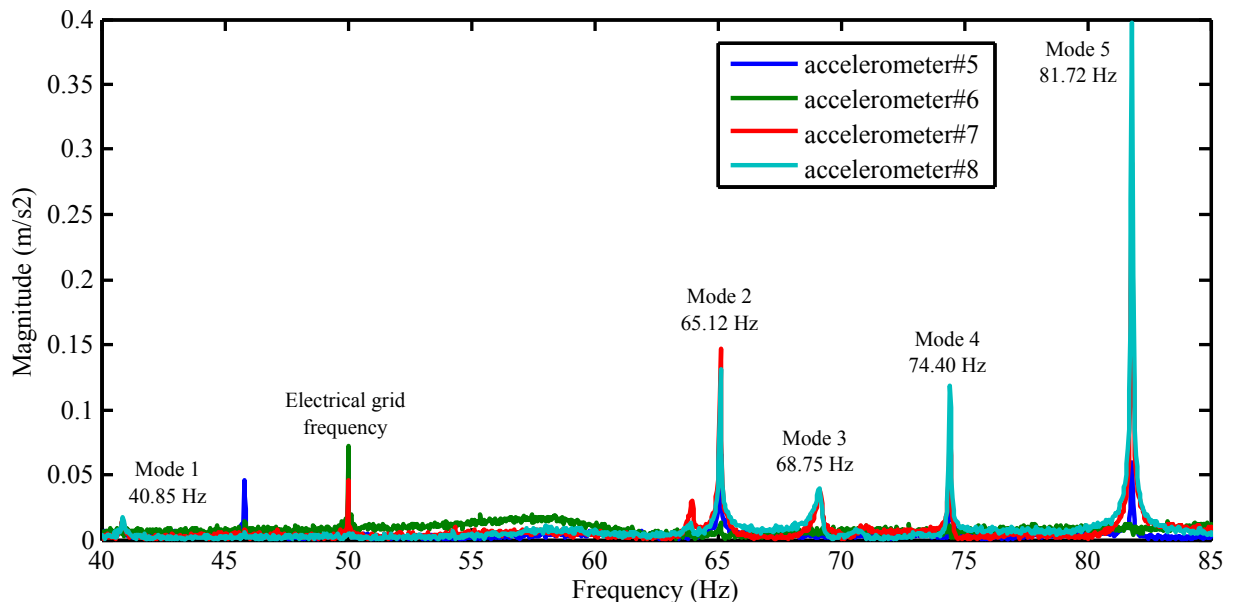
(b) Magnified time domain.

Figure 3.9: Characteristic signal obtained in the impact hammer test.

The stiffness graphs in Figure 3.11 further illustrate that differences are non-significant. Difference regarding stiffness of racking of open side between target and numerical values is 3.05 %. On the other hand, difference for the same condition between target and experimental value is even smaller 0.83 %. The following condition, i.e., stiffness of racking of closed side, showed difference between target and numerical values in the order of 4.76 %, whereas difference for the same condition between target and experimental value is 9.52 %. Longitudinal stiffness difference between target and numerical value is 6.37%, lead-



(a) Power spectrum for X direction.



(b) Power spectrum for Y direction.

Figure 3.10: Eigenfrequencies obtained from the impact hammer test.

ing to the same inference as the two previous cases: non significant. For the remainder case: torsional stiffness, difference between target and numerical value is 26.40%. This difference is significantly higher. However, based on the fact that racking related values presented good concordance, and represent dominant effect, such value was considered appropriate. Moreover, that difference is acceptable in the presence of the various uncertainties regarding container's full scale parameters, like different manufacturers standards, processes, welding, etc.

3.8 Considerations about the Scaled Model

Table 3.9: Comparison between target, numerical, and experimental data of scaled model

Stiffness	Side	Target	Numerical	Experimental
Racking [MN/m]	closed	3.61	3.72	3.58
	open	0.21	0.20	0.23
Longitudinal [MN/m]		3.61	3.84	np
Torsional [kNm/rad]		12.50	15.80	np

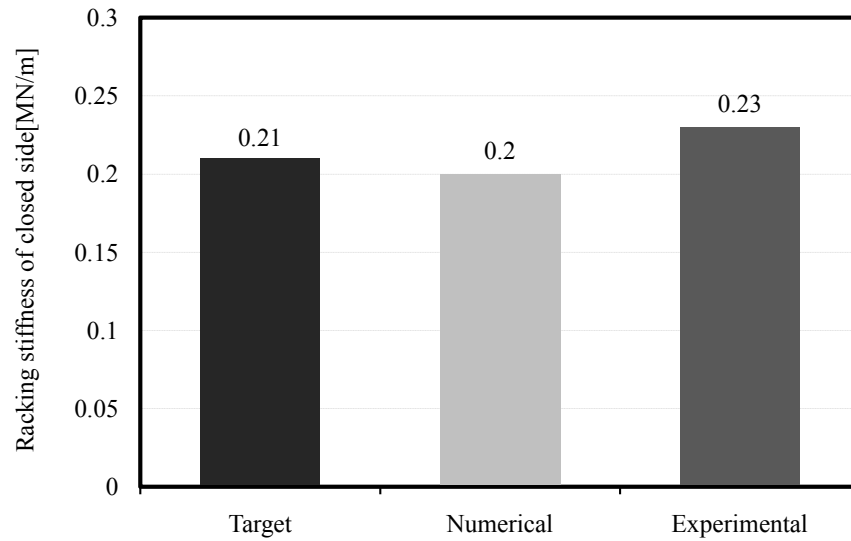
The last part of the study analyzed the frequency components of the structure. Following the example of the first part of the study, frequency related results presented concordance even better than the static cases (please refer to table 3.10). Among the five modes considered for our validation process, differences range from 0.3% to 4.94 %. First, second, third, fourth and fifth modes showed differences of 4.12%, 1.89%, 4.94%, 0.32%, and 1.12%, respectively. Figure 3.12 illustrates frequency comparison for the five first modes between numerical and experimental values.

Table 3.10: Eigenfrequencies obtained from the impact hammer test and frequency extraction numerical analysis

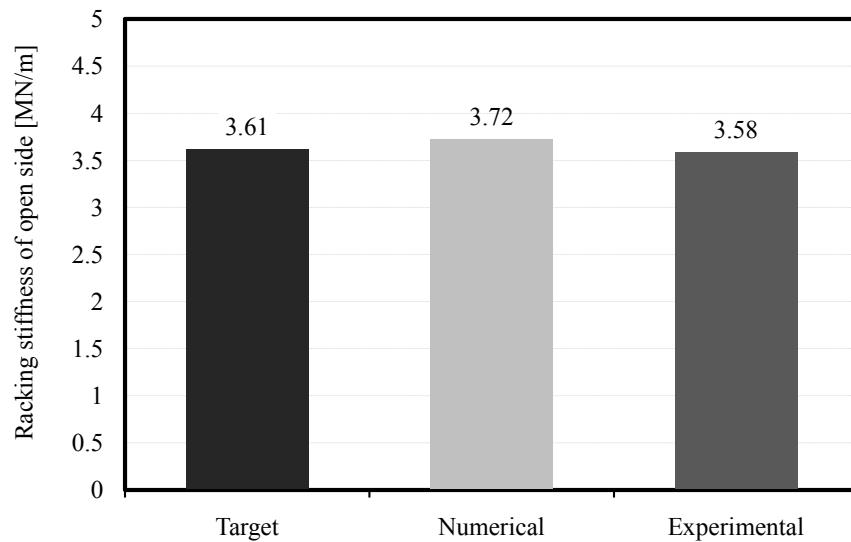
Mode	1	2	3	4	5
Frequency [Hz]–Experimental	40.86	65.11	68.95	74.41	81.83
Frequency [Hz]–Numerical	39.24	66.37	72.54	74.17	82.76

This part of the project was undertaken to design and evaluate a scaled model of a 20 ft container. The study has shown that our approach to validate the proposed design showed good agreement for static and frequency evaluation considering numerical and experimental data. This finding has important implications for development of more complex studies based on the methodology employed in the current study. Moreover, the scaled model developed presents itself as a valid tool to simulate the behavior of full-scale containers in a wide gamma of situations. In this panorama, it may contribute significantly to the understanding about container stack dynamics, an area where intuition and old standards are still preferred over more solid scientific principles.

Finally, some important limitations must be considered. The most important limitation regards the minimum value for vertical stiffness according to ISO standards: 188.44 MN/m. According to Froude scaling, the minimum value for the scaled model must be



(a) Comparison for racking stiffness of closed side.



(b) Comparison for racking stiffness of open side.

Figure 3.11: Summary of results for static cases studied.

10.6 MN/m. However, the vertical stiffness of the proposed geometry exceeds the full-scale value by a factor up to three (3). This limitation can affect greatly the output of a buckling analysis, inducing to wrong predictions for such case. However, this difference has to be accepted in favor of the structural integrity of the rear end frame. The other disparity observed in our proposed design, about the torsional stiffness, was discussed early in this section.

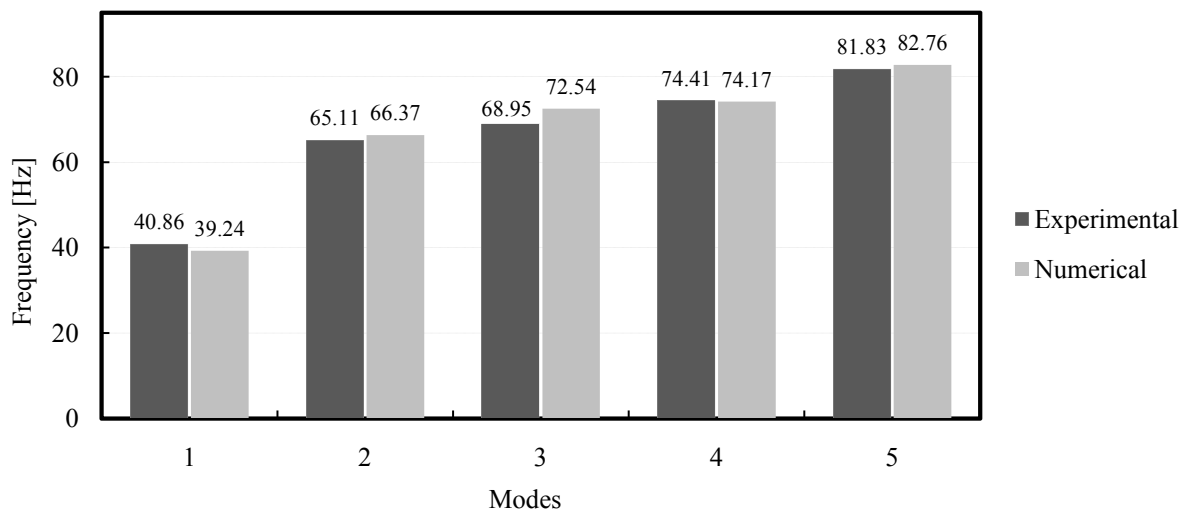


Figure 3.12: Frequency comparison between experiment and finite element analysis.

Chapter 4

Experimental Investigation for the 7x1 and 7x3 Cases

Calibration of the numerical model was performed through a series of experiments that will be explained shortly in sections 4.1 and 4.2. Single stack experiments aimed understanding the effect of some basic variables, described in each pertinent section, whilst three stacks configuration has the main goal of identifying contact.

4.1 Seven-tiers Single Stack (7x1)

The study limited the analysis of displacement of top corner of some individual containers. Furthermore, for means of comparison the highest container was used for evaluation purposes. As mentioned in section 2.5, displacement-time response data was analyzed using three techniques: time history, coefficients of Fourier expansion and RMS value comparison.

All vibrational tests described here were performed using a shaking table (Figure 2.3) with technical specifications summarized in table 2.1. The shaking table test employed seven scaled models of a 20 ft ISO freight container arranged in a single stack (Figure 4.2). The structural and geometrical details of the model were exhaustively discussed in section 3. This arrangement was used to perform dynamical tests with controlled driving excitation employing a sinusoidal function where frequency and amplitude were fixed for every trial. Furthermore, three physical variables were idealized to provide extra information about the system's behavior: dead weight added to the system (Figure 4.1b), shaking table horizontal rotation (Figure 4.1c) and twist lock gap size (Figure 6.3). A quantitative list of the experimental control variables is presented in table 4.1. Additionally a brief explanation and a summary of these variables is presented in section 2.4.

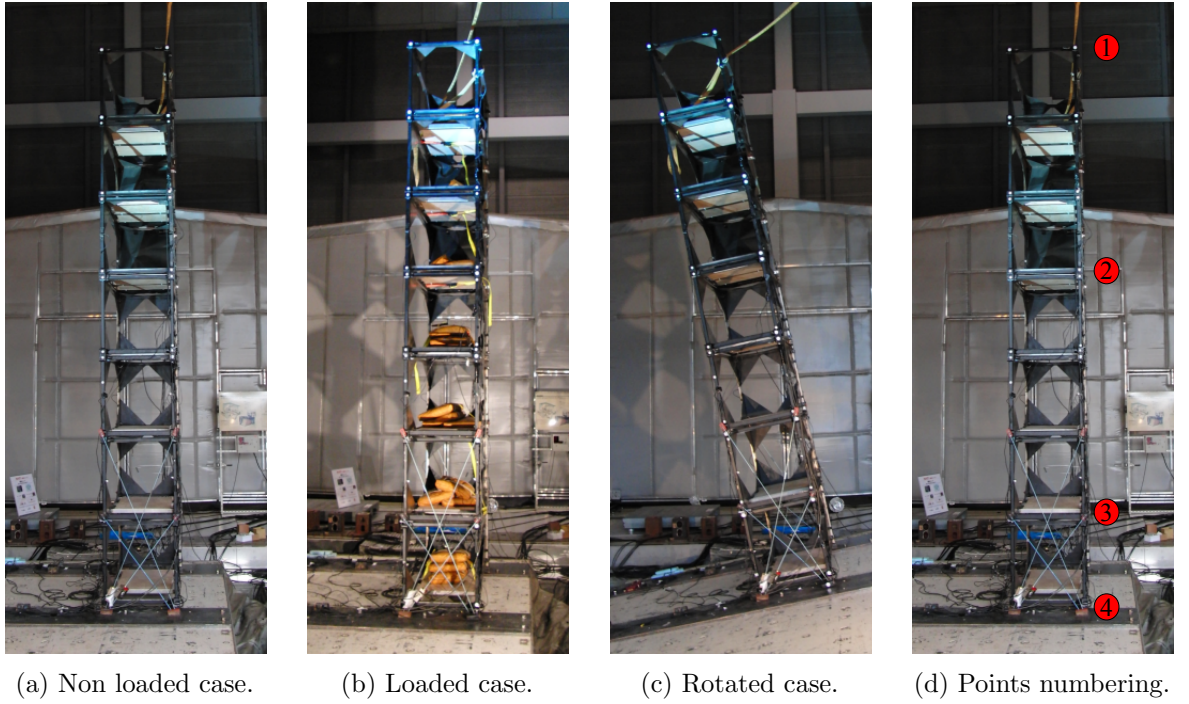


Figure 4.1: Physical parameters and labeling.

Regarding experimentation, each scaled container was linked to its adjacent, upper and lower, counterpart through a bolt placed in the corner castings as can be seen in Figure 6.4a. The stack was fixed to a socket welded to the shaking table in the same fashion depicted in Figure 6.4b. Regardless of lashing system, this arrangement emulates the same conditions faced in a regular securing process administrated before container transportation. Three reflexive markers positioned on the right top corner casting of the scaled models in the first, fourth and seventh tiers, corresponding to their open sides, were used to record displacement using a high-speed camera (section 2.2.2). Moreover, and an extra marker was placed in the shaking table to acquire the driving excitation signal. The sampling rate of the high-speed camera was set to 500 Hz. The numbering of the reflexive markers follows the schematics showed in Figure 4.1d. Finally, the recorded data was filtered using a low-pass technique described in section 2.6.

Table 4.1: Experimental parameters (7x1)

Amplitude [mm]	2	4	6
Frequency [Hz]	0.5	1	2 5
Gap [mm]	1	2	
Payload [kg]	0	45	
Rotation [degree]	0	2	5 10

Table 4.2: Terminology used to refer to the displacement-time response data (7x1)

Description	Nomenclature
Displacement with relation to a fixed reference (ground)	<i>Local motion</i>
Subtraction of displacement-time driving excitation (point 4) and displacement-time response (point 1, 2 and 3)	<i>Relative motion</i>

4.2 Seven-tiers Three Stacks (7x3)

The study limited the analysis of displacement of top corner of some individual containers. Furthermore, for means of comparison the highest container was used for evaluation purposes. In other words, points 1, 4, 5, 10 and 11 were used to analyze the mechanical behavior of the system. As mentioned in section 2.5, displacement-time response data was analyzed using three techniques: time history, coefficients of Fourier expansion and RMS value comparison.

All vibrational tests described here were performed using a shaking table (Figure 2.3) with technical specifications summarized in table 2.1. The shaking table test employed seven scaled models of a 20 ft ISO freight container arranged in three stacks (Figure 4.2). The structural and geometrical details of the model were exhaustively discussed in section 3. This arrangement was used to perform dynamical tests with controlled driving excitation employing a sinusoidal function where frequency was used as variable. Because of the knowhow acquired during the 7x1 study, amplitude was fixed for every trial using the highest proposed value. Furthermore, one extra physical variable was idealized to provide extra information about the system’s behavior: shaking table horizontal rotation (Figure 4.1c). A quantitative list of the experimental control variables is presented in table 4.3. Additionally a brief explanation and a summary of these variables is presented in section 2.4.

Regarding experimentation, each scaled container was linked to its adjacent, upper and lower, counterpart through a bolt placed in the corner castings as can be seen in Figure 6.4a. The stack was fixed to a socket welded to the shaking table in the same fashion depicted in Figure 6.4b. Regardless of lashing system, this arrangement emulates the same conditions faced in a regular securing process administrated before container transportation. Three reflexive markers positioned on the right top corner casting of the scaled models in the first, fourth and seventh tiers, corresponding to their open sides, were used to record displacement using a high-speed camera (section 2.2.2). Moreover, and an extra marker was placed in the shaking table to acquire the driving excitation signal. The sampling rate of the high-speed camera was set to 250 Hz. The numbering of

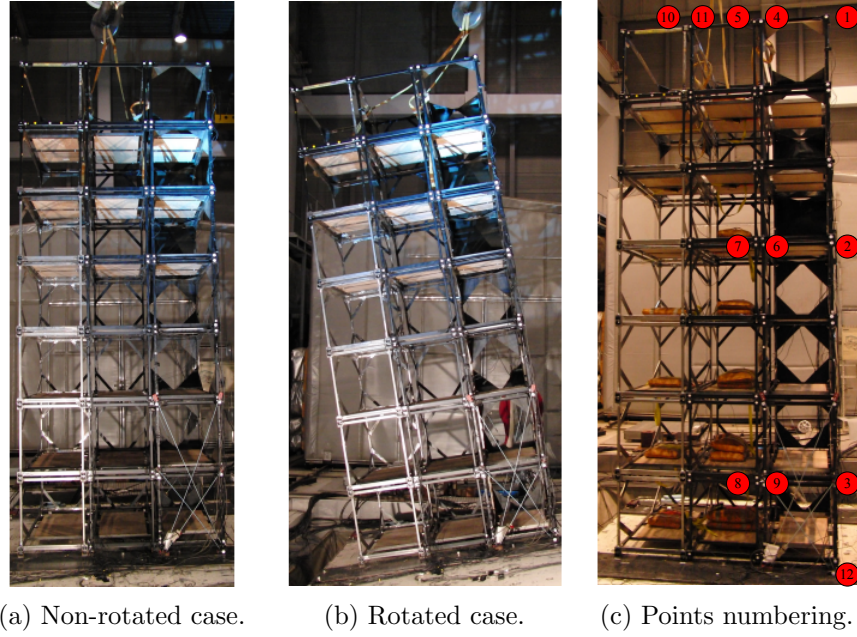


Figure 4.2: Physical parameters, labelling and details of the linking components.

the reflexive markers follows the schematics showed in Figure 4.2c. Finally, the recorded data was filtered using a low-pass technique described in section 2.6.

Table 4.3: Experimental parameters (7x3)

Amplitude [mm]	6		
Frequency [Hz]	2		
Gap [mm]	1		
Payload [kg]	0		
Rotation [degree]	0	2	10

Table 4.4: Terminology used to refer to the displacement-time response data (7x3)

Description	Nomenclature
Displacement with relation to a fixed reference (ground)	<i>Local motion</i>
Subtraction of displacement-time driving excitation (point 12) and displacement-time response (points 1 to 11)	<i>Relative motion</i>

Chapter 5

Numerical Model

5.1 Container Model Structure

Each numerical model (scaled) was considered as steel frames sections compounded of circular and pipe beams. Details of every section are described in table 5.1. Nine nodes define each scaled container: four on the corners and one in the geometric center. This node is employed to adjust moments of inertia and mass for each container using the experimental model values as target. Additionally, this node is connected to the bottom nodes through springs. Additionally, numerical model was calibrated statically and dynamically to comply to structural stiffness and eigenvalue range of the design used for experimentation and described in section 3. The material was assumed an isotropic, linear elastic material with the following properties: Young's modulus $E=210$ GPa, Poisson ratio $\nu=0.3$ and density $\rho=7850$ kg/m³, characterizing steel as mentioned earlier in this section. Furthermore Figure 5.2 depicts the basic geometry of each individual container that compound the numerical model for the seven-tier single stack (7x1) and seven-tier three stack (7x3) cases.

5.2 Twist Lock Non-Linear Behavior

As mentioned in section 1.2.2, in spite of its importance and broad usage, twist lock's technical requirements only account for basic features like dimensions and minimum structural stiffness, neglecting more complex dynamics responses like effect of transient forces on it. Moreover, standards only account for the component itself and do not infer about its role as a link in the container securing system. In addition, recent increases in container losses have heightened the need for a better comprehension of its dynamical behavior and the main factors behind its mechanisms, which it would lead to prevention rather than economical minimization. In this panorama, studies regarding twist lock dynamics is an

Table 5.1: General information about the frame section

Components	Profile	Diameter [mm]	Thickness[mm]
Bottom cross	circular	3.5	–
Closed end	circular	2.5	–
Lateral cross	circular	2.5	–
Open end	circular	0.4	–
Top cross	circular	0.4	–
Longitudinal top and bottom rails	pipe	10	1
Transversal rails	pipe	10	1
Vertical rails	pipe	10	1

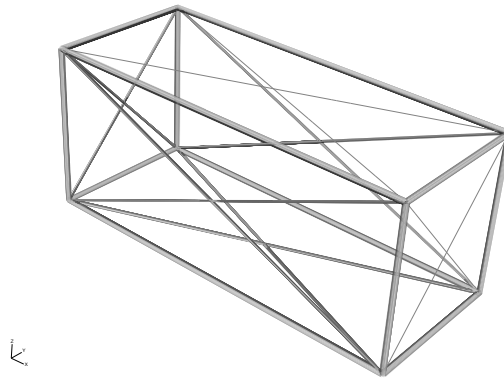


Figure 5.1: Profile of the beams used for the numerical model.

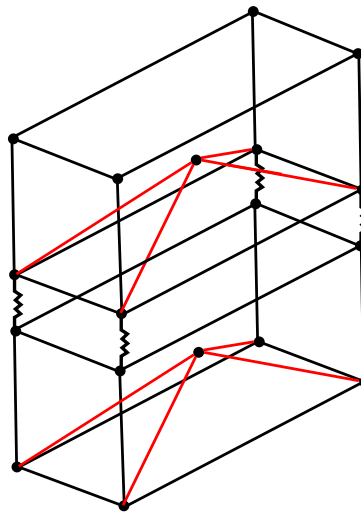


Figure 5.2: Details of the nodes, non-linear springs connecting individual containers and springs (red) used to connect the geometric center.

important step to understand and simulate properly container stack dynamics. Thus, this section will describe an attempt to clarify its nuances and mechanisms using a well established numerical method: finite element analysis, and an well known experimental technique: shaking table testing. This experimental approach has the advantage of allowing a great deal of control over vibrational variables like amplitude and frequency, as well possibility of vibration input following special functions (transient, non-transient, random, recorded, etc.). Although the primary goal of this section is to model the twist lock mechanical behavior, its secondary purpose is to provide a auxiliary mathematical tool to model container stack dynamics. The protocol adopted to find an approach to simulate twist lock's mechanical behavior is explained in the next sections.

5.2.1 Experimental Investigation

5.2.1.1 Slamming Test

The experiment was performed using an empty 20 ft ISO dry freight container (NYK-MTI, Japan) fixed to the shaking table through its corner castings using semi-automatic twist locks (KOEI Kinzoku Industrial) emulating the same conditions faced in regular fixing process before container transportation. Three types of instruments were used during the experimental investigation: shaking table, accelerometers and laser displacement meters. Please refer to Figure 5.3 for positioning of the transducers and other experimental settings. Experimental apparatus is described in sections 2.2.1 and 2.2.2. The system was excited using controlled displacement with a transient characteristic (step function). These displacements were applied on the container in the vertical direction inducing three different velocities characterizing each trial: 0.6 m/s, 0.7 m/s and 0.8 m/s. This kind of transient excitation was chosen because is close to slamming impact, caused by pitching in adverse sea condition, observed during marine transportation. The excitation history is shown in Figure 5.4.

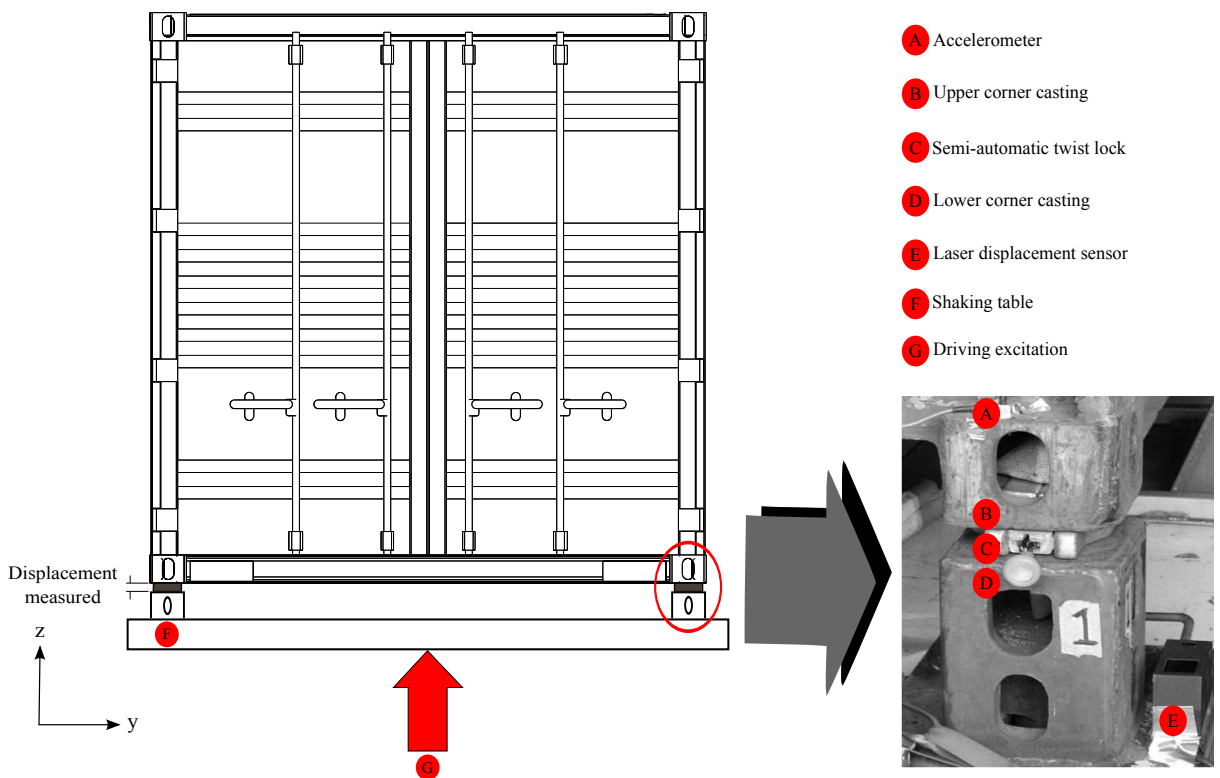


Figure 5.3: Figure at left side is a schematic representation of the experimental settings (door view). The one at right side is a magnified view of the region of interest in this study (corner 1).

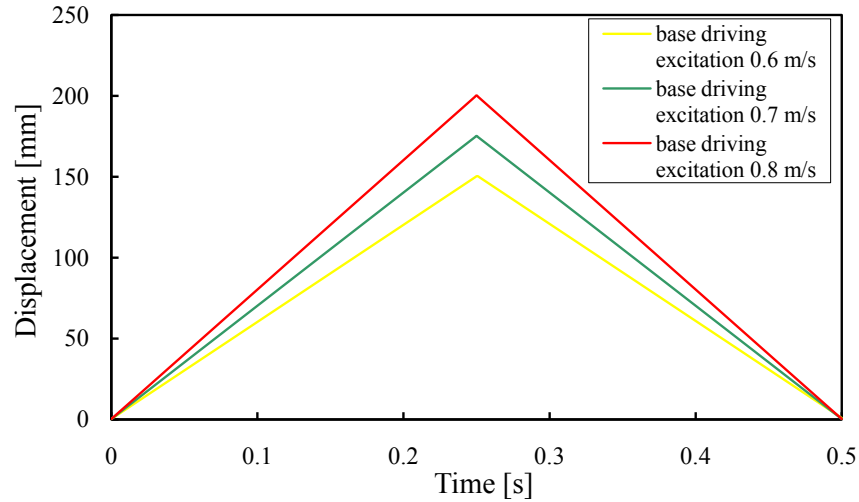


Figure 5.4: Step function used as driving excitation (vertical direction).

5.2.1.2 Tensile Test

Acquire the longitudinal stiffness of the twist lock used for our experiment is an essential step to provide an accurate value to be used in the numerical model. In order estimate this value, an uni-axial tensile test was performed with the same model of twist lock used in the experiment. Result of the uni-axial test performed is depicted in Figure 5.5. Stiffness used for the linear region of the curve depicted in Figure 5.7 was calculated based on the proportional linear region of the experimental data, corresponding to the blue line in Figure 5.5.

5.2.2 Numerical Analysis

A simplified 3-D finite element model of the system: a 20 ft ISO standard size container, twist locks and shaking table was developed using a commercial software (ABAQUS version 6.7, Dassault Systems). Further details of the model are depicted in Figure 5.8. Container was considered an isotropic solid section, consisting of a linear elastic material with the following properties: Young's modulus $E=210$ GPa, Poison ratio $\nu=0.3$ and density $\rho=7850$ kg/m³. The main object of our study, twist locks were modeled as non-linear springs. Furthermore, horizontal and vertical gaps between twist lock and corner castings (see Figure 5.6 for details) were incorporated into the model by describing the backlash phenomenon, i.e., region where twist locks exhibit no stiffness. The mechanical property of the non-linear spring is shown Figure 5.7, where the stiffness of the twist locks were estimated through a uni-axial tensile test described in section 5.2.1.2. At last, shaking table was considered a rigid body where the driving excitation, following

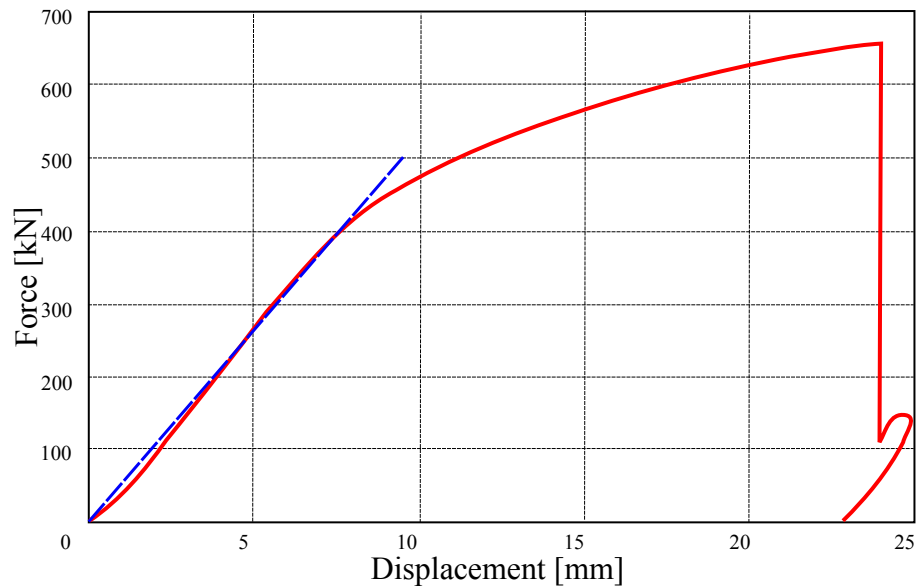


Figure 5.5: Result of the tensile test of the twist lock used for experimentation. Line in blue represents the linear limit where the stiffness value was calculated.

same conditions imposed in experiments (see Figure 5.4), was applied to it. To provide damping, discrete damping elements, denominated dashpots, were included in the 3-D model following the same line of action of the non-linear springs. Finally, dynamic numerical analysis accounted for geometric non-linearity in a implicit integration scheme.

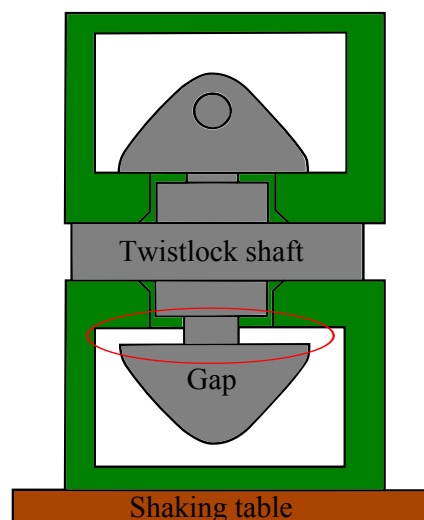


Figure 5.6: Cut view of corner casting-twist lock system (corner fittings or corner castings are depicted in green).

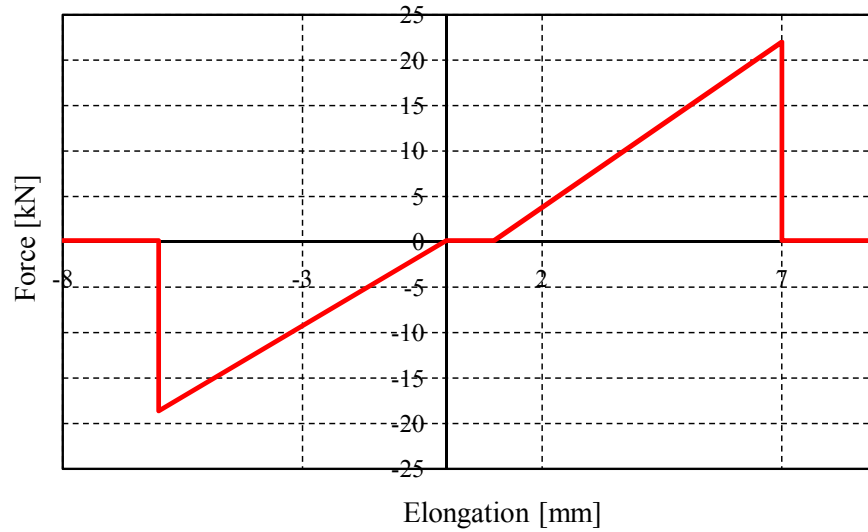


Figure 5.7: Non-linear spring relation used to represent twist lock mechanical behavior.

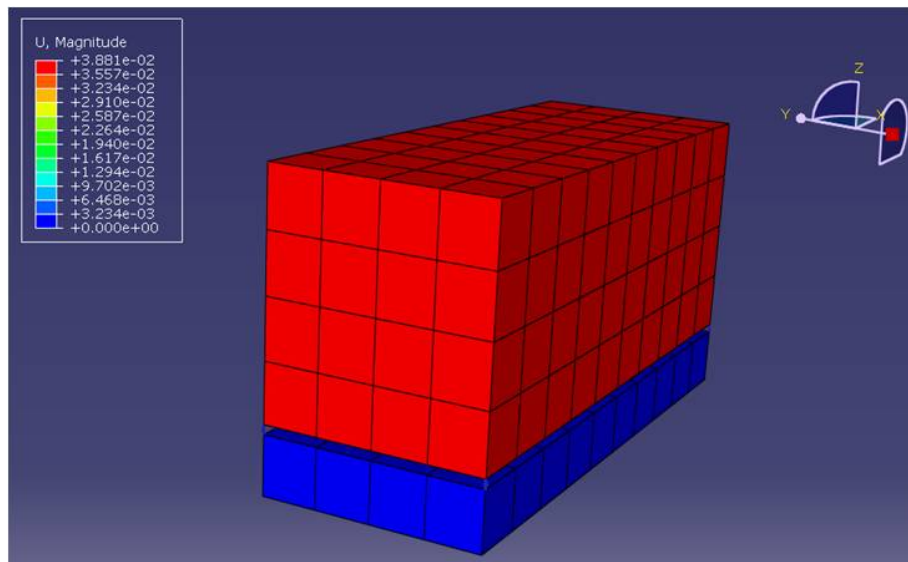


Figure 5.8: Finite element model (20 ft container in red and shaking table in blue). Connecting elements are non-linear spring and dashpots.

5.2.3 Data Analysis

Elongation history of twist lock was calculated using the finite element model and compared to experimental data to validate the numerical approach for the twist lock. As can be observed from the Figure 5.10 simulation and experimental results have similar patterns. However, there some small differences between experimental and numerical results. Differences observed in Figure 5.10 are caused by the way model and real object

experienced the transient displacement applied to the system. Shaking table is activated through a series of hydraulic pistons, which naturally will present a response delay caused by mechanical friction. In the other hand, numerical model does not include this physical phenomenon. Thus, the response curve is prone to present a higher slope angle inclined for the duration of the excitation. In other words, numerical velocity and acceleration present higher curve slope when compared to experimental data. Moreover, numerical model considers twist locks as non-linear springs with zero stiffness for the gap size considering tension region of the curve. For compression, this component behaves linearly so there is the appearance of the successive peaks after the main event until the damping included in the model finally forces the system to rest. Some discrepancies were observed for the elongation measure in every corner. Such differences are attributed to a non-symmetrical distribution of the weight in the real container according to the geometric center of it. Thus, every twist lock experiences slightly different elongations for every corner (please refer to Figure 5.9).

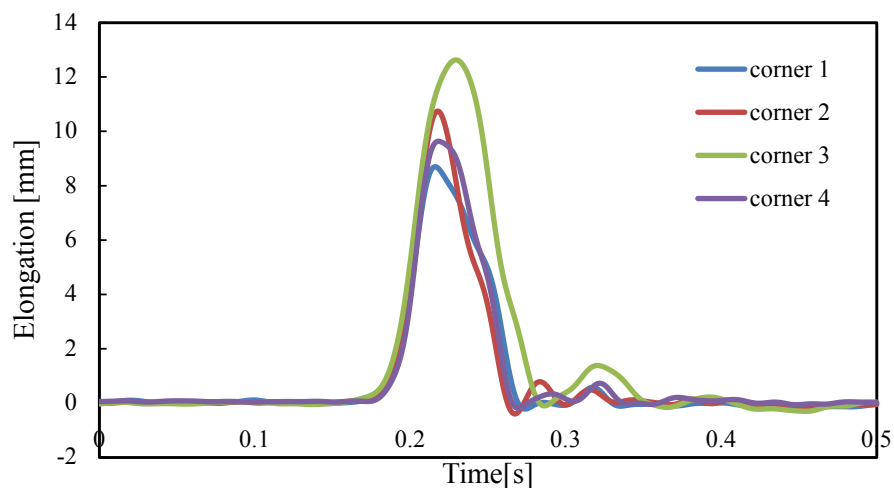


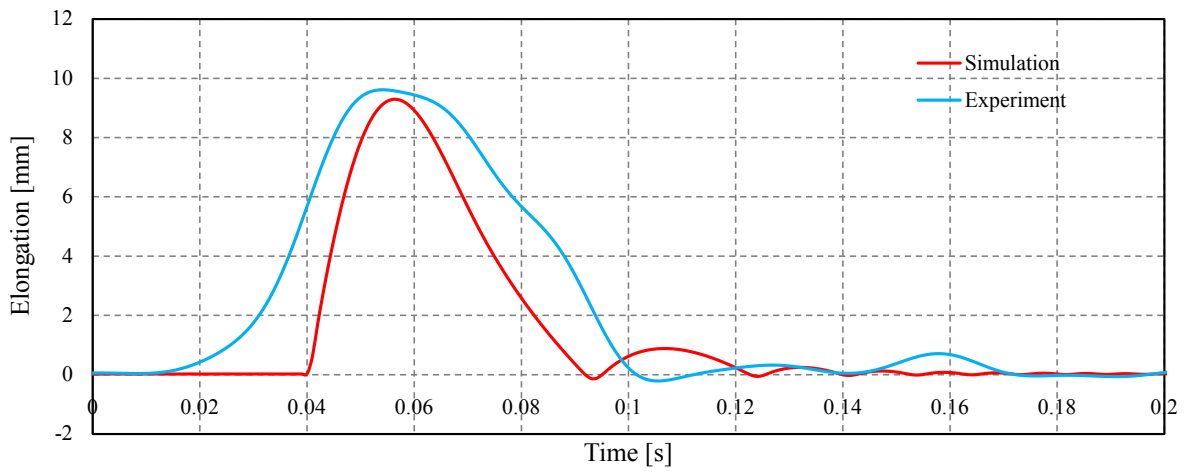
Figure 5.9: Discrepancies observed for experimental data.

There is a proportional relationship between the speed of excitation and the elongation measured in the twist locks, i.e., increase in velocity induces increase in the elongation. Since the excitation was given only in the vertical direction, the gaps existing in the remaining directions, between twist locks and corner castings, do not affect the stack behavior in these directions. It is obvious that these gaps will be active and effective for the other loading conditions such as racking. Because of gaps, force flows pass over from lower corner casting to upper corner casting through the shaft of twist lock directly without delay at compression and move together as one body. However during tension, first gaps are closed and later force transmission starts. The detail of the twist lock-corner

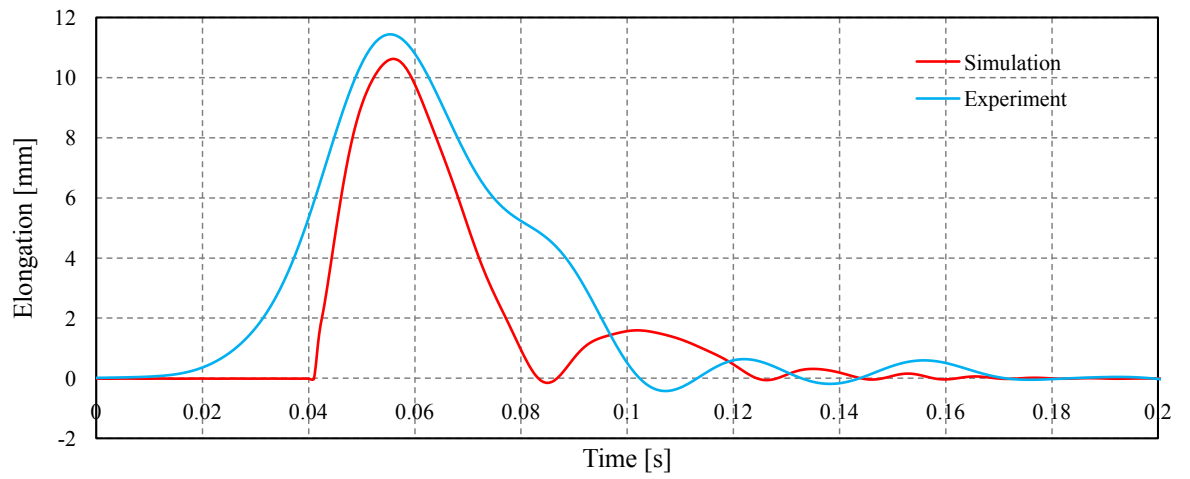
casting connection is shown Figure 5.6. Acceleration data was used to double check the expected mechanical behavior measured through displacement-time response analysis.

The present part of this study was designed to determine the mechanical behavior of the twist lock in a really usual situation faced during maritime transportation. The comparison between numerical and experimental data presents enough body of evidence to ensure that twist lock fundamentals were completely understood. Moreover, such behavior may be described by a mathematical relationship. Undoubtedly, this is one of the most significant findings to emerge from this study. An implication of this is the possibility of simulation of a more complex situation involving the system here described. For instance, this approach can be used to investigate behavior of a container stack considering dynamical loads. Although, analysis considering the system described in this paper are still in its infancy, mainly because of omission of other securing system components, the importance of this step cannot be neglected: twist lock behavior summed to the impact between adjacent stacks are the main responsible for non-linearities observed in the system. Thus, numerical models must include both phenomena in order to present a realistic estimation of container stack dynamics, which would be a major step to identify the causes of some problem faced by the marine transportation industry, e.g., container losses, that have never been approached before.

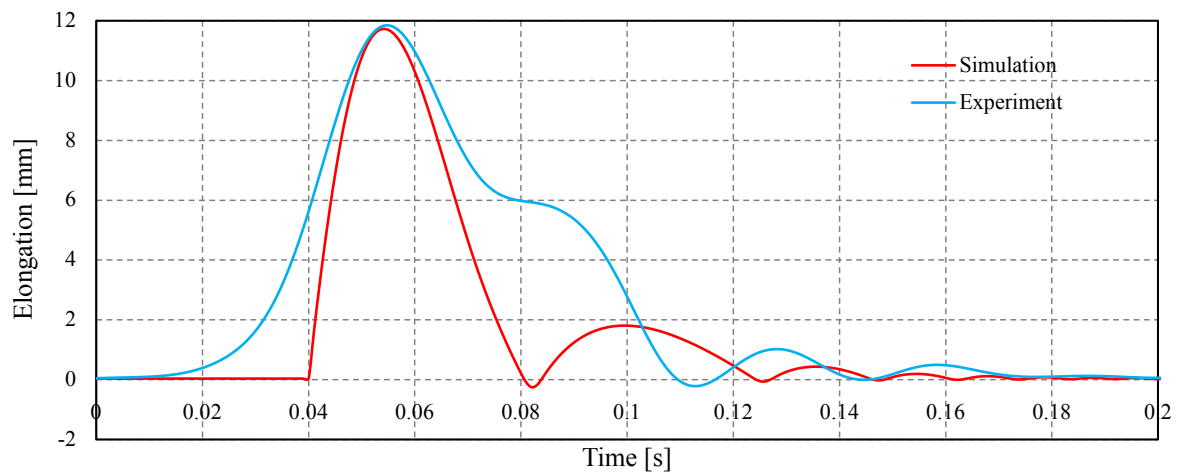
5.2 Twist Lock Non-Linear Behavior



(a) 0.6 m/s case.



(b) 0.7 m/s case.



(c) 0.8 m/s case.

Figure 5.10: Comparison between experimental and numerical data.

5.3 Damping

Hitherto, our knowledge regarding damping is fairly limited, especially when compared to our comprehension about mass and stiffness systems. As a result, predicting vibration parameters regarding damping is actually a difficult task in real situations [49]. However, neglect damping when modeling or experimenting is an unrealistic assumption, because it is responsible for controlling the dynamic response and attenuation in structures subjected to dynamical regimes. Additionally, conventional engineering materials like steel and high strength aluminum alloys provide small amounts of internal material damping, not enough to prevent large amplification at or near resonant frequencies. Thus, include damping in the analysis is a crucial step to properly model a real structure, and even for experimental purposes, damping assumption is important.

There are different methods to define damping in order to be used in practical situations like experiments, e.g., logarithmic decrement commonly used in vibration tests, or energy loss per cycle for cyclic tests. Moreover, there are some others approaches for damping as complex modulus, rise-time or spectrum ratio for wave propagation analysis, only to mention [68]. Theoretically, damping assumptions used for single degree of freedom systems can be extended to multi degree of freedom systems. Among these theoretical approaches, three are notably in use: viscous damping, Coulomb damping and structural damping. Viscous damping is introduced in the structures through a viscous damping element called dashpot, in which the force is assumed to be proportional to the relative velocity between the two ends of it. In case of complex structures, like the one modeled in this study, dashpots did not present a good option. The inclusion of damping through dashpots had as consequence the appearance of beat phenomenon and excessive attenuation of the response, which is completely unrealistic. These two effects are shown in Figure 5.11 below.

To better understanding and illustrate the advantage of using Rayleigh damping instead of discrete damping elements, it is better to plot displacement curves for the same model built considering damping in two types, mentioned a priori. The curve in blue represents our model considering discrete damping. In the other hand, the curve in red represents damping using a proportional form, in this case Rayleigh damping, which is characterized by two parameters: alpha (α) and beta (β). Both curves are depicted in Figure 5.11. A formal treatment for this kind of damping will be explained in the next paragraphs. As can be seen in the Figure 5.11 inclusion of Rayleigh damping avoids both phenomena observed in the discrete approach (Figure 5.11). Notice that the signals have a phase difference. Nevertheless, in this section, rather than emphasizing this problem domain, we would like to present the advantage of one approach in detriment of the other.

Resuming damping assumptions, Coulomb damping, is caused by the relative motion of surfaces sliding against each other, i.e., bodies sliding in dry surfaces (Meirovitch, 1986), whilst structural damping is introduced to model energy dissipation of continuous elements. For means of numerical analysis of dynamical problems a theoretical approach is often used: Rayleigh damping also referred as proportional damping. Rayleigh damping is a mathematical tool frequently used to approximate continuous systems that are modeled by finite element method. The next section will present a mathematical treatment of this technique.

5.3.1 Rayleigh Damping

The differential equations of motion of a multi degree of freedom system can be derived from the equilibrium of forces associated to each degree of freedom, i.e., the differential equation of motion for the system is derived by Newton's second law. The system of second order differential equations obtained, and that governs the movement of structures subject to dynamic load, has the following form:

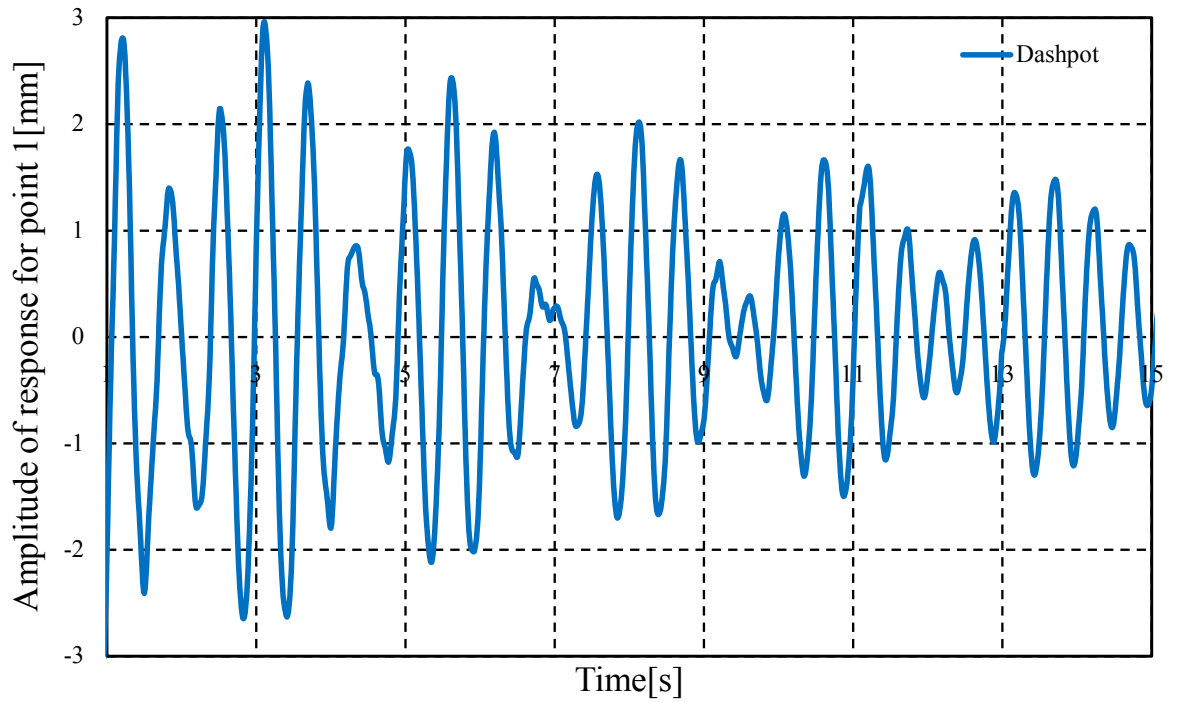
$$[M]\ddot{q}(t) + [C]\dot{q}(t) + [K]q(t) = F(t) \quad (5.1)$$

Where $[M]$, $[C]$ and $[K]$ are the mass, damping and stiffness matrices of the system, $\ddot{q}(t)$, $\dot{q}(t)$ and $q(t)$ are the acceleration, velocity and displacement vectors and $F(t)$ is the driving or excitation force. To assemble mass and stiffness matrices is a relatively easy task. However defining the damping matrix of the system can prove to be very difficult. Additionally, solving the system represented above, which has n size, is time consuming since they are coupled and the bandwidth is large [52]. Remembering that the system is solved for every time step which increases the overall time.

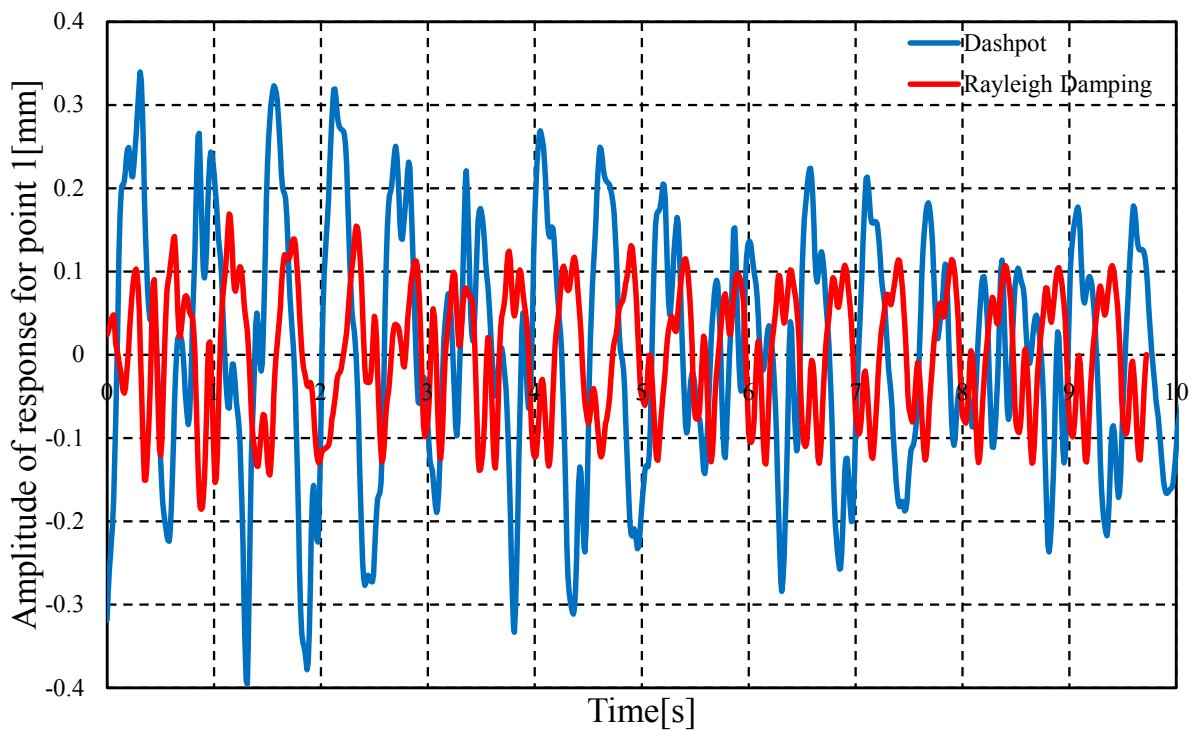
Researchers like [Bathe & Wilson](#) made some attempts to rewrite these equations in a way that they become decoupled. The main advantage of this process is that the total number of equations necessary to solve the system decreases drastically. Returning to the main topic: damping approximation. [Caughey & OKelly](#) proposed a damping with the following general form

$$[C] = M \sum_{k=0}^{p-1} \sigma_k ([M]^{-1}[K])^k \quad (5.2)$$

Which seems a reasonable approximation for small levels of damping. Nevertheless, the main outcome of this assumption is the decoupling of the system's equations guaranteed



(a) Horizontal direction case.



(b) Vertical direction case.

Figure 5.11: Comparison between dashpot and Rayleigh coefficients approach.

by the existence of real modes. If only two terms are considered in the above expression, i.e., in the special case where $p=2$, we obtain the classical Rayleigh damping form [62]

$$[C] = \alpha[M] + \beta[K] \quad (5.3)$$

Where α and β are constant coefficients. The main advantage of this approach is that it preserves the simplicity of the real normal modes as in the undamped case [2]. Consequently, the calculated response is greatly simplified because of the system's equation decoupling. The equivalent decoupled form of equation 5.2 is

$$2\zeta = \sum_{k=0}^{p-1} \alpha_k \omega_i^{2k-1} \quad (5.4)$$

It is easy to identify that the damping ratios depend on the natural frequencies to an odd power. Considering the two parameter equation 5.3, equation 5.4 yields:

$$\zeta = \frac{\alpha}{2\omega_i} + \frac{\beta\omega_i}{2} \quad (5.5)$$

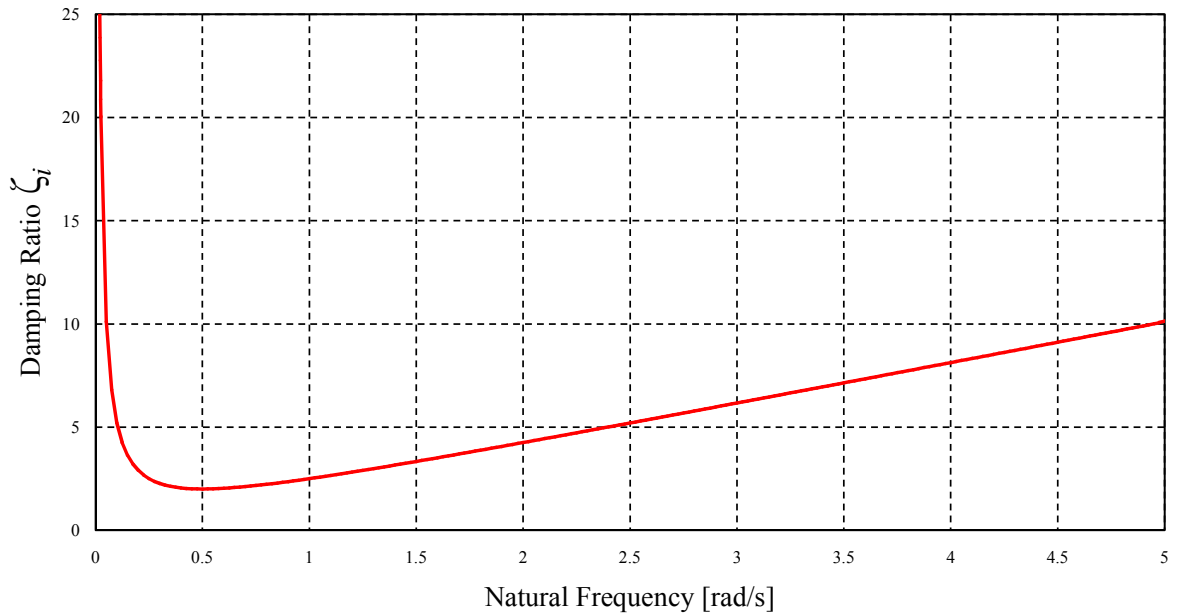


Figure 5.12: Relation of damping ratio (ζ_i) and natural frequency ($\alpha = \beta = 1$).

From the Figure 5.12 is easy to notice that for small frequencies the first term in equation 5.5 governs the overall behavior of the curve (hyperbole). In the other hand, when frequency range is increasing, the second term in equation 5.5 is responsible for dictating curve behavior (linear). The main concern here is for systems with very low fundamental

frequency where the curve is non-linear. Outside this region the curve converges quickly to a linear proportionality with frequency. Thus considering that the non-linear range is very small, non-linear effects from damping may be neglected. Consequently, damping ratio for every mode, from now on, will be considered linearly proportional to the frequency of the system. Considering a discrete set of frequencies $\omega_1, \omega_2, \dots, \omega_m$, and damping ratios $\zeta_1, \zeta_2, \dots, \zeta_m$ they have the following expression

$$\zeta_i = \frac{\zeta_m - \zeta_1}{\omega_m - \omega_1} (\omega_i - \omega_1) + \zeta_1 \quad (5.6)$$

Where ζ_1 and ω_1 are the damping ratio and natural frequency for the first mode, respectively. ζ_i and ω_i are the damping ratio and natural frequency for the i -th mode (for all $i \leq m$) and ζ_m and ω_m are the damping ratio and natural frequency for the last significant mode used in analysis.

The next step is to perform an eigenvalue analysis. For a system with n degrees of freedom there are n eigenfrequencies. However, many of these eigenfrequencies have only theoretical value; in other words, a real structure will never present most of the values in the eigenfrequencies spectrum and subsequent eigenmodes. Some researchers claim that for most structures the number of significant modes, mass participation majority (about 95%), is usually 3 at minimum and 25 at maximum [19].

Thus based on the eigenvalue solution and modal mass participation one can identify the number of relevant modes, in our notation m . After that, proceed to a frequency extraction (eigenfrequencies) for $2.5 m$. After that, one just has to assume the damping ratio range for the problem, i.e., choose ζ_1 and ζ_m . Using these values, interpolate other values of damping ratio for intermediate modes i ($1 \leq i \leq m$), using equation 5.6. The remainder damping ratios for modes greater than m ($m \leq i \leq 2.5 m$), can be extrapolated using

$$\zeta_i = \frac{\zeta_m - \zeta_1}{\omega_m - \omega_1} (\omega_i - \omega_m) + \zeta_m \quad (5.7)$$

One obtains a first set of data consisting of $\zeta_1, \zeta_m, \omega_1$, and ω_m . This set will be denominated half range damping ratio because α and β are calculated based only on the first m modes. Based on the above set of data obtain β from the equation

$$\beta = \frac{2\zeta_1\omega_1 - 2\zeta_m\omega_m}{\omega_1^2 - \omega_m^2} \quad (5.8)$$

Back-substituting the value of β in the expression

$$2\zeta_i\omega_i = \alpha + \beta\omega_i^2 \quad (5.9)$$

Table 5.2: Eigenvalue analysis results

Mode	Frequency[Hz]	Angular Frequency[rad/s]
1	1.62	10.15
2	4.86	30.54
3	5.91	37.12
4	11.36	71.40
5	11.79	74.10
6	14.65	92.02
7	20.74	130.34
8	22.70	142.60
9	24.50	153.93
10	29.28	183.99

Obtain the value of α . The second set of data consists of ζ_1 , $\zeta_{2.5m}$, ω_1 , and $\omega_{2.5m}$. This set will be denominated full range damping ratio because α and β are calculated based on all modes. Similarly the first set, one has to calculate the values of α and β using equations 5.8 and 5.9. A natural way to obtain a third is through the average between the two previous sets. To find the best values of α and β , one must plot the four sets based on equation 5.5 and check which data fits the best with the linear interpolation curve for the first m significant modes. The flowchart for this calculation is depicted in Figure 5.13.

The numerical values obtained from frequency analysis using ABAQUS can be seen in the Table 5.2. Physically, is possible to state that only the first three modes are relevant. Nevertheless, to use this approach more modes are needed.

Based on these values of frequency, one can calculate the damping ratio range based on a linear interpolation described in the previous paragraphs.

Using these values three kind of calculations were performed: half range, full range and average. Values for each approximation are presented in table

Next step is to plot these four curves and choose the best values for α and β . The four curves are depicted in the Figure 5.14. As mentioned before, the first modes are the most important ones, from a physical point of view. In this panorama, one has to choose the values of α and β that best fit these modes. From simple inspection the values in question are

$$[!]\alpha = 0.1198[s^{-1}], \text{ and } \beta = 0.0028[s] \quad (5.10)$$

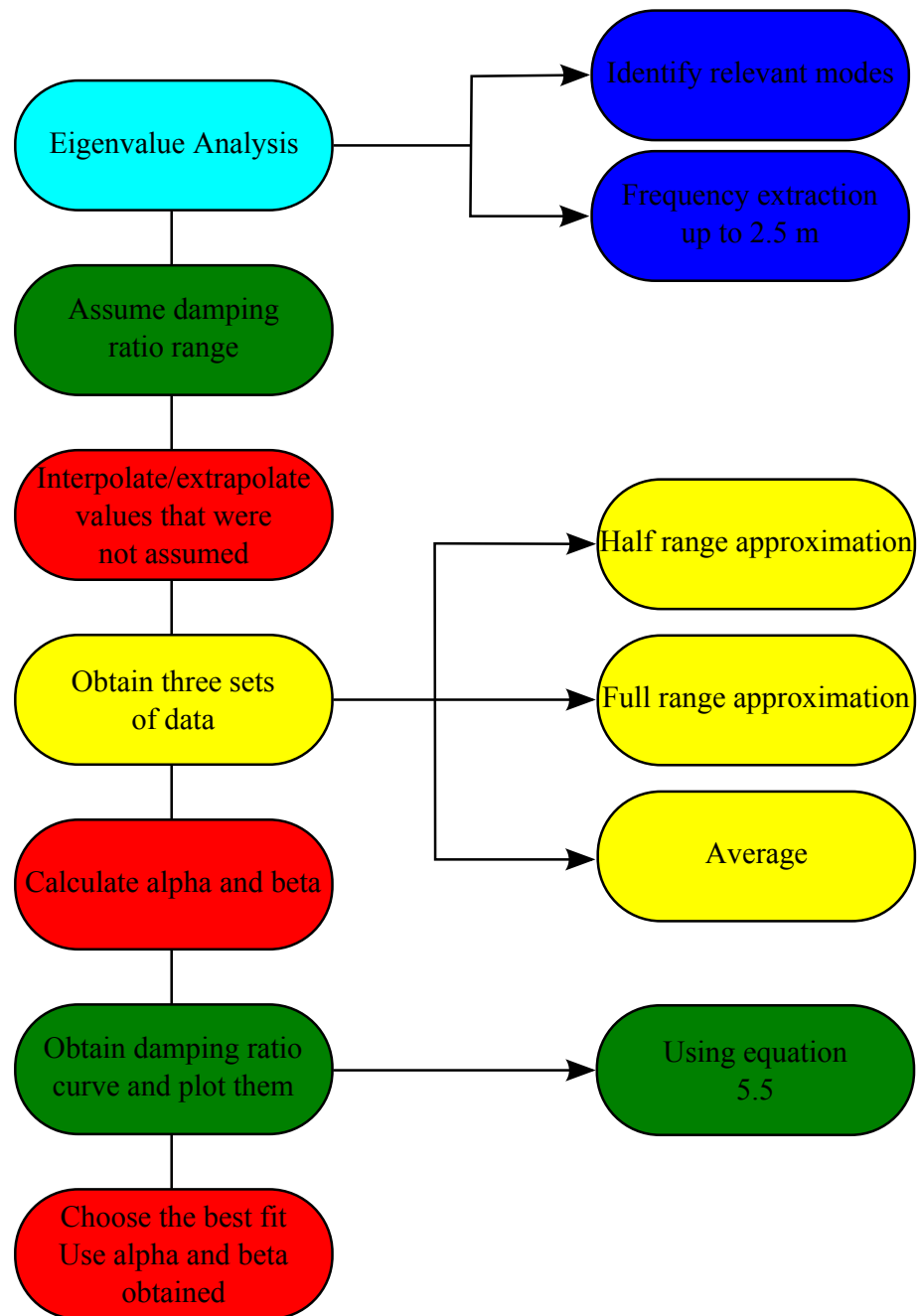


Figure 5.13: Algorithm used to calculate the coefficients in the Rayleigh damping approximation.

Table 5.3: Linear damping ratio interpolated/extrapolated from equations 5.8 and 5.9. Values for the first and the fourth modes were assumed for the problem

Mode	Frequency[Hz]	Linear damping ratio ζ_i
1	10.15	0.02
2	30.54	0.047
3	37.12	0.055
4	71.40	0.1
5	74.10	0.104
6	92.02	0.127
7	130.34	0.177
8	142.60	0.192
9	153.93	0.208
10	183.99	0.247

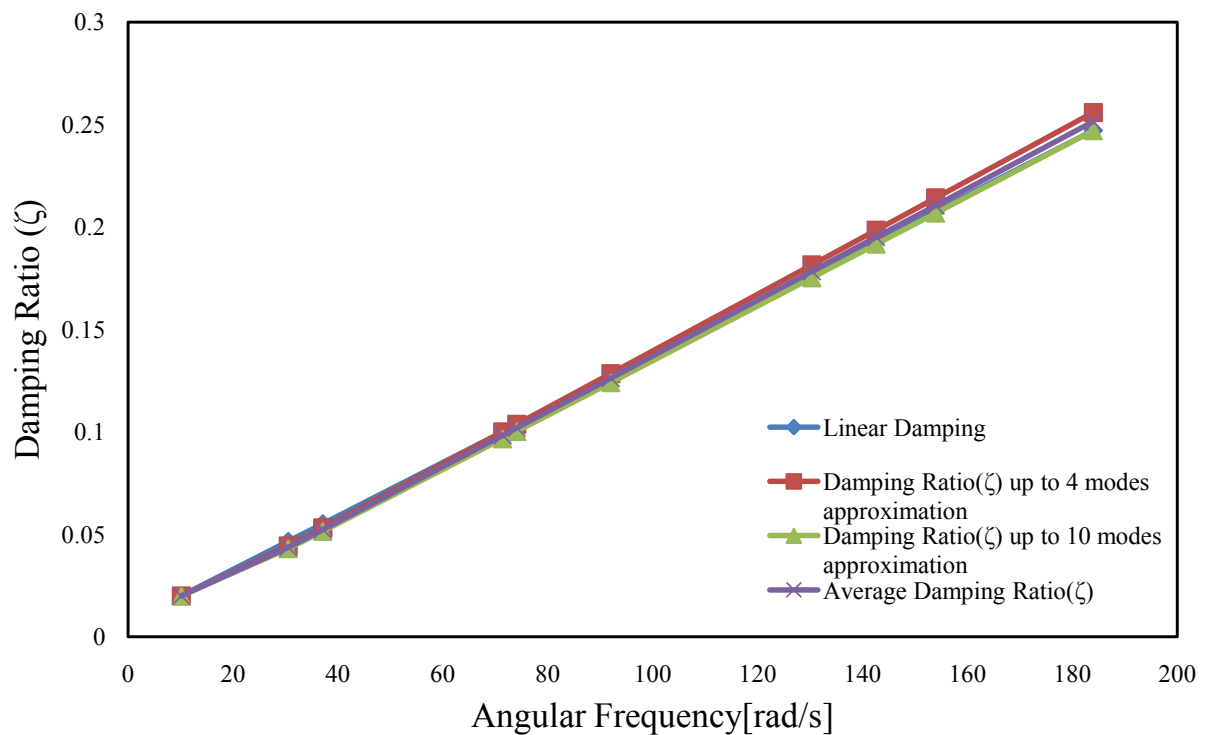


Figure 5.14: Plot of the four approximations.

Table 5.4: Values for the full, half range and average approximations

Mode	Angular Frequency[rad/s]	Damping ratio ζ_i			
		Interpolation/Extrapolation	Half range	Full range	Average
1	10.15	0.02	0.02	0.002	0.02
2	30.54	0.047	0.044	0.043	0.044
3	37.12	0.055	0.053	0.052	0.052
4	71.40	0.1	0.1	0.097	0.098
5	74.10	0.104	0.104	0.1	0.102
6	92.02	0.127	0.128	0.124	0.126
7	130.34	0.177	0.181	0.175	0.178
8	142.60	0.192	0.198	0.191	0.195
9	153.93	0.208	0.214	0.207	0.210
10	183.99	0.247	0.256	0.247	0.251

5.4 Contact

Contact is a physical phenomenon that is difficult to be emulated numerically. There are three methods to model contact. Important information about each is presented in table 5.5. Among these three methods we opt for method II, i.e., contact among stacks was modeled through the inclusion of a non-linear spring-damper between adjacent nodes. Merits and demerits are explained in table 5.5. This approach was chosen for its simplicity, however some other points must be emphasized. First, contact in the container stack is strictly restrict to the corner castings, macroscopically speaking, which avoids the necessity of defining surface to surface interaction, e.g. friction. Second, this approach is time saving compared to any contact approach provide in the commercial package. However, the disadvantage of the non-linear spring-damper element is that uniform dissipation of energy during the approach and restitution periods is not realistically due to the fact that its viscous component is constant (same damping coefficient) during the whole time of collision [32, 83]. Furthermore, it is the most frequently used type of an impact element and is also referred as Kelvin-Voigt model [6, 8, 37, 38, 83]. The non-linear spring follows the mathematical relation depicted in Figure 5.15b. For a complete state-of-the-art review about this kind of approach please refer to the paper written by *Cole et al.* in 2010.

The value of the stiffness was set as 10 times the stiffness of the racking stiffness of the container's closed end. Although this value is largely arbitrary, as long the value itself is not too small or too big, it has non-significant effect in the impact force observed among stacks. The damping coefficient was calculated based in the following formulas presented by *Anagnostopoulos*

$$c = 2\zeta \sqrt{k \frac{m_1 m_2}{m_1 + m_2}} \quad (5.11)$$

$$\zeta = -\frac{\ln e}{\sqrt{\pi^2 + (\ln e)^2}} \quad (5.12)$$

Where k is the stiffness of the linear part of the curve 5.15b, c is the damping constant, ζ is the damping ratio for the collision element and e is the coefficient of restitution. Theoretically, a value of $e = 1$ deals with the case of a fully elastic collision, and a value of $e = 0$ with a fully plastic one. Regardless the fact that there are few experimental evidence about the estimation of this value, researchers like *Jankowski* and *Anagnostopoulos & Spiliopoulos* recommended values ranging from 0.5 to 0.75. More recently *Cole et al.* stated that this range is wider than it was believed before: 0.4 to 1.0. The value used for this study was $e = 0.65$ based on experimental evidence presented by *Goland et al.*,

Table 5.5: A summary of contact algorithms [97]

Method	I	II	III
Capable of	Rigid body to rigid body (mass point to mass point)	Point to point (node to node)	Point to surface (node to surface)
Theory and assumptions	Impulse-momentum law	Contact spring, Hertz law of contact and Predefined contact pairs	Allowing material overlaps, Rigid surface during contact
Algorithm	To judge velocities of contact bodies according to their status before contact	FEM Contact element composed of spring and dashpot	FEM Lagrange multiplier method
Merits	Experiments based, with clear physical meaning. Useful basic concepts for other contact algorithms	Clear physical meaning. Simple algorithm utilize dashpots to simulate energy dissipate	Capable of a wide range of static and dynamic problems with material and geometric non-linearities
Demerits	Unsuited for FEM analysis in general cases	Incapable of 3D arbitrary contacts	Relatively complicated algorithm. Unsuited to be used to a structure composed of bar elements
Applied area	Stereomechanics (classic applications)	Building and bridge structures analysis	Mechanical (car collision, metal forming, etc.)
Notes		Lagrange multiplier method can also be applied for this category.	

Conoscente *et al.*, Zhu *et al.* Chau *et al.* and Shakya *et al.*. Additionally, the coefficient of restitution is obtained from the equation

$$e = \frac{v_2' - v_1'}{v_1 - v_2} \quad (5.13)$$

The expression is derived from the theory of impact among colliding bodies where v_1 and v_2 are the velocities before impact and v_2' and v_1' are the post impact velocities. The coefficient itself is an accounting of how much energy was dissipated during impact and incorporates response non-linearities [37]. The value of this coefficient can be determined experimentally by dropping a sphere on a massive plane plate of the same material from a height h and observing the rebound height h^* . Then, the following formula is used [32]:

$$e^2 = \frac{h^*}{h} \quad (5.14)$$

5.5 Failure

Failure was included in the numerical model by defining zero stiffness after a certain displacement value. This value was decided based on the tensile test described in section 5.2.1.2.

5.6 Euler Buckling

A classical and elegant way to define buckling for structures consisting of slender beams is the Euler buckling theory.

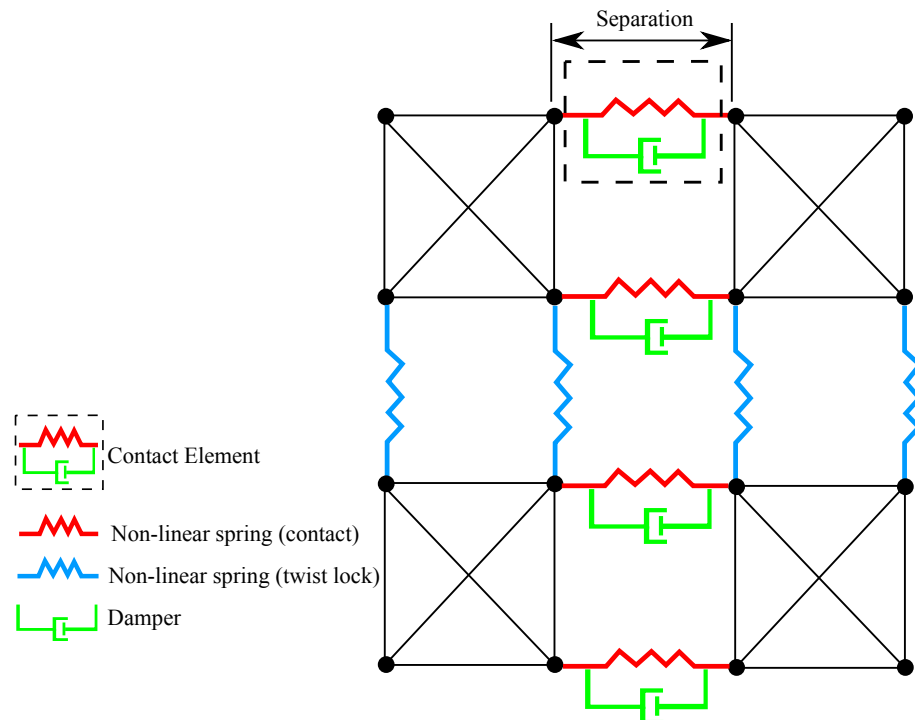
$$[h]P_{critical} = \frac{\pi^2 EI}{L_{effective}^2} \quad (5.15)$$

$$[h]I = \frac{\pi^2 (R^4 - r^4)}{64} \quad (5.16)$$

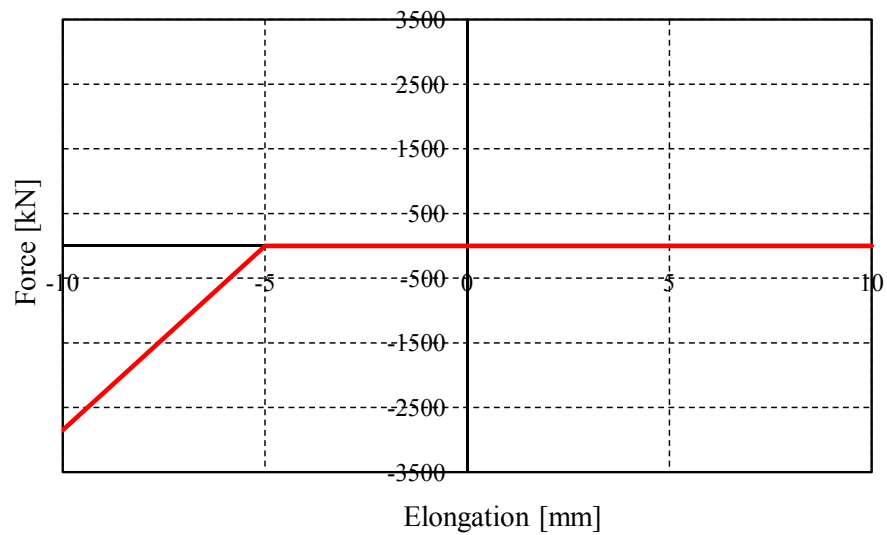
5.7 Time Increment

Time increment was calculated according to the stability condition presented by Courant *et al.*. Analytically:

$$\Delta t_{critical} = L \sqrt{\frac{\rho}{(\lambda + 2\mu)}} \quad (5.17)$$



(a) Schematic representation of the model (front view).



(b) Contact relationship.

Figure 5.15: Details of the contact element used for the numerical simulation.

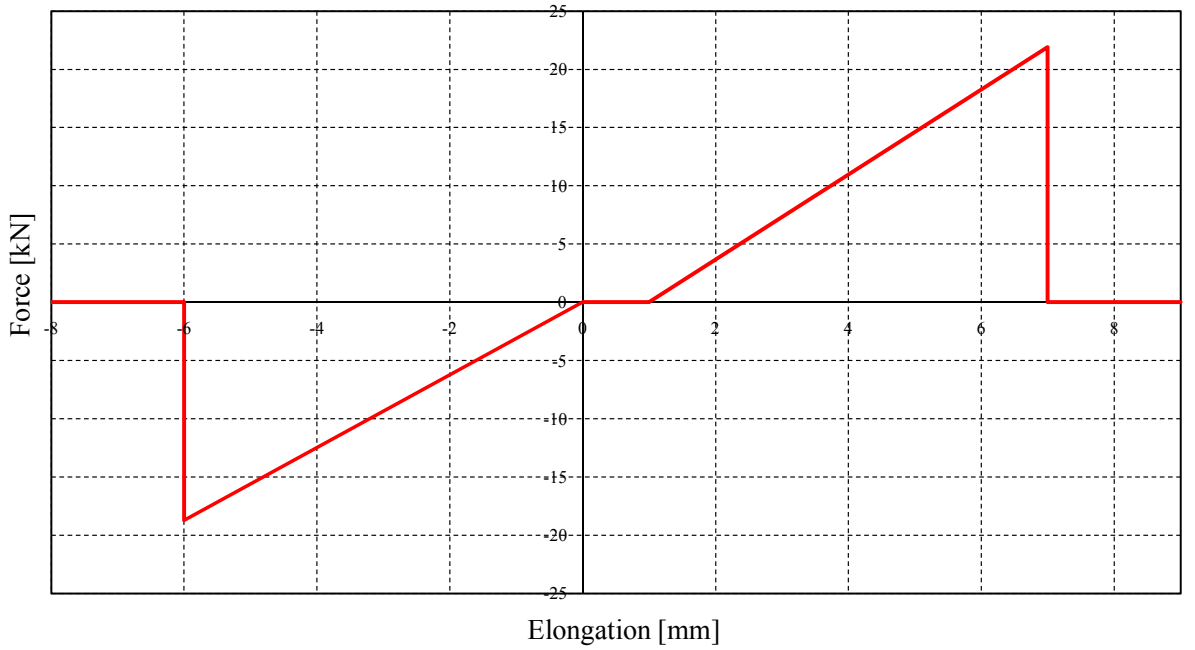


Figure 5.16: Zero stiffness included in the twist lock non-linear relationship to simulate failure.

Where L is the maximum element length, ρ is the material density and λ , μ are the Lamé constants. Where the Lamé constants can be calculated using

$$\lambda = \frac{\nu E}{(1 + \nu)(1 - 2\nu)} \quad (5.18)$$

$$\nu = \frac{E}{2(1 + \nu)} \quad (5.19)$$

For the case of the structure used in this dissertation the characteristic values are: $L = 1647.11$ [mm], $E = 210 \times 10^3$ [N/mm^2] and $\rho = 7.85 \times 10^{-6}$ [kg/mm^3]. Using equations 5.18 and 5.19 yields $\lambda = 9.695 \times 10^4$ [N/mm^2] and $\nu = 7.617 \times 10^4$ [N/mm^2]. Finally placing these two values and ρ in equation 5.17 gives $\Delta = 9.24 \times 10^{-3}$ [s].